University of Turin

PhD School of

Natural Sciences and Innovative Technologies

PhD in

Pharmaceutical and Biomolecular Sciences

(XXXIII cycle)

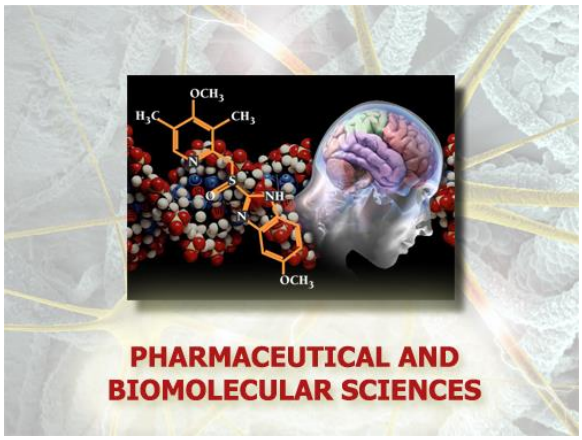

Drug targeting of key proximal drivers of the inflammatory unbalance in cardiometabolic diseases

Candidate: Debora Collotta **Tutor: Professor Massimo Collino**

Università degli Studi di Torino

PhD in

Pharmaceutical and Biomolecular Sciences

Thesis carried out at:

Department of Drug Science and Technology

CYCLE: XXXIII

Thesis title: Drug targeting of key proximal drivers of the inflammatory unbalance in cardiometabolic diseases

CANDIDATE: Debora Collotta

TUTOR: Professor Massimo Collino

COORDINATOR: Professor Roberta Cavalli

ACCADEMIC PERIOD: 2018-2021

SCIENTIFIC-DISCIPLINARY SECTOR OF AFFERENCE: Pharmacology

To my daughter Marina, who during these months, waiting for her birth, has listened to more pharmacology than fairy tales.

Summary

Chapter 1 – Diabesity

"Diabesity" is a term, coined in the 1970s by Sims and colleagues [1] to describe the strong link between diabetes and obesity.

Over the last decade, the escalation in diabetes cases has paralleled the rapid increase in obesity rates, thus the diabesity has been recognized as a major public health problem that is evolving to become a dangerous worldwide epidemic [2]. The International Obesity Task Force estimates that globally, at least 1.1 billion adults are overweight, of whom 312 million are obeses. In adults, the prevalence of obesity is estimated to have doubled or even tripled in less than two decades. More worrisome is that the rate of obesity in children has risen at an even faster rate. In certain parts of Italy and other countries up to 36% of children are overweight.

1.1. Insulin resistance and type 2 diabetes mellitus

Obesity is the prominent risk factor for insulin resistance and results in type 2 diabetes mellitus (T2DM) and other features of cardiovascular disorders associated. The emerging comprehension of risk factors for cardiometabolic disorders underlines the need of additional knowledge on molecular mechanisms involved in their pathophysiology.

Insulin resistance is a pathological metabolic condition determined by impaired sensitivity to insulin of its main target organs (adipose tissue, liver and muscle). Insulin resistance occurs when the body's cells cannot properly perceive insulin because they became less sensitive and eventually resistant to insulin, the hormone that is produced by the pancreas to facilitate glucose absorption. Glucose cannot longer be absorbed by the cells but remains in the blood, triggering the need for more and more insulin (hyperinsulinemia) to be produced in an attempt to induce glucose disposal. The production of ever-increasing amounts of insulin strains and may eventually wear out the beta cells in the pancreas, responsible for insulin production. Once the pancreas is no longer able to produce enough insulin then a person becomes hyperglycaemic. Insulin resistance is strongly associated with irregularities in both glucose and lipid metabolism, in fact, Insulin regulates glucose uptake and circulating free fatty acid (FFA) and triglyceride (TG) concentrations. In adipose tissue, insulin decreases lipolysis thereby reducing FFA efflux from adipocytes; in liver, insulin inhibits gluconeogenesis by reducing key enzyme activities and in skeletal muscle insulin predominantly induces glucose uptake by stimulating the translocation of the GLUT4 glucose transporter to the plasma membrane [3]. Insulin resistance leads to increased circulating FFA and TG concentrations and ectopic fat accumulation, in insulin target tissues, which impair insulin-mediated glucose uptake in skeletal muscle and elevated glucose production in liver [4].

1.2. The insulin signalling pathway

As before, insulin is a hormone released by pancreatic beta cells in response to elevated levels of nutrients in the blood. Insulin triggers the uptake of glucose, fatty acids and amino acids into liver, adipose tissue and muscle and promotes the storage of these nutrients in the form of glycogen, lipids and protein respectively. However, failure to uptake and store nutrients

results in diabetes. The insulin receptor (Figure 1.1) is composed of two extracellular α subunits and two transmembrane β subunits linked together by disulphide bonds. Binding of insulin to the α subunit induces a conformational change resulting in the autophosphorylation of a number of tyrosine residues present in the β subunit [5]. These residues are recognized by phosphotyrosine-binding (PTB) domains of adaptor proteins such as members of the insulin receptor substrate family (IRS) [6]. Receptor activation leads to the phosphorylation of key tyrosine residues on IRS proteins, some of which are recognized by the Src homology 2 (SH2) domain of the p85 regulatory subunit of PI3-kinase (a lipid kinase). The catalytic subunit of PI3-kinase, p110, then phosphorylates phosphatidylinositol (4,5) bisphosphate leading to the formation of Ptd (3,4,5) P3. A key downstream effector of Ptd (3,4,5) P3 is Protein Kinase B (AKT), which is recruited to the plasma membrane. Activation of AKT also requires the protein kinase 3phosphoinositide dependent protein kinase-1 (PDK1), which in combination with an as yet unidentified kinase leads to the phosphorylation of AKT. Once active, AKT enters the cytoplasm where it leads to the phosphorylation and inactivation of glycogen synthase kinase 3β (GSK-3β). A major substrate of GSK-3β is glycogen synthase, an enzyme that catalyzes the final step in glycogen synthesis. Phosphorylation of glycogen synthase by GSK-3β inhibits glycogen synthesis; therefore, the inactivation of GSK-3β by AKT promotes glucose storage as glycogen. In addition to promoting glucose storage, insulin inhibits the production and release of glucose by the liver by blocking gluconeogenesis and glycogenolysis. Insulin directly controls the activities of a set of metabolic enzymes by phosphorylation and dephosphorylation events and also regulates the expression of genes encoding hepatic enzymes involved in gluconeogenesis. A key action of insulin is to stimulate glucose uptake into cells by inducing translocation of the glucose transporter, GLUT-4, from intracellular storage to the plasma membrane. PI3-kinase and AKT are known to play a role in GLUT-4 translocation [7].

Moreover, insulin promotes the uptake of fatty acids and the synthesis of lipids due to an increase in the transcription factor steroid regulatory element-binding protein (SREBP)-1c [8].

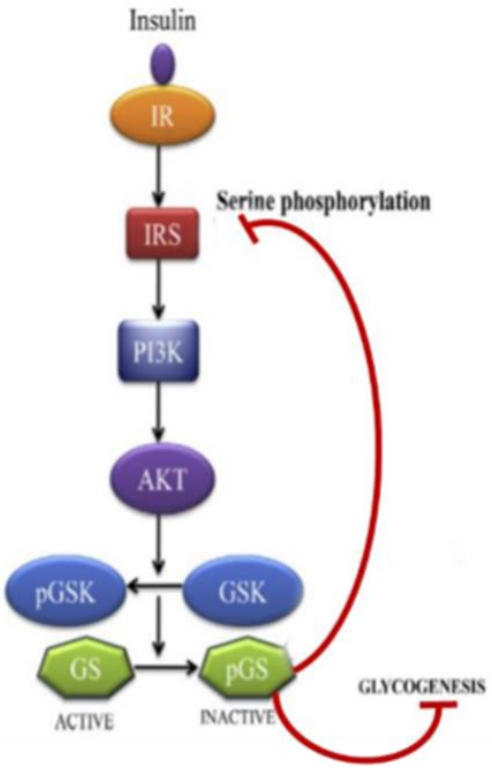

Figure 1.1 Insulin Signallig pathway

The inhibition of signalling downstream of the insulin receptor is a primary mechanism through which inflammatory signalling leads to insulin resistance (Figure 1.2). Exposure of cells to TNF-α or elevated levels of FFA stimulate inhibitory phosphorylation of serine residues of IRS-1. This phosphorylation reduces both tyrosine phosphorylation of IRS-1 in response to insulin and the ability of IRS-1 to associate with the insulin receptor and thereby inhibits downstream signalling and insulin action. Several serine/threonine kinases are activated by inflammatory or stressful stimuli and contribute to inhibition of insulin signalling, including JNK, inhibitor of nuclear factor-κB (NF-κB) kinase (IKK) and conventional protein kinase C (PKC). They have all been reported to be able to inhibit insulin action by serine phosphorylation of IRS-1 [9]. In addition to serine/threonine kinase cascades, other pathways contribute to inflammation-induced insulin resistance. In particular, suppressor of cytokine signalling-3 (SOCS-3), a protein involved in both inflammation and insulin resistance, seem to inhibit insulin action at the level of insulin receptor substrates IRS-1 and IRS-2, although by a different mechanism. SOCS-3 has also been demonstrated to regulate central leptin action. Inflammatory cytokine stimulation can also lead to induction of inducible nitric oxide synthase (iNOS). iNOS produces large amounts of nitric oxide (NO) as a defence mechanism; this also seems to contribute to impairment of both muscle cell insulin action and β cell function in obesity. Thus, induction of SOCS-3 proteins and iNOS represents two additional and potentially important mechanisms that contribute to cytokine-mediated insulin resistance [10].

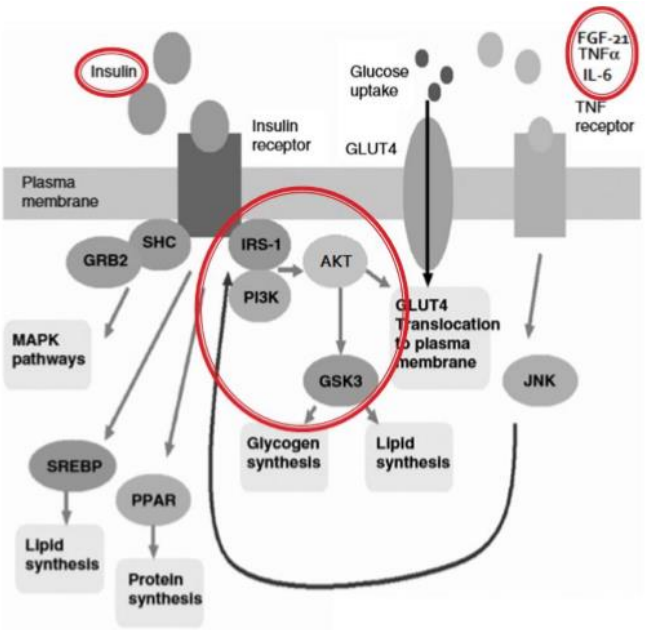

Figure 1.2 Crosstalk between insulin pathway and inflammatory pathway

Modified from: Journal of Clinical Investigation (2011).

Chapter 2 – Cardiovascolar diseases

Metabolic disorders are associated with unfavorable changes in cardiovascular morphology and function including cardiac and vascular remodeling, neointimal formation, decreased myocardial contractility, endothelial injury and compromised vascular compliance [11]. It is well perceived that individual components of metabolic syndrome serve as independent risk factors for the overall prevalence of cardiovascular diseases, with the prevalence dramatically escalating with concurrent risk factors [12].

Chapter 3 – Cardiometabolic disorders: meaning, risk factors and social impact

Cardiometabolic disorders (CMD) are a cluster of interrelated factors which increase the risk of cardiovascular diseases and T2DM which occur together more often than by chance alone [13].

The risk factors include hypertension (increased blood pressure: systolic BP ≥135 mmHg or diastolic BP ≥85), dyslipidemia (increased triglycerides and lower high-density lipoprotein cholesterol), increased glucose levels (fasting pGL ≥7 mmol/L, an HbA1C ≥6.5%, a 2 h plasma glucose ≥11.1 mmol/L during a glucose tolerance test (GTT) or a random measurement of glucose ≥11.1 mmol/L) and abdominal obesity (measured by waist circumference, waist-to-hip ratio, waist-to-height ratio and body mass index).

The growing prevalence of Cardiometabolic disorders worldwide is becoming a serious health problem and economic burden. Data in letterature show significant increase in the prevalence of abdominal obesity in young adults [14] underlining the importance of implementing lifestyle intervention programs to promote healthy eating habits, physical activities and better awareness of the risk of abdominal obesity in this particular age group.

The existence of several definitions of Cardiometabolic disorders has been overcome with a harmonised definition [15]: that is, the presence of three out of five risk factors as follows:

Table 1: The new International Diabetes Federation (IDF) definition

According to the new IDF definition, for a person to be defined as having the metabolic syndrome they must have: **Central obesity** (defined as waist circumference* with ethnicity specific values) **plus** any two of the following four factors:	
Raised triglycerides	≥ 150 mg/dL (1.7 mmol/L) **or specific treatment for this lipid abnormality**
Reduced HDL cholesterol	< 40 mg/dL (1.03 mmol/L) in males < 50 mg/dL (1.29 mmol/L) in females **or specific treatment for this lipid abnormality**
Raised blood pressure	systolic BP ≥ 130 or diastolic BP ≥ 85 mm Hg **or treatment of previously diagnosed hypertension**
Raised fasting plasma glucose	(FPG) ≥ 100 mg/dL (5.6 mmol/L), **or previously diagnosed type 2 diabetes** If above 5.6 mmol/L or 100 mg/dL, OGTT is strongly recommended but is not necessary to define presence of the syndrome.

** If BMI is >30kg/m², central obesity can be assumed and waist circumference does not need to be measured.*

Chapter 4 – The pivotal role of Metaflammation in Cardiometabolic Disorders

Metaflammation is defined as a low-grade, chronic inflammatory response orchestrated by metabolic cells in response to excess nutrients and calories in metabolic tissues. In the vicious circle where vascular defects and metabolic disturbances worsen and reinforce each other, metaflammation has been suggested to serve as the pathophysiological link that binds endothelial and metabolic dysfunctions. A growing body of evidences indicates indeed that excessive fatty acids and sugar intake participates in the development and progression of cardiovascular diseases, including myocardial infarction, by increasing the local inflammatory response and, at the same time, by reducing the efficiency of protective responses that are usually activated by transient oxygen deprivation [16].

A previus publication of our lab [17] clearly demonstrate that a high-fat high-fructose (HFHF) diet alters different signaling pathways involved in cardiac injury. While elements of cardioprotective pathways are downregulated, those of inflammatory processes are upregulated by HFHF diet and ischemia reperfusion (IR) injury is exacerbated by these maladaptive pathway modulations. These results offered further improvements on the understanding of the link between cardiovascular and metabolic injuries.

In particular, the diet-induced inhibition of protective signaling pathways was associated with a robust increase in myocardial protein levels of NLRP3 inflammasome, a central mediator in the inflammatory response to tissue injury during either myocardial infarction or insulin resistance [18- 19]. Strong correlations between the expression of NLRP3 inflammasome-related genes and insulin resistance have been recently reported in obese male subjects with impaired glucose tolerance and in type 2 diabetic patients [20].

Chapter 5 – Markers of common mechanisms of cardiometabolic disorders

The need to facilitate the complex management of CMD have prompted the search and identification of some biomarkers. Desirable characteristics of any cardiovascular disorders (CVD) biomarker include that its measurement should be easy, preferably at point-of-care over a short time period with adequate precision and accuracy and the demonstration of low intra-individual variability.

5.1. Cytokines

The finding a decade ago that tumour necrosis factor-α (TNF-α) is overexpressed in the adipose tissue of multiple rodent-obesity models provided the first clear link between cardiometabolic disorders and chronic inflammation. TNF-α is a proinflammatory cytokine that activates various signal transduction cascades and impairs insulin-action. Also now it is clear that, in addition to TNF-α, various other pro-inflammatory mediators and cytokines such as Interleukin (IL)-6, IL-1β, IL-18 are overexpressed in adipose and other tissues in mice models of obesity in humans.

Adipokines (such as leptin and adiponectin) are secreted by adipose tissue, with well-established metabolic functions, that can regulate the immune response. Leptin controls food intake and energy expenditure and plays significant roles in both adaptive and innate immunity. Leptinemia is increased in obesity, having a proinflammatory role, indeed it is consistent with the increase in inflammatory cytokines and a reduction in adiponectin level [21]. Adiponectin has important anti-atherogenic, antidiabetic, anti-inflammatory properties and immunological activity. Unlike most other adipokines, adiponectin is decreased in obesity, diabetes and other insulin-resistant states. This may be explained by the increased secretion of TNF-α from visceral fat [22].

Lipids themselves also participate in the coordinate regulation of inflammation and metabolism. Elevated plasma lipid levels are characteristic of obesity infection and other inflammatory states.

The high level of coordination of inflammatory and metabolic pathways is highlighted by the overlapping biology and function of macrophages and adipocytes. Preadipocytes under some conditions can exhibit phagocytic and antimicrobial properties and appear to even be able to differentiate into macrophages in the right environment, which suggests a potential immune role for preadipocytes. Macrophages in adipose tissue are likely to contribute to the production of inflammatory mediators either alone or in concert with adipocytes, which suggests a potentially important influence of macrophages in promoting insulin resistance. Besides macrophages, obesity is associated with aberrant expansion of other leukocytes (T cells, B cells, eosinophils, neutrophils and mast cells) in adipose tissue that contribute to chronic inflammation. In particular, the increased neutrophils lead to a rise of myeloperoxidase (MPO) activity, a marker of neutrophil infiltration, in the damaged tissue during inflammation.

Regarding the direct link between cytokines and cardiovascular disorderes recently studies on the cardiovascular comorbidity that arises in autoimmunity are revealing additional roles for cytokines in atherosclerosis. Arterial inflammation is a hallmark of atherosclerosis and appropriate management of this inflammation represents a major unmet therapeutic need for cardiovascular disease patients. Randolph and colleagues underlied the diverse

contributions of immune cells to atherosclerosis including mechanisms of activation in this context and the cytokine circuits (specially involving IL-1β, TNF-α and IL-17) that disease progression and discussed the recent application of these insights immunotherapy to treat cardiovascular disease [23].

5.2. AGEs

An important factor to the metaflammation concerns the accumulation of Advanced glycation end products (AGEs).

AGEs are a heterogeneous and irreversible group of compounds that is formed by a non-enzymatic reaction known as Maillard Reaction (Figure 5.1). This reaction, specifically, occurs between the carbonyl group of a reducing sugar and the amino group of proteins. At high temperatures shiff bases are formed which undergo a rearrangement of the double bonds to the formation of the Amadori compounds. At this point, a large number of reactions, including successions of dehydrations, oxidation-reduction reactions, take place influenced by pH and high temperatures and by the presence of oxidation products the formation of multiple by-products, including highly reactive dicarbonyl compounds such as methylglyoxal (MGO), which as a last step to the formation of AGEs.

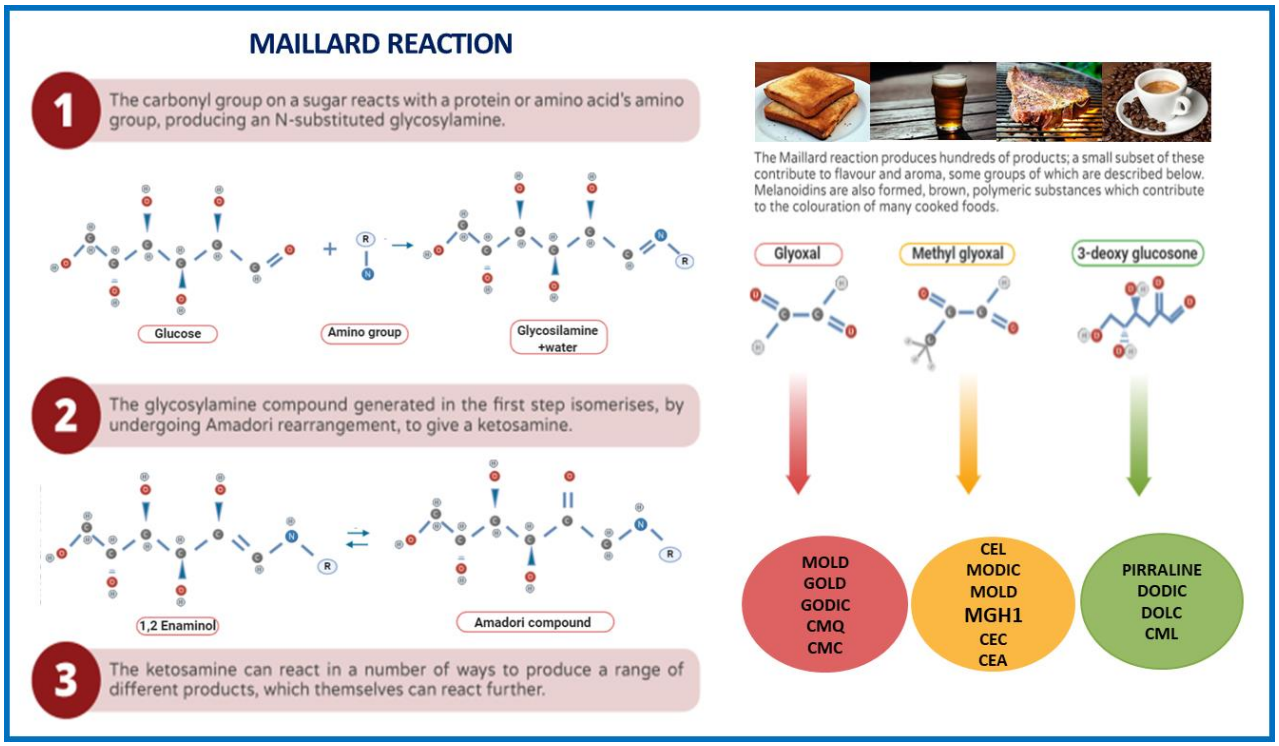

Figure 5.1 Maillard reaction scheme

AGEs can therefore be formed exogenously in foods that have undergone a heating process at high temperatures, during the processing of food products or even endogenously following a high intake of sugars with the diet.

AGEs are prevalent in the diabetic vasculature and contribute to the development of atherosclerosis. The presence and accumulation of AGEs in many different cell types affect extracellular and intracellular structure and function. Their biological effects translate to accelerated plaque formation in diabetes as well as increased cardiac fibrosis with consequent effects on cardiac function. AGEs infact contribute to a variety of microvascular and macrovascular complications, in patients with T2DM and obesity, leading to the development of atherosclerosis [24]. Activation of receptor for advanced glycation end products (RAGE) by AGEs causes upregulation of the transcription factor NF-κB and its target genes, triggering metaflammation. Moreover, AGEs block nitric oxide activity in the endothelium and cause the production of reactive oxygen species (ROS).

5.3. ROS

AGEs are associated with an increase in oxidative stress since they mediate the production of ROS, increasing the intracellular levels of hydrogen peroxide (H2O2), superoxide (O2-) and nitric oxide (NO). The interaction of AGEs with RAGE enhances oxidative stress through ROS production by NADPH oxidases [25] inside the mitochondria affecting its function and ultimately influences cell metabolism under various pathological conditions [26].

ROS play an essential role in mediating the RAGE signal transduction. According to this, ROS generated in the cellular environment directly activate p21RAS [27] and in RAGE-bearing cells expressing a mutant form of p21RAS, suppression of the activation of ERK1/2 upon exposure to AGEs was found [28]. Furthermore, AGE-RAGE mediated activation of ERK1/2 kinases is enhanced in the presence of glutathione depletion. ROS are also necessary for sustaining the phosphorylation of p38 [29] and JNK [30] caused by AGEs by inhibiting the inactivating phosphatases, allowing the activation of the proinflammatory NF-κB pathway [31].

Chapter 6 – Selective inflammatory pathways involved in cardiometabolic disorders

A growing body of evidence support that metabolic and cardiovascular diseases are intimately related to chronic inflammation.

Initiation and resolution of inflammation are both necessary: an inappropriate inflammatory response would not be able to fight invading pathogens, while uncontrolled inflammation can damage the host. The inflammatory response is indeed a defense and protection mechanism usually followed by a resolution phase, a physiological active process, which is highly coordinated and regulated by several endogenous mediators. If the resolution does not occur the inflammatory process became chronic with consequent damage to organs and tissues.

The endogenous mechanisms that deactivate excessive inflammation and urge its resolution timely are of considerable interest since unresolved inflammation is the common mechanism of cardiometabolic disorders.

6.1. Proinflammatory pathways

6.1.1. NLRP3 Infammasome pathway

Most recent evidences suggest a substantial role of the NLRP3 inflammasome in regulating meta-inflammation. The term “inflammasome” was coined by Tschopp and co-workers in 2002 to describe a high-molecular-weight complex present in the cytosol of stimulated immune cells that mediates the activation of inflammatory caspases [32]. The inflammasomes are signalling platforms, which are assembled in response to pathogen-associated and damage-associated molecular pattern molecules and environmental irritants. Currently, inflammasomes are distinguished into two families: the NOD-like receptor (NLR) family and the pyrin and HIN200 (haematopoietic interferon-inducible nuclear antigens with 200 amino-acid repeats) domain-containing protein (PYHIN) family. The NLR family consists of NLRP1, NLRP2, NLRP3, NLRP6, NLRC4 and NLRP12. The PYHIN family consists of AIM2 and IFI16. Each inflammasome is induced by numerous different exogenous and endogenous signals. Among the inflammasomes, the most studied in the area of metabolic diseases is the NLRP3 inflammasome (Figure 6.1): a multiprotein, large cytoplasmic complex (>700 kDa), which interacts with an apoptosis associated speck-like protein containing a caspase recruitment domain (ASC), thus recruiting and activating caspase-1. Because caspase-1 is an IL-1β-converting enzyme, it mediates the processing of pro-IL-1β into mature IL-1β and the consequent release of IL-1β, thereby causing inflammation. Yet, the induction of IL-1β release requires the transcriptional induction of pro-IL-1β. Thus, a system including pro-IL-1β induction and inflammasome-mediated IL-1β maturation seems necessary for the regulation of this inflammatory cytokine.

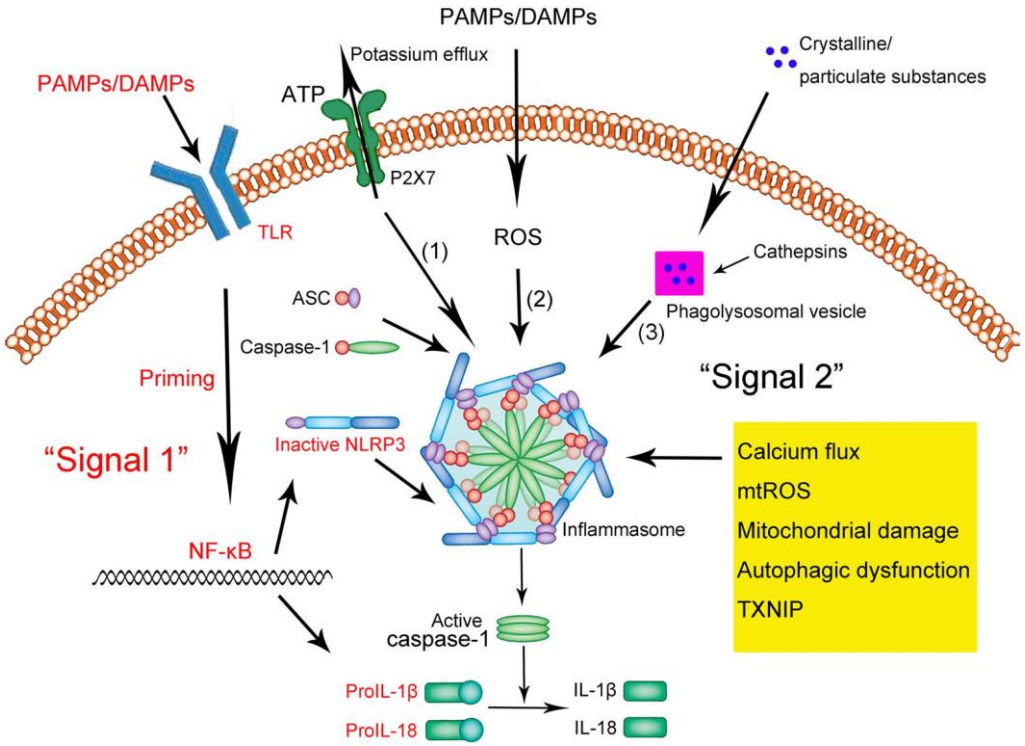

Figure 6.1 Mechanism of action of NLRP3 Inflammasome.
(Bo-Zong Shao et all. Front. Pharmaco 2015l)

There are a number of potential mechanisms for the assembly of the NLRP3 inflammasome. According to one hypothesis, mitochondria are the principal source of ROS required for inflammasome activation; several recent studies have implicated ROS produced by mitochondria, rather than phagosomes, in NLRP3 activation exerting an indirect effect on pathways of metabolism [33]. A second mechanism involves the disruption of lysosomal membrane integrity by crystalline materials and peptide aggregates [34]. Upon uptake of such substances, lysosomal rupture leads to the leakage of lysosomal proteases, specifically cathepsins B and L, into the cytosol where they could possibly mediate NLRP3 inflammasome activation by an as-yet-undefined cleavage event. Vajjhala and colleagues [35] have shed light on the molecular details of the complex mechanisms of NLRP3 inflammasome assembly and activation, identifying multiple binding sites on the PYD domain (N-terminal pyrin domain) of the adaptor protein ASC which allowes self-association and interaction with binding partners.

The assembly of functional NLRP3 inflammasome requires two distinct steps, priming and activation, respectively at the transcriptional and post-transcriptional levels. Furthermore, it is necessary to prime for a long time to increase the cellular expression of NLRP3 through NF-κB signaling. Post-transcriptional molecular mechanisms controlling NLRP3 activation that can respond quickly to *stimuli* without the need for NF-κB activation and new protein synthesis have also been identified. Extracellular signal-regulated kinase 1 (ERK1) - mediated post-translational modifications also permit the NLRP3 inflammasome to respond to the second signal, ATP, by inducing post-translational events that are independent of any new production of pro-IL-1β or NLRP3 protein.

As explained in previous chapters, metaflammation plays an important role in the development of CVD and metabolic diseases. Over the last years, several studies have shown

that NLRP3 inflammasome can play an important role in the crosstalk between inflammation and deranged pathways.

The role of the NLRP3 Inflammasome complex as pharmacological target for metaflammation is the main topic of an editorial I contributed to write, published on "Diabetes research Openvention J.", and reported in the discussion section.

6.1.2. NF-ϰB pathway

The NF-kB protein complex (Figure 6.2) controls DNA transcription for a multitude of proinflammatory and immunological molecules. NF-kB is found in almost all animal cell types and it is important in regulating cellular responses because it belongs to the category of "rapid-acting" primary transcription factors, that are present in cells in an inactive state and do not require new protein synthesis in order to become activated. This allows NF-kB to be a first responder to harmful cellular *stimuli*.

Known inducers of NF-kB activity are highly variable and include ROS, TNF-α, IL-1β and bacterial LPS. NF-kB plays a key role in regulating the immune response to infection (κ light chains are critical components of immunoglobulins).

In unstimulated cells, the NF-kB dimers are sequestered in the cytoplasm by a family of inhibitors, called IκBs (Inhibitor of kB), which mask the nuclear localization signals of NF-kB proteins and sequester NF-kB as an inactive complex [36].

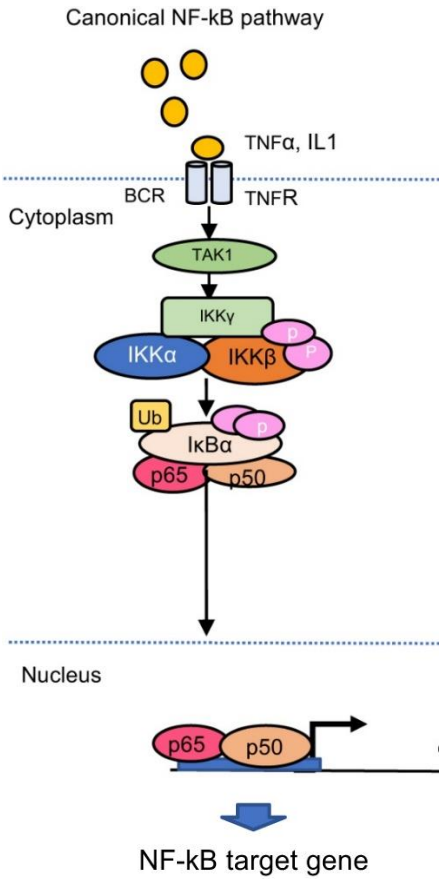

Figure 6.2 The canonical pathway for NF-kB activation

Modified from: Endocrine-Related Cancer 26, 6; 10.1530/ERC-19-0087

Thus in physiological conditions NF-κB is found in an inactive form in the cytosol, linked to IκB, which prevents its translocation and transcription at nuclear level. The IκB family includes

several members, in particular IκBα, a 37 kDa protein, which is the NF-κB inhibitor most involved in the signaling mediated by it.

NF-κB is characterized by two different activation pathways, the canonical pathway which, if triggered, leads to a rapid and transient activation of NF-κB and the non-canonical pathway which instead determines slow and persistent activation of the transcription factor under exam. The activation of the canonical pathway occurs, as mentioned before, upon arrival of a stressogenic or pro-inflammatory *stimulus*. In particular, there is the activation, through phosphorylation on $Ser^{176/180}$ amino acid residues of the IKK kinase complex (IKKα, IKKβ) which, in turn, is able to phosphorylate IκBα on $Ser^{32/36}$ residues. IκBα is associated with the dimers of p50 and the members of the REL family (RELA or c - REL), while p105 is associated with p50 or REL (RELA or c - REL). After IKK phosphorylation, IκBα and p105 are targeted for ubiquitin (Ub) -dependent degradation in the proteasome, resulting in nuclear translocation of members of the canonical NF-κB pathway that bind to specific DNA elements in the form of various dimeric complexes, including RELA - p50, c - REL - p50 and p50 - p50. Conversely, the activation pathway of non-canonical NF-κB is based on the processing of p100, a molecule similar to IκB that regulates mainly, although not exclusively RelB. The non-canonical NF-κB pathway selectively responds to the subfamily of the Tumor Necrosis Factor Receptors (TNFR) which target activation of the NF-κB-inducing kinase (NIK) kinase. NIK phosphorylates and activates IKKα, which phosphorylates the carboxterminal serine residues of p100, triggering the degradation of the IκB-like carboxyerminal structure of p100 and leading to the generation of p52 and the nuclear translocation of p52 and RELB52.

6.1.3. JAK-STAT pathway

The Janus kinase (JAK) – signal transducer and activator of transcription (STAT) pathway (Figure 6.3) is a master regulator of more than 50 cytokines or hormone receptors, many of which play a pivotal role in the pathophysiology of metaflammation [37].

The mammalian JAK family has four members, named JAK1, JAK2, JAK3 and tyrosine kinase 2 (TYK2), which selectively bind different receptors [38]. Over the past few years, Jak signaling has been demonstrated to be dysregulated in metabolic diseases including obesity and T2DM [39]. JAK proteins are recruited to the intracellular domains of various receptors upon binding of their ligand, where they are dimerized and activated through autophosphorylation. When activated, JAKs in turn phosphorylates and activates STAT proteins, which themselves dimerize and translocate to the nucleus where they regulate gene transcription, including cytokine production.

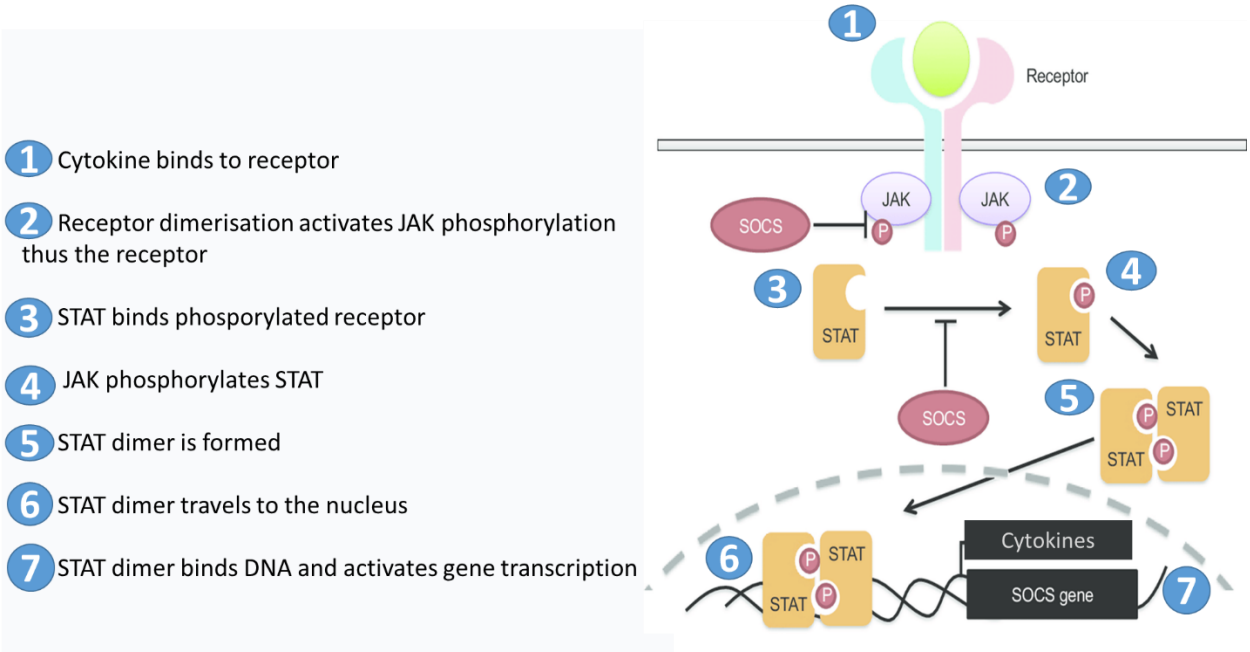

Figure 6.3 JAK-STAT pathway

Modifed from: Zhaoqi Yan et all. Clinical Immunology 2016

Cytokine signaling *via* JAKs plays an important role in the pathogenesis of metabolic diseases, as recently documented by both clinical and basic science research studies [40]. Studies in knock-out mice confirmed a pivotal role for JAK signaling, mainly JAK2, in the regulation of a multitude of metabolic processes including, but not limited to glucose tolerance, insulin sensitivity, leptin sensitivity, energy expenditure and adiposity.

Several published papers reporting a cross-talk between the insulin receptor and JAK signaling pathway [41]. Infact, in response to the administration of physiological concentrations of insulin in rats, JAK2 associates with the insulin receptor and is then phosphorylated in insulin-sensitive tissues [42]. Interestingly, JAK2 overactivation has been demonstrated to contribute to the downregulation of Akt phosphorylation and glucose uptake in models of insulin resistance, whereas JAK2 knockdown in L6 myotubes alleviated insulin resistance by interfering with the negative regulation of Akt phosphorylation and activity [43]. A recently published study on rats with streptozotocin-induced diabetes investigated the effects of the pharmacological inhibition of JAK signaling. The authors demonstrated that combination therapy of tofacitinib (10 mg/kg BW) and aspirin (100 mg/kg BW) in rats significantly improved glucose homeostasis and insulin secretion compared to diabetic (untreated) rats [44]. However, tofacitinib is a JAK3 inhibitor. Other authors have convincingly demonstrated that loss of JAK3 in mice results in body weight gain, impaired glycemic and lipid homeostasis and early symptoms of liver steatosis [45]. In contrast, JAK2 deficiency in the liver, macrophages, or adipocytes protects against high-fat diet induced metabolic inflammation [46-47], suggesting that JAK2 may be a promising target for the treatment of obesity, metabolic syndrome and T2DM.

6.2. Antinflammatory pathways

During the past years, the study of inflammation was limited to the mere understanding of the proinflammatory signals that mediated its onset and evolution. Currently, there is evidence of how the resolution of inflammation and return to physiological homeostasis are not passive phenomena, but represent active and highly regulated biochemical processes at the tissue level. Recently the existence of endogenous pro-resolving pathways has been demonstrated [48]. Some mediators have been highlighted endogenous pro-resolutours that include lipids, like Resolvins, such as Resolvin D1 (RvD1), the lipoxins (LXA4, LXB4, ATL), the protectins, such as Annexin A1, the maresins, which guide actively terminating inflammation, stimulating and accelerating resolution processes through multifactorial mechanisms [49].

At the cellular level, these endogenous mediators, through binding to specific receptors lead to a reduction in the migration and infiltration of neutrophils and increasing their phagocytosis through macrophages. Their action also translates into a decrease in the production of pro-inflammatory factors such as cytokines, chemokines, prostaglandins and ROS, thereby decreasing the extent of the inflammatory response. The inflammatory process has always been considered a passive process that ends when the pro-inflammatory impulses and lipid mediators are lacking, such as leukotrienes and prostaglandins. For this reason, most of the anti-inflammatory drugs have been made against those lipid mediators that are responsible for the inflammatory process. Highlighting the existence of endogenous mechanisms that block the inflammatory event with synthesis and the release of anti-inflammatory mediators permits to obtain significant positive effects for the treatment of inflammatory diseases confirming that resolution of the inflammatory progression is an active process [50].

6.2.1. Annexine A1 pathway

Annexin superfamily is composed of 13 members, grouped in view of their unique Ca2+ binding-site architecture, which enables them to peripherally attach to negatively charged membrane surfaces [51]. Annexin A1 (AnxA1), also known as lipocortin I, was originally identified as a glucocorticoid-induced protein active on phospholipase- (PL-) A2 inhibition and prevention of eicosanoid synthesis [52]. This 37 kDa protein consists in a homologous core region of 310 amino acid residues, representing almost 90% of the structure, attached to a unique N-terminal region. In addition to mediating membrane binding, Ca2+ ions can also induce a conformational change that leads to the exposure of the bioactive N-terminal domain. In fact, studies on the anti-inflammatory activity of AnxA1 revealed not only that the different functions of the protein lie within the unique N-terminus, but also that synthetic peptides from the N-terminal domain may mimic the pharmacological property of the whole protein, specifically binding to formyl peptide receptors (FPRs) [53]. In inflammatory conditions intact AnxA1 can be cleaved by proteinase-3 and neutrophil elastase generating the 33 kDa cleaved isoform, which is believed to be inactive and peptides derived from the AnxA1 N-terminus [54].

AnxA1 is an endogenous glucocorticoid-regulated protein, which is able to counterregulate the inflammatory events restoring homeostasis. AnxA1 and its mimetic peptides inhibit neutrophil tissue accumulation by reducing leukocyte infiltration and activating neutrophil apoptosis. AnxA1 also promotes monocyte recruitment and clearance of apoptotic leukocytes by macrophages.

More recently, some evidence has suggested the ability of AnxA1 to induce macrophage reprogramming toward a resolving phenotype, resulting in reduced production of proinflammatory cytokines and increased release of immunosuppressive and proresolving molecules. [55].

The combination of these mechanisms results in an effective resolution of inflammation, pointing to AnxA1 as a promising tool for the development of new therapeutic strategies to treat inflammatory diseases.

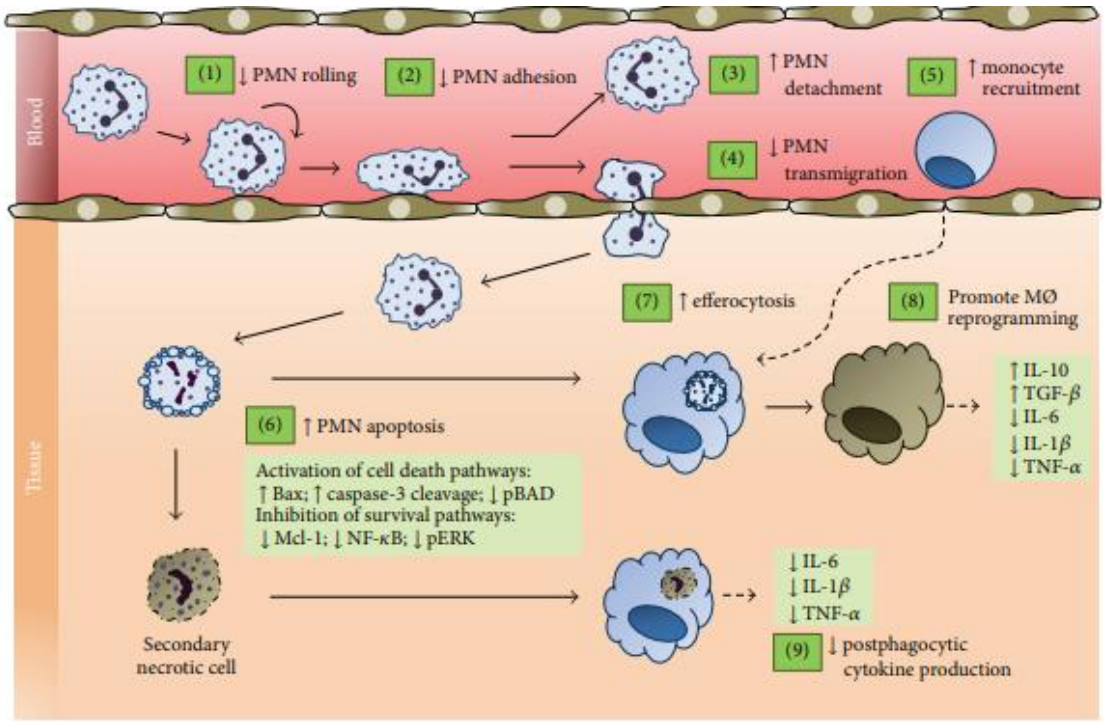

Figure 6.4 Cellular events associated with the anti-inflammatory and proresolving effects of AnxA1 and its mimetic Nterminal peptides

AnxA1 modulates a wide range of cellular and molecular steps of the inflammatory response and is deeply involved in the endogenous mechanisms that are activated to bring about proper resolution. Pharmacological administration of AnxA1 results in decreased neutrophil rolling (1) and adhesion (2) to endothelium, increased detachment of adherent cells (3) and inhibition of neutrophil transmigration (4). In addition, AnxA1 is able to induce apoptosis, overriding the prosurvival signals that cause prolonged lifespan of neutrophils at the inflammatory site (6). Endogenous and exogenous AnxA1 also promote monocyte recruitment (5) and clearance of apoptotic neutrophils by macrophages (7). Phagocytosis of apoptotic neutrophils by macrophages is coupled with release of anti-inflammatory signals, including transforming growth factor-β, and lower levels of proinflammatory cytokines (8). Besides, AnxA1 is related to macrophage reprogramming toward a proresolving phenotype (8). Initial in vitro studies using AnxA1 knock-down leucocytes demonstrate that AnxA1 prevents proinflammatory cytokine production after phagocytosis of secondary necrotic cells. This effect provides an important fail-safe mechanism counteracting inflammatory responses when the timely clearance of apoptotic cells has failed (9). Source Journal of Immunology Research 2016 Michelle A et all

AnxA1 exerts many of its anti-inflammatory and proresolving actions through the formyl peptide receptor type 2/lipoxin A4 receptor (FPR2/ALX). This receptor, along with FPR1 and FPR3, composes a family of seven-transmembrane domain G protein-coupled receptors which share significant sequence homology [56]. FPR2/ALX receptor is shared by a variety of other peptide/protein and lipid ligands, mediating diverse biological functions of relevance for host

defence and inflammation. Interestingly, FPR2/ALX agonists are associated with both proinflammatory and proresolving signalling pathways [57]. However, how FPR2/ALX can promote both inflammatory response and limit its duration and intensity still remains to be fully elucidated. It is noteworthy that distinct FPR2/ALX domains are required for signalling by different agonists [58]. Moreover, it has been shown that proresolving mediators such as resolvins and LXA4 induce further antiinflammatory molecules *in vivo*, such as interleukin- (IL-) 10 [59]. Taken together, these data suggest that a proresolving cascade may be operating during resolution with FPR2/ALX playing a central role in this process.

Chapter 7 – Aim

CMD describe a spectrum of interconnected pathological alterations in organs involved in metabolic and cardiovascular functions. Despite the recent publication of several papers suggesting clinical and social interventions to prevent CMD, the identification of the common mechanisms of these diseases are far from clear. Most recent evidences suggest a substantial role of a low-grade chronic inflammatory response, known as metaflammation, in fomenting CMD. So far selective inflammatory pathways have been proven to be involved in metaflammation, including the well-known NF-kB pathway and more innovative cascades such as NLRP3 inflammasome and the JAK/STAT cascades, but their effective contribution in these clinical contexts and the consequences of their pharmacological modulation are still under investigation.

The general aim of the project was to study the effects of the pharmacological targeting of selective inflammatory pathways involved in metabolic diseases and cardiovascular disorders and to identify the cross-talk mechanisms suitable for pharmacological modulation that link these comorbidities.

The specific objectives were:

1) to study the impact of different diet components in the pathophysiological mechanism(s) involved in the development of metabolic derangements

2) to study the effects of the pharmacological modulation of selective pro- and anti inflammatory pathways of metaflammation in experimental models of cardiometabolic diseases.

3) Targeting metaflammation as new pharmacological strategy for cardio-metabolic diseases

The experiments here reported were conducted in the laboratory of cardiometabolic pharmacology at the Department of Drug Science and Technology of the University of Turin, under the supervision of Professor Massimo Collino. During my three-year PhD programme I spent six months of lab training: three months at the University of Oviedo (Institute of Oncology “Principado de Asturias”, Oviedo, Spain), under the supervision of Professor Rosa Maria Saiz Menendez and three months at the National University of Ireland (Advanced Glycoscience Research Cluster, NCBES Biomedical Science, Galway, Ireland), under the supervision of Professor Lokesh Joshi.

Chapter 8 – Animal models and experimental procedures

8.1. Diet-induced metabolic derangements

For all the models we used male C57BL/6 mice of 6 weeks of age housed in a controlled environment at 25±2 °C with a 12 h light/dark cycle. All groups received drink and food *ad libitum*. All along the experimental protocol, body weight, glycaemia and food intake were strictly monitored recording weekly. Mice were cared in compliance with the European Council directives on the protection of animals used for scientific purposes and with the Principles of Laboratory Animal Care. The scientific projects were approved by the Ethical Committee of the Turin University and by the Italian Ministry of Health.

- Mastrocola R, Ferrocino I, Liberto E, Chiazza F, Cento AS, Collotta D, QuerioG, Nigro D, Bitonto V, Cutrin JC, Rantsiou, Durante M, Masini E, Aragno M, Cordero C, Cocolin L, Collino M. **Fructose liquid and solid formulations differently affect gut integrity, microbiota composition and related liver toxicity: a comparative in vivo study**. Journal of Nutritional Biochemistry 55 (2018) 185–199

12 weeks of dietary manipulation		
(ND group n=10)	**(Fr-L group n=10)**	**(Fr-S group n=10)**
Normocaloric diet +water	Normocaloric diet and drinking a 60% fructose (w/vol) syrup solution	Solid diet providing the 60% of calories from fructose and drinking tap water

Normocaloric diet composition was 62.1% of calories in carbohydrates (36.2% from corn starch, 14.9% from dextrin and 11% from sucrose), 5.1% of calories in fat, 5% of calories in fibers and 17.6% of calories from proteins. L-Fr syrup was prepared dissolving 60% of fructose in water with 3.5% citric acid as preservative. S-Fr diet composition was 70% of calories in carbohydrates (8.9% from corn starch, 1% from sugar and 60% from fructose), 10% of calories in fat and 20% of calories from proteins. The ND and Fr-S diets provided the same amount of calories (3.85 kcal/g). Mice of both S-Fr and L-Fr groups were fed with the same amount of daily fructose intake.

- D. Collotta, L. Lucarini, F. Chiazza, A. S. Cento, M. Durante, S. Sgambellone, J. Chini, F. Baratta, M. Aragno, R. Mastrocola, E. Masini and M. Collino **Reduced Susceptibility to Sugar-Induced Metabolic Derangements and Impairments of Myocardial Redox Signaling in Mice Chronically Fed with D-Tagatose when Compared to Fructos.** Hindawi Oxidative Medicine and Cellular Longevity Volume2018, Article ID5042428,11pages

24 weeks of dietary manipulation				
(ND group n=6)	**(Fr-L group n=6)**	**(Fr-S group n=6)**	**(Tg-L group n=6)**	**(Tg-S group n=6)**
Normocaloric diet + water	Normocaloric diet and drinking a 30% fructose syrup	30% fructose solid diet and drinking water	Normocaloric diet and drinking a 30% D-tagatose syrup	30% D-tagatose solid diet and drinking water

- Mastrocola R, Collotta D, Gaudioso G, Le Berre M, Cento AS, Ferreira Alves G, Chiazza F, Verta R, Bertocchi I, Manig F, Hellwig M, Fava F, Cifani C, Aragno M, Henle T, Joshi L, Tuohy K, Collino M. **Effects of Exogenous Dietary Advanced Glycation End Products on the Cross-Talk Mechanisms Linking Microbiota to Metabolic Inflammation**. Nutrients. 2020 Aug 19;12(9):E2497.

22 weeks of dietary manipulation	
(ND group n=15)	**(AGE-D group n=15)**
Normocaloric diet	AGE-enriched Diet

AGE-D was prepared replacing casein in the ND (200 g/kg of diet) by an equal amount of modified casein where 10% of arginine was glycated with MGO (methylglyoxal 5) in order to obtain a total of 4 µmol of MG-H1 per g of diet. The diet was prepared thanks to the collaboration of the Thomas Henle's Lab in the University of Dresden, Germany.

- F. Chiazza, A. S. Cento, D. Collotta, D. Nigro, G. Rosa, F. Baratta, V. Bitonto, J. C. Cutrin, M. Aragno, R. Mastrocola and M. Collino **Protective Effects of Pyridoxamine Supplementation in the Early Stages of Diet-Induced Kidney Dysfunction** Hindawi BioMed Research International Volume 2017, Article ID 2682861, 12 pages

12 weeks of dietary manipulation			
(ND group n=15)	**(ND + P group n=5)**	**(HFHF group n=20)**	**(HFHF + P group n= 10)**
Normocaloric diet	Normocaloric diet + Pyridoxamine (1 g/L, the equivalent of about 150mg/kg/day)	High-fat high fructose diet	High-fat high fructose diet + Pyridoxamine (1 g/L, the equivalent of about 150mg/kg/day)

- D.Collotta, W.Hull R.Mastrocola, F.Chiazza, A.S.Cento, C.Murphy, R.Verta, G.F.Alves, G.Gaudioso, F.Fava, M.Aragno, K.Tuohy, C.Thiemermann M.Collino **Baricitinib counteracts metaflammation thus protecting against diet-induced metabolic abnormalities in mice**

22 weeks of dietary manipulation		
(ND group n=15)	**(HFHF group n=15)**	**(HFHF + Bar group n=15)**
Normocaloric diet	High fat high sugar diet	High fat diet for 22 weeks and treated with baricitinib (10 mg/kg die, p.o.) for the last 16 weeks

- G. S.D. Purvis, M. Collino, R.A. Loiola, A. Baragetti, F. Chiazza, M. Brovelli, M. H. Sheikh, D. Collotta, A. Cento, R. Mastrocola, M. Aragno, J. C. Cutrin, C. Reutelingsperger, L. Grigore, A. L. Catapano, M. M. Yaqoob, G. Danilo Norata, E. Solito and Christoph Thiemermann **Identification of AnnexinA1 as an Endogenous Regulator of RhoA and Its Role in the Pathophysiology and Experimental Therapy of Type-2 Diabetes** Front. Immunol., 27 March 2019

10 weeks of dietary manipulation			
Wild type or ANXA1 -/-	**Wild type or ANXA1 -/-**	**Wild type or ANXA1 -/-**	**Wild type or ANXA1 -/-**
Normocaloric diet	High fat high sugar diet	Normocaloric diet + vehicle (Hepes 50Mm,NaCl 40Mm i.p.) or hrANXA1 (40ug/kg i.p.) treated for the last 6 weeks	High fat diet diet + vehicle (Hepes 50Mm,NaCl 40Mm i.p.) or hrANXA1 (40ug/kg i.p.) treated for the last 6 weeks

8.2. Cecal ligation and puncture (CLP) in Mice with Pre –existing Type 2 Diabetes

The animal protocols followed in this study were approved by the local Animal Use and Care Committee in accordance with the derivatives of both, the Home Office Guidance in the Operation of Animals (Scientific Procedure Act 1986) published by Her Majesty's Stationary Office, the Guide for the Care and Use of Laboratory Animals of the National Research Council (home office project license, PPL: 70/8350) and by the local ethical committee (DGSAF 0021573-P-12/11/2013) and are in keeping with the European Directive 2010/63/EU as well as the 2011 Guide for the Care and Use of Laboratory Animals.

This study was conducted on 56 male C57BL/6 mice aged 10 weeks (Charles River, Kent, UK) weighing 25–30 g, receiving a standard diet and water *ad libitum* (before starting the experiments). Mice were housed 5 per cage in a temperature controlled room with a 12-h light/dark cycle. High Fat Diet Model of Type 2 Diabetes Mellitus in this model of diet-induced obesity and insulin resistance, mice (Charles River UK, Kent) were randomized to receive normocaloric diet or high fat diet with free access to water for 12 weeks. Body weight, food intake and calories intake were measured weekly through the experiment to monitor feeding behavior. At 12 weeks after starting the HFD, mice fed either chow or HFD were randomized to undergo either sham operation or Cecal ligation and puncture (CLP) surgery. Before surgery, mice were anaesthetised using (1.5 ml/kg, i.p.) of 2:1 ketamine (100 mg/ml): xylazine (20 mg/ml) solution. To obtain adequate analgesia, buprenorphine (0.05 mg/kg, i.p.) was administered just before starting the surgery. The fur of the abdomen was removed using Veet® hair removing cream and the area cleaned with 70% ethanol. A 1.5 cm midline incision of the abdomen was made and the caecum was exposed. The caecum then was ligated below the ileocecal valve and two punctures were made one at each end using an 18-G needle. A small amount of faecal matter was then squeezed from both punctures before the caecum was returned to its anatomical position and the cut in the abdomen was then sutured. Each mouse then received a resuscitation fluid (1 ml 0.9 % NaCl, s.c.). Mice were left on a homeothermic blanket to recover then placed back into fresh clean cages. At 1 h after CLP surgery, mice from the HFD group were randomised to receive linagliptin (10 mg/kg, i.v), IKK-16 (1 mg/kg i.v.) or vehicle (2% DMSO; 3ml/kg, i.v.). At 6 and 18 h after surgery, antibiotic (imipenem/cilastatin, 20 mg/kg) dissolved in resuscitation fluid (15 ml/kg 0.9% NaCl, s.c.) was administered along with analgesia (buprenorphine, 0.05 mg/kg, i.p.). At 24 h, mice were anaesthetised for assessment of cardiac function *in vivo*. As a terminal procedure, mice were anaesthetised using high dose isoflurane (3 % delivered in 0.9 L/min O2) before being sacrificed. Blood samples were collected by cardiac puncture and vital organs were collected and snap frozen using liquid nitrogen then stored for further analysis at -80°C freezer. Mice underwent sham surgery were not subjected to perforation of the cecum, but otherwise treated the same.

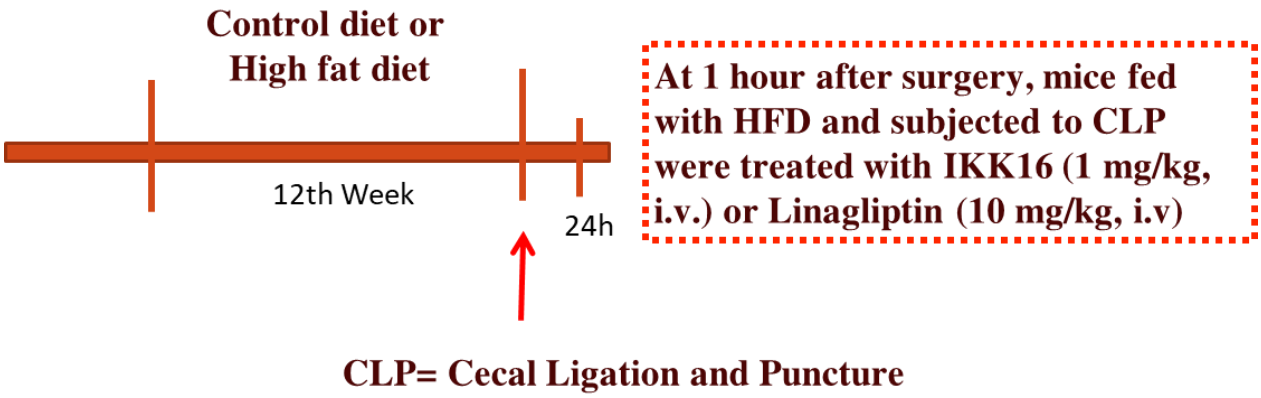

Figure 8.1 Scheme of the performed surgery protocol

- Al Zoubi S, Chen J, Murphy C, Martin L, Chiazza F, Collotta D, Yaqoob MM, Collino M, Thiemermann C. **Linagliptin Attenuates the Cardiac Dysfunction Associated with Experimental Sepsis in Mice with Pre –existing Type 2 Diabetes by Inhibiting NF-κB** *Front Immunol. 2018 Dec 18;9:2996.*

12 weeks of dietary manipulation					
ND n=8 Normocaloric diet	**HFD n=8** High fat diet	**ND + CLP n=10** Normocaloric diet + Cecal ligation and puncture	**HFD + CLP n=10** High fat diet + Cecal ligation and puncture + vehicle (2% DMSO; 3ml/kg, i.v.)	**HFD+ CLP +IKK16 n=10** High fat diet + Cecal ligation and puncture + IKK-16 (1 mg/kg i.v.)	**HFD+ CLP + LINA n=10** High fat diet + Cecal ligation and puncture + linagliptin (10 mg/kg, i.v)

Chapter 9 – Methods and materials

9.1. Analysis in vivo

9.1.1. Oral glucose tolerance test (OGTT)

Oral glucose tolerance test (OGTT) is performed after an overnight fasting period by administering glucose (2 g/kg) by oral gavage. Once before administration and 15, 30, 60, 120 min afterward, blood obtained from the saphenous vein and glucose concentration is measured with a conventional glucometer (GlucoMen LX kit, Menarini Diagnostics, Italy).

9.1.2. Insulin tolerance test (ITT)

Mice were fasted for 4 h with free access to water. At the end of the 4 h fasting, the body weight and fasting blood glucose were measured using tail vein blood. Mice then received a dose of insulin aspart (NovoRapid) (0.75 U/kg, i.p.). Blood glucose level was then measured at 15, 30, 45, 60, 90, and 120min post insulin administration using blood glucose meter Accu-Chek (Accu-Chek Compact System; Roche Diagnostics, Basel, Switzerland).

9.1.3. Assessment of Baseline Kidney Function

The evaluation of renal dysfunction in animals is developed by measuring levels of creatinine and urea in plasma and urine.

Firstly, the mice are anesthetized using isoflurane (3 L/min) and oxygen (1 L/min) before being sacrificed. Then the thoracic cage is opened with scissors and through cardiac puncture, approximately 0.7 mL of blood is collected with a G25 needle andnon-heparinized syringes. The blood must be immediately decanted into 1.3 ml plasma gel tubes (Sarstedt, Nürnbrecht, Germany) (it is very important that the samples are keep on ice).

The blood samples should be centrifuged for 3 minutes at 9,000 RPM to separate the plasma, and then about 100 µL of plasma are pipetted into an aliquot and snap frozen in liquid nitrogen to be stored at −80ºC for further analysis.

Through colorimetric assays, the quantification of urea and creatinine in biological fluids can be determined to identify kidney damage.

Usually during the last week of the experiment, mice were housed in the metabolic cages to collect urine. They were housed (one mouse per cage) for 24 h with free access to water. Urine creatinine, urin albumin and serum creatinine were assessed or blindly by IDEXX the commercial veterinary testing laboratory (IDEXX Ltd; West Sussex, UK) or using ELISA kit following manufacturer instructions.

Then creatinine clearance (CrCl) and urine albumin to creatinine ratio (ACR) were calculated using the following equations:

$$\mathrm{CrCl} = \frac{\mathrm{Urine\ \ Creatinine}}{\mathrm{Serum\ \ Creatinine}} \times \frac{\mathrm{Urine\ \ Volume}}{\mathrm{Time}}$$

Equation 1: Creatinine clearance (ml/min) is calculated using four measurements (a) urine creatinine (µmol/L), (b) serum creatinine (µmol/L), (c) urine volume (ml), and (d) time (minutes).

$$\mathrm{ACR} = \frac{\mathrm{Urine\ \ Albumin}}{\mathrm{Urine\ \ Creatinine}}$$

Equation 2: Urine albumin to creatinine ratio is calculated using 2 (a) urine albumin (µg/L) and (b) urine creatinine (mg/L).

9.1.4. Creatinine in urine

The concentration of plasma creatinine is assessed by using commercial kits (Arbor Assays, Ann Arbor, MI, USA). Creatinine (2-amino-1-methyl-5H-imidazol-4-one) is a metabolite of phosphocreatine (p-creatine), a molecule used as a store for high-energy phosphate that can be utilized by tissues for the production of ATP. Creatine either comes from the diet or synthesized from the amino acids arginine, glycine, and methionine. This occurs in the kidneys and liver, although other organ systems may be involved and species-specific differences may exist. Creatine and p-creatine are converted non-enzymatically to the metabolite creatinine, which diffuses into the blood and is excreted by the kidneys. In vivo, this conversion appears to be irreversible and in vitro it is favored by higher temperatures and lower pH. Creatinine forms spontaneously from p-creatine. Under normal conditions, its formation occurs at a rate that is relatively constant and as intra-individual variation is < 15% from day to day, creatinine is a useful tool for normalizing the levels of other molecules found in urine. Additionally, altered creatinine levels may be associated with other conditions that result in decreased renal blood flow such as diabetes and cardiovascular disease. The DetectX® Urinary Creatinine Kit is designed to quantitatively measure creatinine present in urine samples. Please read the complete kit insert before performing this assay. A creatinine standard, calibrated to a NIST creatinine standard, is provided to generate a standard curve for the assay and all samples should be read off the standard curve. Standards or diluted samples are pipetted into a clear microplate plate. The color generating reaction is initiated with the DetectX® Creatinine Reagent, which is pipetted into each well. After a short incubation the intensity of the generated color is detected in a microplate plate reader capable of measuring 490nm wavelength. The concentration of the creatine in the sample is calculated, after making a

suitable correction for the dilution of the sample, using software available with most plate readers. The Jaffe reaction used in this kit has been modified to read creatinine levels in urine.

9.1.5. Creatinine in serum

The DetectX® Serum Creatinine Kits are designed to quantitatively measure creatinine present in serum samples. Please read the complete kit insert before performing this assay. A creatinine standard, calibrated to a NIST creatinine standard, is provided to generate a standard curve for the assay and all samples should be read off the standard curve. Standards or samples are pipetted into a clear microplate plate. An assay diluent is added to all standards, controls and samples. The color generating reaction is initiated with the DetectX® Creatinine Reagent, which is pipetted into each well. The assay utilizes a kinetic absorbance method to overcome interference by colored compounds in serum. The absorbance of the colored product is read after 1 minute in a microplate plate reader capable of measuring 490nm wavelength. At 30 minutes the optical density is read again. The concentration of creatinine is calculated using the delta of the optical density readings at 30 and 1 minute compared to the curve generated from the standards, or by using the Excel worksheet available for free download at our web site. The Jaffe reaction used in this kit has been modified to read creatinine levels in serum.

9.1.6. Albumin in urine

Urine albumin was measured using a mouse albumin ELISA kit following manufacturer instructions (Cambridge Bioscience, Cambridge, UK). The RayBio® Human Albumin ELISA kit is an in vitro enzyme-linked immunosorbent assay for the quantitative measurement of human Albumin in serum, plasma, and cell culture supernatants. This assay employs an antibody specific for human Albumin coated on a 96- well plate. Standards and samples are pipetted into the wells and Albumin present in a sample is bound to the wells by the immobilized antibody. The wells are washed and biotinylated anti-human Albumin antibody is added. After washing away unbound biotinylated antibody, HRP-conjugated streptavidin is pipetted to the wells. The wells are again washed, a TMB substrate solution is added to the wells and color develops in proportion to the amount of Albumin bound. The Stop Solution changes the color from blue to yellow, and the intensity of the color is measured at 450 nm.

9.1.7. Proteinuria assay

UP ELISA kit applies the quantitative sandwich enzyme immunoassay technique. The microplate plate has been pre-coated with a monoclonal antibody specific for UP. Standards or samples are then added to the microplate plate wells and UP if present, will bind to the antibody pre-coated wells. In order to quantitatively determine the amount of UP present in the sample, a standardized preparation of horseradish peroxidase (HRP)-conjugated polyclonal antibody, specific for UP are added to each well to “sandwich” the UP immobilized on the plate. The microplate plate undergoes incubation, and then the wells are thoroughly washed to remove all unbound components. Next, substrate solutions are added to each well.

The enzyme (HRP) and substrate are allowed to react over a short incubation period. Only those wells that contain UP and enzyme-conjugated antibody will exhibit a change in color. The enzyme-substrate reaction is terminated by addition of a sulphuric acid solution and the color change is measured spectrophotometrically at a wavelength of 450 nm. A standard curve is plotted relating the intensity of the color (O.D.) to the concentration of standards. The UP concentration in each sample is interpolated from this standard curve.

9.2. Histological analysis

9.2.1. Hematoxylin/eosin (H&E) staining and histology score on tissue sections

Liver and ileum mucosa morphology was evaluated by standard H&E staining on dewaxed 5-µm sections. The NAFLD activity score (NAS) evaluating the grade of steatosis, the number of inflammatory foci, the presence of ballooning and the fibrosis staging has been performed as described by Kleiner et al. [62] paralleled by the histology activity index of damage, a semiquantitative necroinflammatory grading based in the Knodell score system which evaluates the degree of periportal interface hepatitis, focal lytic necrosis, apoptosis and focal inflammation. Histologic scores have been performed on 10 fields at 200× magnification per liver section by a blinded pathologist.

9.2.2. Periodic-acid Schiff stain

Histology was carried out on formalin-fixed-paraffin-embedded (FFPE) samples that were subsequently stained with periodic-acid Schiff stain (PAS) before being visualized using a Nanozoomer digital pathology scanner (Hamamatsu Photonics K.K., Japan). These samples were then analyzed using the Nanozoomer NDP viewer software (Hamamatsu Photonics K.K., Japan). Two cross-sectional measurements (at 90° to one another) were taken for 10 renal corpuscles and glomeruli and averaged before an area for each was established using the formula $A=\pi r2$.

9.2.3. Oil Red O staining

Liver lipid accumulation was evaluated by Oil Red O staining on 7-µm ileum cryostatic sections. Stained tissues were viewed under an Olympus Bx4I microscope (×10 magnification) with an AxioCamMR5 photographic attachment (Zeiss, Gottingen, Germany).

Lipid droplets are found in all eukaryotic organisms. They function as reservoirs of neutral lipids, primarily triacylglycerol and cholesterol esters. The stored lipids can be used for energy, steroid synthesis, or membrane formation. Lipid droplet accumulation is a normal function in cells. Adipocytes consist predominantly of lipid droplets. However excessive lipid droplet accumulation within cells can be an indicator of metabolic deficiency or pathogenesis. For

example, excessive accumulation of lipids in liver cells (steatosis) can lead to cellular dysfunction. The ORO method is able to detect and analyze neutral lipids based on the lysochrome ORO (C26H24N4O). ORO is a fat-soluble diazol dye, with a maximum absorption at 518 nm, which stains neutral lipids and cholesteryl esters but not biological membranes. The principle for staining is that ORO is minimally soluble in the solvent, and the solubility is further decreased by dilution of ORO in water before use. The hydrophobic dye will therefore move from the solvent to associate with the lipids within tissue sections.

9.2.4. Sirius Red Analysis

Slices were deparaffinized in xylol, rehydrated in a graded ethanol series, and incubated with a saturated aqueous solution of picric acid containing Sirius Red (1mg/ml) for 1 h. After washing twice in acidified water (containing 0.2% glacial acetic acid), slices were dehydrated in 100% ethanol and cleared with xylol for microscope evaluation.

Collagen is the principal load-bearing polymer in all connective tissues ranging from skin to bone. Collagen networks strongly stiffen when a mechanical force is applied, thus preventing

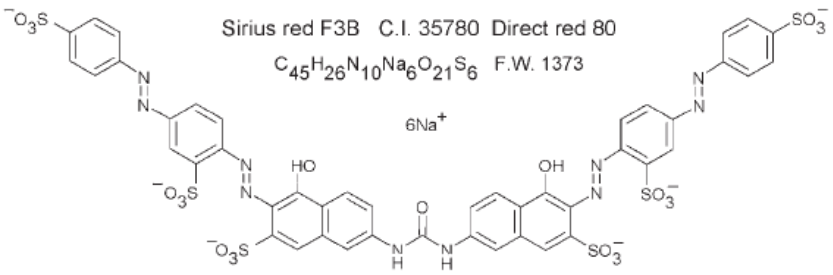

Figure 9.1 Stuctural formula of sirius red F3B.

Modified from Dapson et al. *Biotechnic & Histochemistry;* 2011

excessive deformation of the tissue. There are 16 types of collagen, of which the type I, II, and III nearly comprise the 80% of the collagen in the body that are packed together to form long thin fibrils. Collagen type IV forms a two-dimensional reticulum; while several other collagen types are associated with fibril-type collagen, linking them to each other or to other matrix components. These collagens along with the other components of the extracellular matrix (ECM) undergo constant remodeling to provide required biochemical properties like tensile strength and elasticity. In tissues, the basement membrane is rich in collagen, in addition it is found in the stroma and lining the connective tissues. Physical, mechanical or chemical damage of a tissue or organ would lead to disruption of collagen deposition, and organization. Hence, assessing the patterns of collagen distribution would provide us an idea about the tensile strength of the tissue/organs. Any alterations from normal patterns of collagen distribution would imply tissue damage. Sirius red is a histology stain used to mark total collagen as well as differentiate between varying collagen types for evaluation of collagen distribution in tissues. The sulphonic acid group of Sirius red reacts with basic amino groups of lysine and hydroxylysine and guanidine group of arginine (present in the collagen molecule). Thereby, being an anionic dye, it attaches to all the varying types of collagen isoforms. In bright field, collagen appears as bundles of pink to red fibers which get disturbed in pathological conditions. The same larger collagen fibers under polarized light appear bright yellow to orange and the thinner ones, including reticular fibers, look green. This birefringence or

double refraction, whereby incident light is split by polarization into two different paths, is highly specific for collagen. The amount of polarized light absorbed by the Sirius red dye stringently depends on the orientation of the collagen bundles enabling to differentiate different collagen types. This method is very simple, quick, economic and reliable in comparison with other commonly used staining methods for collagen.

9.2.5. Immunohistochemistry Analysis

RAGE was analyzed by immunohistochemistry on 4m formalin-fixed, paraffin embedded kidney. Slices were deparaffinized in xylol, rehy drated in a graded ethanol series, and subjected to retrieval (20 minutes, 100°C, in tris-EDTA buffer solution, pH 9). Endogenous peroxidase activity was blocked using 0.6%hydrogen peroxide. After blocking, sections were incubated overnight with primary antibody (goat anti-RAGE, 1:100, Chemicon International) and subsequently for 1 h with HRP-conjugated anti-goat secondary antibody. Immunohistochemica staining was performed using the Detection System Peroxidase/DAB. Nuclei were counterstained with hematoxylin.

9.3. Analysis ex vivo

9.3.1. Quantitative determination of Triglycerides

Triglycerides in plasma are measured according to Trinder reaction. Glycerol, released by triglycerides after hydrolysis with lipoprotein-lipase (LPL) is transformed by glycerol-kinase (GK) into glycerol-3-phosphate which is oxidized by glycerol-phosphate-oxidase (GPO) into de-hydroxyacetone phosphate, with formation of hydrogen peroxide. In presence of peroxidase (POD), hydrogen peroxide reacts with ethyl-sulphopropyl-toluidine (ESPT) and 4-aminophenazone to form a colored complex, whose color intensity is directly proportional to triglycerides concentration in the sample.

9.3.2. Skeletal muscle TGs level

TGs were extracted from total tissue homogenates of skeletal muscle and assayed using reagent kits according to the manufacturer’s instructions (Triglyceride Quantification Kit, Abnova Corporation, Aachen, Germany).

9.3.3. Quantitative determination of Total cholesterol

Total cholesterol in plasma is measured according to Trinder reaction. Esterified cholesterol is hydrolyzed into free cholesterol and fatty acid by cholesterol esterase (COE). Cholesterol oxidase (COD) oxidizes the free cholesterol into cholestene-3-one with formation of hydrogen peroxide. In presence of peroxidase (POD), hydrogen peroxide reacts with hydroxybenzoate

and 4-aminoantipyrine, to produce a colored complex whose color intensity is directly proportional to the total cholesterol concentration in the sample.

9.3.4. Quantitative determination of HDL cholesterol

The kit for quantitative determination of HDL Cholesterol in plasma is made up in two steps: in the first phase the HDL-cholesterol present in the sample is masked by a specific detergent, to make enzymes present in the first reagent eliminate only the non-HDL-cholesterol. In the second step cholesterol esterase (COE) liberates HDL-cholesterol and hydrolyzes it into free cholesterol and fat acids.

Cholesterol oxidase (COD) oxidizes free cholesterol into cholestene-3-one with formation of hydrogen peroxide. In the presence of peroxidase (POD), hydrogen peroxide reacts with disulphobutyl-mtoluidine (DSBmT) and 4-aminophenazone, to produce a colored complex whose color intensity is directly proportional to the concentration of HDL-cholesterol in the sample.

9.3.5. Quantitative determination of LDL cholesterol

This method directly defines the LDL cholesterol by some particular surface acting agents, which eliminate the cholesterol portions in chilomicrons, VLDL fraction and 2 step HDL reaction. In the first step, cholesterol in VLDL, HDL and chilomicron fractions is eliminated in particular conditions by a specific oxidation reaction (cholesterol esterase, cholesterole oxidase) and catalase of correspondent oxygenated water formed. In the second step the remaining LDL-C, in presence of particular surface-acting agents is transformed into a colored quinonic derivate (cholesterol esterase, cholesterol oxidase, peroxidase) which color intensity is proportional to the LDL-C quantity present in the sample.

9.3.6. Measuring Fasting Plasma Insulin

Mice were fasted for 6 h with free access to water. At the end of the 6 h fasting period, blood samples were collected from the tail vein. Fasting plasma insulin levels were then measured using Abcam's human insulin ELISA (Enzyme-Linked Immunosorbent Assay) kit that is an *in vitro* enzyme-linked immunosorbent assay for the quantitative measurement of Human Insulin and Proinsulin in serum, plasma, cell culture supernatants.

This assay employs an antibody specific for Human Insulin coated on a 96-well plate. Standards and samples are pipetted into the wells and Insulin present in a sample is bound to the wells by the immobilized antibody. The wells are washed and biotinylated anti-Human Insulin antibody is added. After washing away unbound biotinylated antibody, HRP-conjugated Streptavidin is pipetted to the wells. The wells are again washed, a TMB substrate solution is added to the wells and color develops in proportion to the amount of Insulin bound. The Stop Solution changes the color from blue to yellow, and the intensity of the color is measured at 450 nm.

9.3.7. Measuring Myeloperoxidase (MPO) Activity

MPO was extracted from the tissues according to the methods described by Barone et al. (Barone FC, Hillegass LM, Price WJ, White RF, Lee EV, Feuerstein GZ, et al. Polymorphonuclear leukocyte infiltration into cerebral focal ischemic tissue: myeloperoxidase activity assay and histologic verification. J Neurosci Res Cell Sci. (1991) 29:336–45.) with slight modifications to measure neutrophil accumulation in the tissue examineted. For samples preparation, a piece of lung was diluted (1:20wt/vol) with 5mM potassium phosphate buffer to homogenize the sample using a POTTER-ELVENHIEM homogenizer. For measurements of MPO activity, the homogenate was centrifuged (at 13000g, 30min, 4°C). The resulted supernatant was discarded and the pellet was extracted: a 5-time dilution with 0.5% hexadecyl-trimethyl-ammonium bromide (Sigma) in 50mM potassium phosphate buffer was used to suspend and homogenize the pellet (pH 6,0 25°C). The resulted solution was then frozen and thawed three times followed by 10 s sonication at room temperature. After the last sonication, the samples were incubated at 4°C for 20 minutes and centrifuged at 12500g (15 min,4°C). MPO activity was measured in the supernatant by mixing 100 µl of the supernatant with 0.167 mg/ml o-dianiside dihydrochloride and 0.0005% hydrogen peroxide in 2.9ml 50mM potassium phosphate buffer. UV visible spectrophotometer was used to measure the change in absorbance at 460 nm for 90 min. MPO activity was presented as the quantity of the enzyme degraded 1 µmol of peroxide/min at 25°C and expressed as µU/gram of the wet tissue.

9.3.8. Measuring N-acetyl-b-D-glucosaminidase (NAG) Activity

NAG activity was analyzed to measure macrophage accumulation in the tissue examineted. For samples preparation, a piece of lung was diluted with 0.01M phosphate buffer saline and homogenized at 4°C. The resulted solutions were then frozen and thawed three times followed by 10 seconds sonication at room temperature to break the cells. For measurements of NAG activity, the homogenate was centrifuged (at 5,000 RPM, 30 minutes, 4°C). The resulted supernatants were then used to measure NAG activity using a NAGase ELISA kit following manufacturer instructions (Elabscience, Houston, Texas, USA). The micro ELISA plate provided in the kit has been pre-coated with an antibody specific to Human NAGase. Standards or samples are added to the micro ELISA plate wells and combined with the specific antibody. Then a biotinylated detection antibody specific for Human NAGase and Avidin-Horseradish Peroxidase (HRP) conjugate are added successively to each micro plate well and incubated. Free components are washed away. The substrate solution is added to each well. Only those wells that contain Human NAGase, biotinylated detection antibody and Avidin-HRP conjugate will appear blue in color. The enzyme-substrate reaction is terminated by the addition of stop solution and the color turns yellow. The optical density (OD) is measured spectrophotometrically at a wavelength of 450 nm ± 2 nm. The OD value is proportional to the concentration of Human NAGase. You can calculate the concentration of Human NAGase in the samples by comparing the OD of the samples to the standard curve.

9.3.9. Bioplex Pro Assay

The Bio-plex system is a flexible, easy to use microplate based multiplex immunoassay system. It capable of quantifing up to 100 different analytes in a sigle well of a 96 well plate in 3-4

hours. Bio plex assays are designed using microscopic beads, each with a different color code (spectral address) to permit discrimination of individual ratios of two fluoropheres and are thus classified into 100 unique bead regions (xMAP technology).

Coupled beads: a bio plex assay uses a selection of beads with different spectral addresses, each coupled to antibodies against a different target

Samples: samples types ranging from serum, urine, milk and plasma to cell lysates can be used

Detection antibodies: biotin-labeled detection antibodies are specific for secondary epitopes on each target.

Reporter: fluorescently labeled streptavidin reporter binds to the biotin-laveled detection antibodies

Assay: the bio plex reader first classifies beads by spectral addresses and then quantifies the associated reporter signal intensity

Bio-plex immunoassay workflow

- Add coupled beads to wells of a 96-well plate (50 µl 1 x beads to wells)
- Wash 2 x 100 µl
- Add 50 µl of standard, blank, samples
- Incubate at RT shaking 30 minutes
- Wash 3 x 100 µl
- Add 25 µl 1x detection antibodies to wells
- Incubate 30 minutes at RT
- Wash 3 x 100 µl
- Add reporter to wells (50 µl 1x streptavidin-PE)
- Incubate 10 minutes at RT
- Wash 3 x 100 µl
- Resuspend in 125 µl assay buffer and shake
- Read the plate

Note:

- Dyed beads are identified by their internal fluorescent signature (bead region)
- Level of target bound to beads is indicated by intensity of reporter signal
- Multiplex data are reported simultaneously

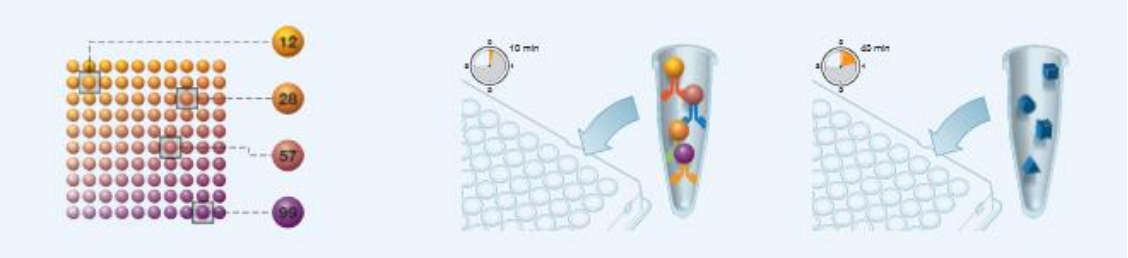

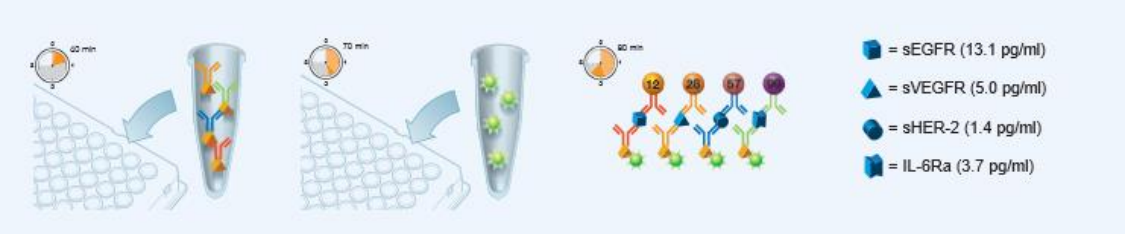

Figure 9.2 Bioplex immunoassay scheme

Source: www.bio-rad.com

Assay Format

Bio-Plex Pro™ assays are essentially immunoassays formatted on magnetic beads. The assay principle is similar to that of a sandwich ELISA. Capture antibodies directed against the desired biomarker are covalently coupled to the beads. Coupled beads react with the sample containing the biomarker of interest. After a series of washes to remove unbound protein, a biotinylated detection antibody is added to create a sandwich complex. The final detection complex is formed with the addition of streptavidin-phycoerythrin (SA-PE) conjugate. Phycoerythrin serves as a fluorescent indicator or reporter.

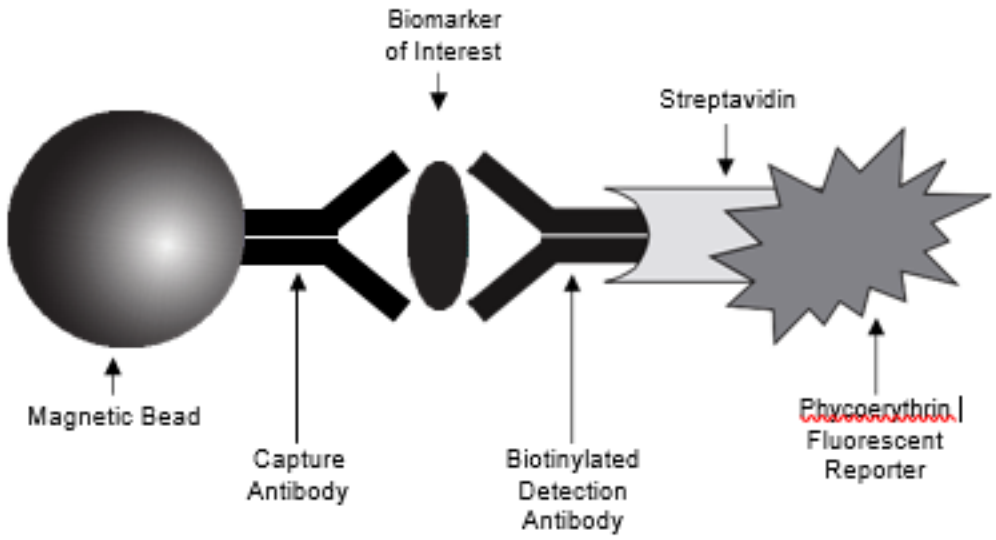

Figure 9.3 Bio-Plex sandwich immunoassay

Data Acquisition and Analysis

Data from the reactions are acquired using a Bio-Plex system or similar Luminex-based reader. When a multiplex assay suspension is drawn into the Bio-Plex 200 reader, for example, a red (635 nm) laser illuminates the fluorescent dyes within each bead to provide bead classification and thus assay identification. At the same time, a green (532 nm) laser excites PE to generate a reporter signal, which is detected by a photomultiplier tube (PMT). A high-speed digital processor manages data output, and Bio-Plex Manager™ software presents data as median

fluorescence intensity (MFI) as well as concentration (pg/ml). The concentration of analyte bound to each bead is proportional to the MFI of reporter signal. Using Bio-Plex Data Pro™ software, data from multiple instrument runs can be combined into a single project for easy data management, quick visualization of results, and simple statistical analysis.

Component	1 x 96-Well Format	10 x 96-Well Format
Standard diluent	10 ml	100 ml
Sample diluent	40 ml	80 ml
Assay buffer	50 ml	500 ml
Wash buffer	200 ml	1.5 L
Detection antibody diluent	5 ml	50 ml
Streptavidin-PE (100x)	1 tube	1 tube
Filter plate and/or flat bottom plate (96-well)	1 plate	10 plates
Sealing tape	1 pack of 4	10 packs of 4
Assay Quick Guide	1 booklet	1 booklet
Standard	1 vial	10 vials
Human and Mouse Cytokine (Group I and II)		
Coupled magnetic beads (10x)	1 tube	1 tube
Detection antibodies (10x) Mouse Cytokine (Group III) and Rat Cytokine (Group I)	1 tube	1 tube
Coupled magnetic beads (20x)	1 tube	1 tube
Detection antibodies (20x)	1 tube	1 tube

Table 9.1 Kit Contents

Prepare Standards

It is essential to reconstitute and dilute standards exactly as described in this section. Incorrect preparation may lead to low signal, high background, or inconsistent measurements from plate to plate

Refer to Table 1 for recommended diluents based on different sample types.

As a general rule, reconstitute and dilute standards in a diluent similar to the final sample type or sample matrix.

Sample Type	Diluent for Standards	Add BSA
Serum and plasma	Standard diluent	None
Culture media, with serum	Culture media	None
Culture media, serum-free	Culture media	To 0.5% final
Lavage, sputum, other fluids	Bio-Plex® sample diluent	To 0.5% final*
Lysate	Bio-Plex sample diluent	To 0.5% final*

* At least 0.5% final w/v BSA is recommended to stabilize analytes and reduce absorption to labware.

Table 9.2 Summary of recommended diluents fro standards

Reconstitute a Single Vial of Standards

This procedure prepares enough material to run each dilution in duplicate.

1. Gently tap the vial containing the lyophilized standard.

2. Add 500 µl of the appropriate diluent. Do not use assay buffer to reconstitute the standards.

3. Gently vortex the reconstituted standard for 5 seconds then incubate on ice for 30 min.

Prepare Standard Dilution Series from a Single Antigen Vial

The following procedure produces an eight-point standard curve with a fourfold dilution between each point. Pipet carefully using calibrated pipets and use new pipet tips for every volume transfer.

1. Label nine 1.5 ml polypropylene tubes S1 through S8 and Blank.

2. Add the specified volume of standard diluent to each tube

3. Vortex the reconstituted standards gently for 5 seconds before removing any volume. Add 128 µl into the S1 tube containing 72 µl of standard diluent. Vortex at medium speed for 5 sec, then use a new pipet tip to transfer 50 µl from S1 tube to S2 tube. Vortex.

4. Continue with 1:4 (fourfold) serial dilutions from tube S2 to S8 as shown in Figure 9.6.

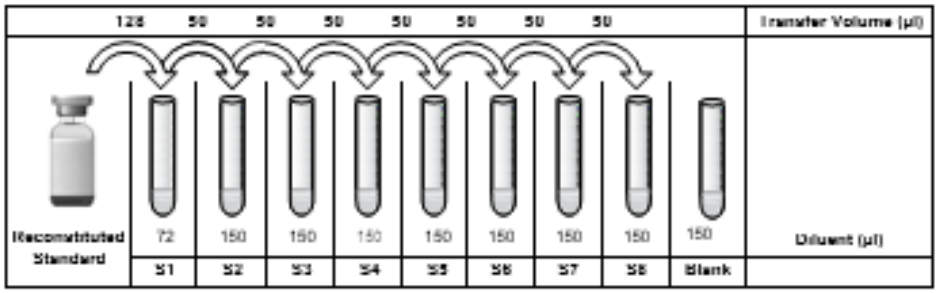

Figure 9.3 Preparing a fourfold dilution series of cytokine standards

Sample Preparation

Serum and Plasma

EDTA or citrate is preferred as an anticoagulant. Heparin-treated plasma, while compatible with Bio-Plex Pro™ assays, may absorb certain soluble proteins of interest.

1. Draw whole blood into collection tubes containing anticoagulant. Invert tubes several times to mix.

2. For serum, allow blood to clot at room temperature for 30 to 45 min. For plasma, proceed directly to the centrifugation steps.

3. Perform centrifugation at 1,000 x g for 15 min at 4°C and transfer the serum or plasma to a clean polypropylene tube.

4. To completely remove platelets and precipitates, centrifuge again at 10,000 x g for 10 min at 4°C.

5. Dilute samples fourfold (1:4) by adding 1 volume of sample to 3 volumes of Bio-Plex sample diluent (for example, 40 µl sample + 120 µl sample diluent).

Prepare Coupled Beads

1. Calculate the volume of coupled beads and assay buffer needed.

2. Add the required volume of Bio-Plex assay buffer to a 15 ml polypropylene tube.

3. Vortex the stock coupled beads at medium speed for 30 seconds. Carefully open the cap and pipet any liquid trapped in the cap back into the tube. This is important to ensure maximum bead recovery.

4. Dilute coupled beads to 1x by pipetting the required volume into the 15 ml tube. Vortex.

Each well of the assay plate requires either 2.5 µl (20x stock) or 5.0 µl (10x stock) adjusted to a final volume of 50 µl in assay buffer.

5. Protect the beads from light with aluminum foil. Equilibrate to room temperature prior to use.

Prepare and add detection antibodies

Instructions are provided for diluting the detection antibodies to a 1x concentration

Assay	Stock Concentration of Detection Antibodies
Human and mouse cytokines (groups I, II)	10x
Mouse cytokines (group III)	20x
Rat cytokines (group I)	20x
Human, mouse, and rat diabetes	20x

Table 9.3 Stock concentration of detection antibodies

1. While the samples are incubating calculate the volume of detection antibodies and detection antibody diluent needed. Detection antibodies should be prepared 10 min before use.

2. Add the required volume of Bio-Plex detection antibody diluent to a 15 ml polypropylene tube.

3. Vortex the stock detection antibodies for 15–20 sec at medium speed, then perform a 30 sec spin to collect the entire volume at the bottom of the tube.

4. Dilute detection antibodies to 1x by pipetting the required volume into the 15 ml tube.

Each well of the assay requires either 1.25 µl (20x stock) or 2.5 µl (10x stock) adjusted to a final volume of 25 µl in detection antibody diluent.

Prepare and Add Streptavidin-PE (SA-PE)

1. Calculate the volume of SA-PE (100x) and assay buffer needed. Streptavidin-PE should be prepared 10 min before use.

2. Add the required volume of assay buffer to a 15 ml polypropylene tube.

3. Vortex the 100x SA-PE for 5 sec at medium speed.

Perform a 30 seconds spin to collect the entire volume at the bottom of the tube.

4. Dilute SA-PE to 1x by pipetting the required volume into the 15 ml tube. Vortex and protect from light until ready to use.

Each well of the assay requires 0.5 µl (100x stock) adjusted to a final volume of 50 µl in assay buffer.

# of Wells	100x SA-PE, µl	Assay Buffer, µl	Total Volume, µl
96	60	5,940	6,000
48	30	2,970	3,000

T**able 9.4 Preparing 1x SA-PE from 100x stock (includes 25% excess volume)**

5. After the detection antibody incubation, slowly remove and discard the sealing tape.

6. Wash the plate three times with 100 µl wash buffer.

7. Vortex the diluted (1x) SA-PE at medium speed for 5 sec. Pour into a reagent reservoir and transfer 50 µl to each well using a multichannel pipet.

The protocol and the data acquisition was performed by BIOCLARMA.

The plasma hormons level and inflammatory profile were determined also using enzyme-linked immunosorbent assay (ELISA) kits, already described.

9.3.10. HbA1C

Glycated hemoglobin (HbA1c) is a form of hemoglobin that is measured primarily to identify average plasma glucose concentration. HbA1c is a measure of the beta-N-1-deoxy fructosyl component of hemoglobin. BioVision's HbA1c ELISA kit is a sandwich ELISA assay for the quantitative measurement of HbA1c in serum, plasma and cell culture supernatants. The density of color is proportional to the amount of HbA1c captured from the samples.

9.3.11. PgE2 Measurement

Tissue fragments were homogenized –4 at 0–4°C in the presence of 10 µmol/liter indomethacin so as to prevent PG production during the procedure, and then they were centrifuged at 600g. Five hundred µl of tissue homogenates were used for PgE2 determination using a com petitive enzyme immunoassay kit (Cayman Chemical Co., Ann Arbor, MI).

Prostaglandin E2 (PGE2) in a primary product of arachidonic acid metabolism in many cells. Like most eicosanoids, it does not exist preformed in any cellular reservoir. When cells are activated or exogenous free arachidonate is supplied, PGE_2 is synthesized de novo and released into the extracellular space. In vivo, PGE_2 is rapidly converted to an inactive metabolite (13,14-dilydro-15keto PGE_2) by the PG 15-dehydrogenase pathway. The half-life of PGE_2 in the circulatory system is approximately 30 seconds and normal plasma levels are 3-12 pg/ml. Because of the rapid metabolism of PGE_2, the determination of in vivo PGE_2 biosynthesis is often best accomplished by the measurement of PGE_2 metabolites. This PGE Metabolite Assay Kit converts all major PGE metabolites into a single stable derivative which is easily measurable by ELISA. This assay is based on the competition between PGE2 and a PGE2- acetylcholinesterase (AChE) conjugate (PGE2 Tracer) for a limited amount of PGE2 Monoclonal Antibody. Because the concentration of the PGE2 Tracer is held constant while the concentration of PGE2 varies, the amount of PGE2 Tracer that is able to bind to the PGE2 Monoclonal Antibody will be inversely proportional to the concentration of PGE2 in the well. This antibody-PGE2 complex binds to goat polyclonal anti-mouse IgG that has been previously attached to the well. The plate is washed to remove any unbound reagents and then Ellman's Reagent (which contains the substrate to AChE) is added to the well. The product of this enzymatic reaction has a distinct yellow color and absorbs strongly at 412 nm.

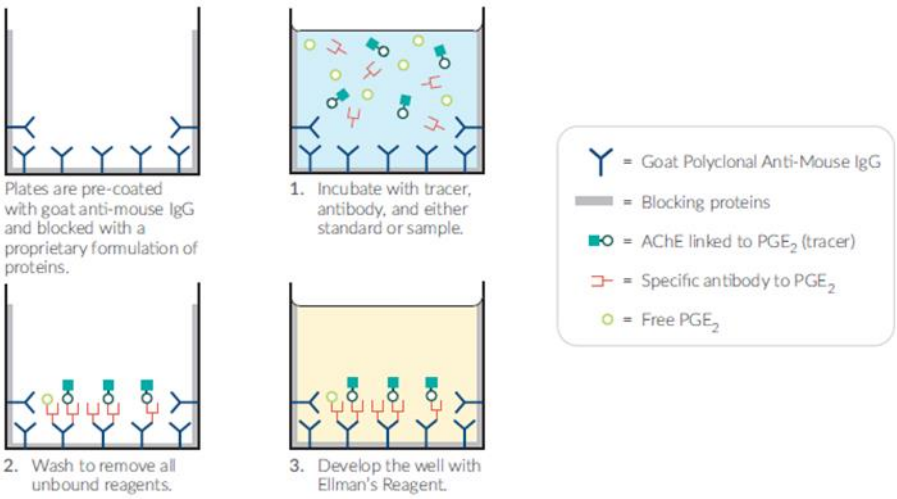

Figure 9.4

Modified from Prostaglandin E2 ELISA kit – Monoclonal. Cayman Chemical

The intensity of this color, determined spectrophotometrically, is proportional to the amount of PGE2 Tracer bound to the well, which is inversely proportional to the amount of free PGE2 present in the well during the incubation.

Absorbance ∝ [Bound PGE2 Tracer] ∝ 1/[PGE2]

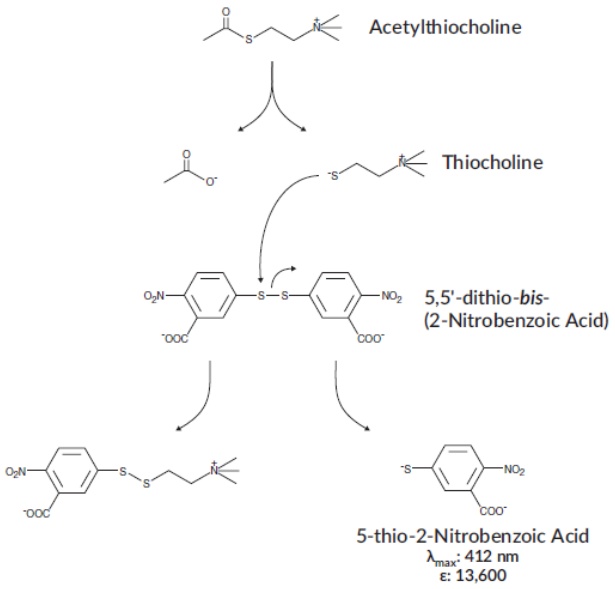

Figure 9.5 Reaction catalyzed by acetylcholinesterase

Modified from Prostaglandin E2 ELISA kit – Monoclonal. Cayman Chemical

9.3.12. Fecal microbiota analysis

Total genomic DNA extraction from frozen feces was carried out in our experiments using QIAamp PowerFecal® DNA Isolation kit (MoBio Laboratories, Inc., Carlsbad, CA) and then subjected to PCR amplification by targeting 16S rRNA V3-V4 variable regions with specific bacterial primer set 341F (5' CCTACGGGNGGCWGCAG 3') and 806R (5' GACTACNVGGGTWTCTAATCC 3').

Each PCR reaction was carried out in triplicate with 0.2 µmol/L deoxynucleotides, 0.4 µmol/L primers, 0.05 units Taq DNA Polymerase (FastStart High Fidelity PCR System; Roche, Basel, Switzerland), and 40 ng template DNA. The following thermal cycles were used: 95°C for 5 min; 30 cycles at 95°C for 30 s, 58°C for 30 s, and 72°C for 1 min; and a final elongation step at 72°C for 8 min. PCR products were checked by gel electrophoresis and cleaned using Agencourt AMPure XP system (Beckman Coulter, Brea, CA, USA), following manufacturer's instructions. After 7 PCR cycles, (16S Metagenomic Sequencing Library Preparation, Illumina), Illumina adaptors were attached (Illumina Nextera XT Index Primer). Libraries were purified using Agencourt AMPure XP (Beckman) and then sequenced on an Illumina® MiSeq (PE300) platform (MiSeq Control Software 2.0.5 and Real-Time Analysis software 1.16.18). Sequences obtained from Illumina sequencing were analyzed using Quantitative Insights Into Microbial Ecology (QIIME) 2.0 pipeline. Percentage relative abundance of taxa from different dietary groups were compared using nonparametric Wilcoxon statistical test.

The analysis was carried out by Prof Kieran M. Tuohy's laboratory team, at the University of Trento.

9.4. Evaluation of Oxidative Stress

9.4.1. Redox analysis: ABTS assay

In biochemistry, ABTS (2,2'-azino-bis (3-ethylbenzothiazoline-6-sulfonic acid)) is a chemical compound used to observe the reaction kinetics of specific enzymes. It is commonly used as a substrate with hydrogen peroxide for a peroxidase enzyme (such as horseradish peroxidase) or alone with blue multicopper oxidase enzymes (such as laccase or bilirubin oxidase). Its use allows the reaction kinetics of peroxidases themselves to be followed. In this way it also can be used to indirectly follow the reaction kinetics of any hydrogen peroxide-producing enzyme, or to simply quantify the amount of hydrogen peroxide in a sample. The formal reduction potentials for ABTS are high enough for it to act as an electron donor for the reduction of oxo species such as molecular oxygen and hydrogen peroxide, particularly at the less-extreme pH values encountered in biological catalysis. Under these conditions, the sulfonate groups are fully deprotonated and the mediator exists as a dianion.

This compound is chosen because the enzyme facilitates the reaction with hydrogen peroxide, turning it into a green and soluble end-product. Its new absorbance maximum of 420 nm light can easily be followed with a common spectrophotometer. ABTS is also frequently used by the food industry and agricultural researchers to measure the antioxidant capacities of foods. In this assay, ABTS is converted to its radical cation by addition of sodium persulfate. This radical cation is blue in color and absorbs light at 734 nm. The ABTS radical cation is reactive towards most antioxidants including phenolics, thiols and Vitamin C. During this reaction, the blue ABTS radical cation is converted back to its colorless neutral form. The reaction may be monitored spectrophotometrically.

The analysis was carried out in the laboratory of Prof R.M.Saiz Menendez, at the University of Oviedo,Spain.

9.4.2. DPPP protocol in urine

The direct fluorometric detection of hydroperoxides in lipids, serum, tissues and foodstuffs is possible using diphenyl-1-Pyrenylphosphine (DPPP). DPPP was tested to be used as a fluorescent probe to monitor lipid peroxidation in cell membranes. DPPP reacted with organic hydroperoxides and hydrogen peroxide stoichiometrically to give DPPP oxide (DPPPO). DPPP has also been used as a fluorescent probe for the detection of low density lipoprotein and cellular oxidation. Fluorescence of DPPP-O can be monitored using excitation and emission wavelengths of 351 nm and 380 nm, respectively.

DPPP incorporated into phosphatidylcholine liposomal membranes and polymorphonuclear leukocytes (PMNs) reacted with methyl linoleate hydroperoxide rapidly but not with hydrogen peroxide nor with tert-butyl hydroperoxide. This novel method revealed that lipid peroxidation proceeded within membranes of PMNs stimulated with phorbol 12-myristate 13-acetate, which is known to produce several kinds of free radicals. It was found that DPPP is a suitable fluorescent probe to monitor lipid peroxidation within cell membranes specifically.

9.4.3. Determination of Malondialdehyde (MDA)

MDA is determined by measurement of the chromogen obtained from the reaction of MDA with 2-thiobarbituric acid. Briefly heart tissues were homogenized with 1 ml of 50mM Tris-HCl buffer containing 180mM KCl and 10mM EDTA, fina pH7.4. Then, 0,5 ml of 2-thiobarbituric acid (1% w/v) in 50mM NaOH and 0.5 ml of HCl (25% w/v in water) were added to 0.5 ml of sample. The mixture was placed in test tubes, sealed with screw caps, and heated in boiling water for 10 min. After cooling, the chromogen was extracted in 3 ml of 1-butanol, and the organic phase was separated by centrifugation at 2000g for 10 min. The absorbance of the organic phase was read spectrophotometrically at a 532nm wavelength. The values are expressed as nanomoles of thiobarbituric acid-reactive substances (MDA equivalents) per milligram of protein, using a standard curve of 1,1,3,3- tetramethoxypropane.

9.4.4. Evaluation of Catalase (CAT)

CAT activity is measured using the Calbiochem® Catalase Assay Kit (Merck Millipore) following the instructions provided by the manufacturer.

Catalase (CAT) is a ubiquitous antioxidant enzyme that is present in most aerobic cells. CAT is involved in the detoxification of hydrogen peroxide (H2O2), a reactive oxygen species (ROS), which is a toxic product of both normal aerobic metabolism and pathogenic ROS production. This enzyme catalyzes the conversion of two molecules of H2O2 to molecular oxygen and two molecules of water (catalytic activity). CAT also demonstrates peroxidatic activity, in which low molecular weight alcohols can serve as electron donors. While aliphatic alcohols serve as specific substrates for CAT, other enzymes with peroxidatic activity do not utilize these substrates.

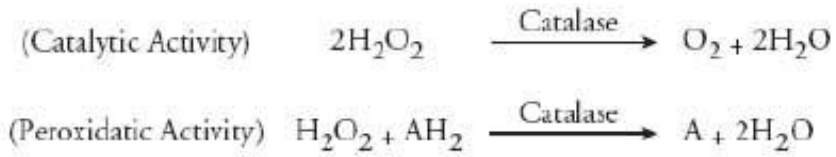

In humans, the highest levels of catalase are found in liver, kidney, and erythrocytes, where it is believed to account for the majority of hydrogen peroxide decomposition.

The Calbiochem® Catalase Assay Kit utilizes the peroxidatic function of CAT for determination of enzyme activity. The method is based on the reaction of the enzyme with methanol in the presence of an optimal concentration of H_2O_2. The formaldehyde produced is measured spectrophotometrically with 4-amino-3-hydrazino-5-mercapto-1,2,4-triazole (Purpald) as the chromogen. Purpald specifically forms a bicyclic heterocycle with aldehydes, which upon oxidation changes from colorless to a purple color. The assay can be used to measure CAT activity in plasma, serum, erythrocyte lysates, tissue homogenates, and cell lysates.

9.4.5. Determination of 8-Hydroxy-deoxyguanosine (8-OHdG)

DNA isolation from cardiac tissue homogenates was performed. In particular, the samples were homogenized in 1 ml of 10 mM phosphate-buffered saline, pH 7.4, sonicated on ice for 1 min, added with 1 ml of 10 mM Tris-HCl buffer, pH 8, containing 10 mM EDTA, 10 mM NaCl, 0.5% SDS, and incubated for 1 h at 37°C with 20 μg/ml RNAse (Sigma). Then, the samples were incubated overnight at 37°C under oxygen-free conditions by insufflating argon, in the presence of 100 μg/ml proteinase K(Sigma). After incubation, the mixture was extracted with chloroform/isoamyl alcohol (10/2 v/v). DNA was precipitated from the aqueous phase with 0.2 vol of 10 M ammonium acetate, solubilized in 200 μl of 20 mM acetate buffer, pH 5.3, and denaturated at 90°C for 3 min. The extract was then supplemented with 10 IU of P1 nuclease in 10 μl and incubated for 1 h, at 37°C with 5 IU of alkaline phosphatase in 0.4 M phosphate buffer, pH 8.8. All the procedures were performed in the dark under argon. The mixture was filtered by an Amicon Micropure–EZ filter (Amicon, MA) and 50 μl of each sample was used for 8-hydroxy-2'-deoxyguanosine (8-OHdG) determination using an ELISA kit (JalCA, Shizuoka, Japan), following the instructions provided by the manufacturer. The absorbance of the chromogenic product was measured at 450nm and expressed as ng/mg of DNA. The results were calculated from a standard curve based on 8-OHdG solution. The values are expressed as ng 8-OHdG/μg total DNA.

The 8-OHdG Check is a competitive in vitro enzyme-linked immunosorbent assay (ELISA) for quantitative detection of the oxidative DNA adduct 8-hydroxy-2'-deoxyguanosine (8-OHdG) .

9.5. Microarray analysis

Incubating printed slides for lectin; microarray applications

TBS: This is a modified low salt version of TBS.

20 mM TRIS (NOT Trizma), 100 mM NaCl, 1 mM $CaCl_2$ and 1 mM $MgCl_2$, pH to 7.2 with HCL.

- ✓ **10X recipe**
  - 200 mM Tris 24.22 g
  - 1 M NaCl 58,44 g
  - 10 mM $MgCl_2$ 0,9521 g
  - 10 mM $CaCl_2$ 1,4702 g

Add 0,5 ml of Tween-20 to the 1X solution (0,5% Tween-20=TBS-T)

For the labeling of the samples Alexa Fluor® 555 Protein Labeling Kit (A20174) was used.

The following protocols should be carried out in the dark at all times.

1. A titration curve should be initially carried out to determine optimum sample concentration in terms of signal to noise ratio and feature overload. Samples are diluted into a final volume of 70 μl with TBS-T.

2. Include two quality control wells and experimental controls (i.e. inhibition) in the experimental design.
3. Check the rubber on the 8-well gasket before aliquoting sample into the wells (70 µl per well)
4. Incubate slide with 70 µl sample per well in a closed container (Agilent 8-well gasket assembled with gasket holder) for 1 hour at desired temperature with gentle rocking/rotation (i.e. in hybridization oven).
5. Remove incubation solution. This is done by opening the slide gasket into a container full of TBS-T to avoid cross contamination by encourage immediate dilution.
6. Wash in TBS-T X3 or 4 (depending on your sample optimization).
7. Wash in TBS-T X1
8. Dry by centrifugation as above
9. Scan immediately

The analysis was carried out in the laboratoty of Prof Lokesh Joshi, at the University of Galway, Ireland

9.6. Tissues analysis

9.6.1. Tissue extracts and proteins count

The protocol for the total exraction of the proteins in the samples consiste in the homogenization of the organs at 10% (w / v) by means of the Potter homogenizer Elvehjem (Wheaton, Millville, NJ, USA), using a compound homogenization buffer enriched with protease inhibitors before use. The homogenates are then centrifuged at 1000 x g for 10 minutes at 4ºC. At the end of the centrifugation the supernatant, separated from the pellet, is stored at -80 ° C.

HOMOGENIZATION BUFFER

Concentration in Final Solution	**STOCK**	**AMOUNT**
20 mM Hepes – KOH pH 7,9	0.5 M	4ml/100ml
1 mM $MgCl_2$	100 mM	1ml/100ml
0,5 mM EDTA	100 mM	0,5ml/100ml
1 mM EGTA	100 mM	1ml/100ml
1% NP-40-IGEPAL (or TRITON-X 100)		1ml/100ml

Make up to volume with MILLI Q water

Add, under the chemical hood, before the use:

Inhibitors	Add in Final Solution
NaF a 4°	1 µl/ml
PMSF A 4°	5 µl/ml
PIC a -20°	10 µl/ml
Sodium Vanadate (Na3VO4) -20°	10 µl/ml

Regarding the Cytosolic and nuclear protein extraction the protocol is:

- Homogenize the tissue with HOMOGENIZAZION BUFFER in ice at concentrations of 1:10 (e.g. 30 mg of tissue in 300 ul of HOMOGENIZAZION BUFFER)
- Centrifuge at 4000 RPM (1320g) for 5 minutes at 4°C.
- Separate the supernatant (Supernatant 1) from the pellet (Pellet 1).
- Centrifuge the Supernatant 1 at 14000 RPM (16215g) for 40 min at 4°C. The obtained supernatant (Supernatant 2) contains the cytosolic proteins.
- Resuspend the Pellet 1 in EXTRACTION BUFFER at concentrations of 1/3 compared to the HOMOGENIZAZION BUFFER (e.g. 100 ul)
- Incubate for 30 min in ice vortexing occasionally.
- Centrifuge at 14000 RPM (16215g) for 20 min at 4°C. The obtained supernatant (Supernatant 3) contains the nuclear proteins.
- Freeze Supernatant 2 (cytosolic proteins) and Supernatant 3 (nuclear proteins).

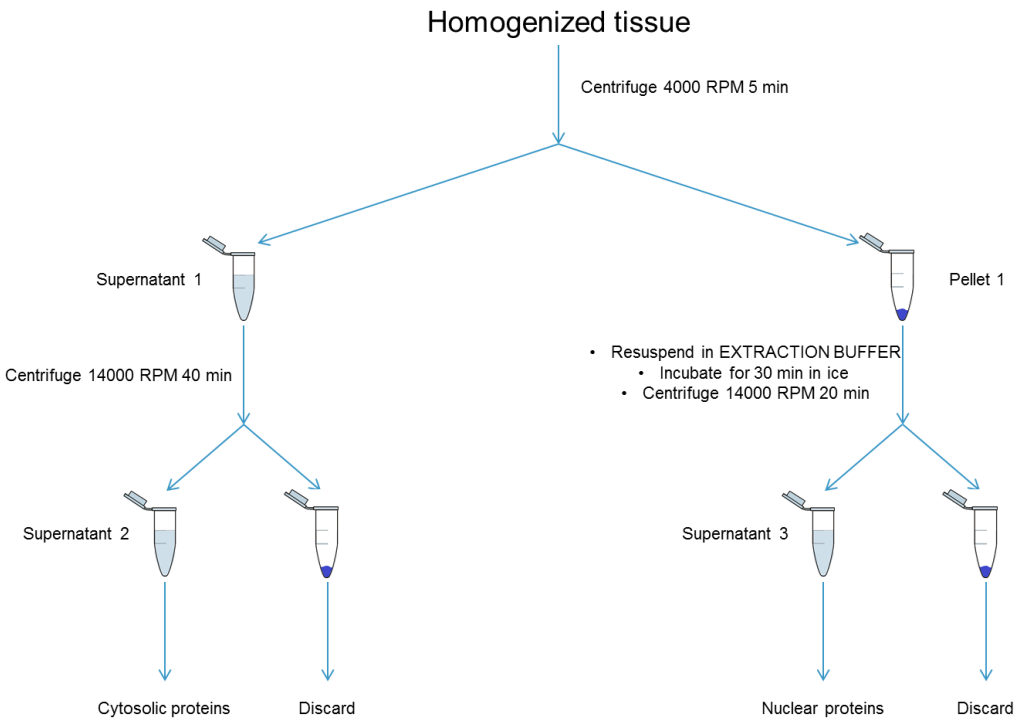

Figure 9.4 Scheme of extraction

HOMOGENIZATION BUFFER

Concentration in Final Solution	**STOCK**	**AMOUNT**
20 mM Hepes – KOH pH 7,9	0.5 M	4ml/100ml
1 mM $MgCl_2$	100 mM	1ml/100ml
0,5 mM EDTA	100 mM	0,5ml/100ml
1 mM EGTA	100 mM	1ml/100ml
1% NP-40-IGEPAL (oppure TRITON-X 100)		1ml/100ml

Make up to volume with MILLI Q water

Add, under the chemical hood, before the use:

Inhibitors	**Add in Final Solution**
NaF a 4°	1 µl/ml
PMSF A 4°	5 µl/ml
PIC a -20°	10 µl/ml
DTT a 4°	1 µl/ml
Sodium Vanadate (Na3VO4) -20°	10 µl/ml

EXTRACTION BUFFER

Concentration in Final Solution	**STOCK**	**AMOUNT**
20 mM Hepes – KOH pH 7,9	0.5 M	2ml/50ml
1,5 mM $MgCl_2$	100 mM	0,75ml/50ml
0,2 mM EDTA	100 mM	0,1ml/50ml
1 mM EGTA	100 mM	0,5ml/50ml

20% Glicerolo	10ml/50ml
420 mM NaCl	1.23g/50ml

Make up to volume with MILLI Q water

Add, under the chemical hood, before the use:

Inhibitors	**Add in Final Solution**
NaF a 4°	1 µl/ml
PMSF A 4°	5 µl/ml
PIC a -20°	10 µl/ml
DTT a 4°	1 µl/ml
Sodium Vanadate (Na3VO4) -20°	10 µl/ml

The protein count was established to determine the volume of samples to be loaded into the gel wells for the Western blot.

A 24-well Costar® 3526 well plate and a pre-purchased BCA Protein Assay kit were used to prepare the samples for counting. It is an analysis method that allows to perform a colorimetric and quantitative detection of proteins.

The Thermo Scientific™ Pierce™ BCA Protein Assay Kit is a detergent-compatible formulation based on bicinchoninic acid (BCA) for the colorimetric detection and quantitation of total protein. This method combines the well-known reduction of Cu+2 to Cu+1 by protein in an alkaline medium (the biuret reaction) with the highly sensitive and selective colorimetric detection of the cuprous cation (Cu+1) using a unique reagent containing bicinchoninic acid. The purple-colored reaction product of this assay is formed by the chelation of two molecules of BCA with one cuprous ion. This water-soluble complex exhibits a strong absorbance at 562 nm that is nearly linear with increasing protein concentrations over a broad working range (20–2000 µg/mL). The BCA method is not a true end-point method; that is, the final color continues to develop. However, following incubation, the rate of continued color development is sufficently slow to allow large numbers of samples to be assayed together.

The macromolecular structure of protein, the number of peptide bonds and the presence of four particular amino acids (cysteine, cystine, tryptophan and tyrosine) are reported to be responsible for color formation with BCA. Accordingly, protein concentrations generally are determined and reported with reference to standards of a common protein such as bovine serum albumin (BSA). A series of dilutions of known concentration are prepared from the protein and assayed alongside the unknowns before the concentration of each unknown is determined based on the standard curve.

Preparation of standards and working reagent (required for both assay procedures)

Preparation of diluted albumin (BSA) standards: Dilute the contents of one Albumin Standard (BSA) ampule into several clean vials, preferably using the same diluent as the samples. Use the following table as a guide to prepare a set of protein standards. Each 1 mL ampule of 2 mg/mL Albumin Standard is sufficient to prepare a set of diluted standards for either working range suggested in the table. There will be sufficient volume for three replications of each diluted standard.

Dilution Scheme for Standard Test Tube Protocol and Microplate Procedure (Working Range = 20–2,000 µg/mL)			
Vial	**Volume of Diluent (µL)**	**Volume and Source of BSA (µL)**	**Final BSA Concentration (µg/mL)**
A	0	300 of Stock	2000
B	125	375 of Stock	1500
C	325	325 of Stock	1000
D	175	175 of vial B dilution	750
E	325	325 of vial C dilution	500
F	325	325 of vial E dilution	250
G	325	325 of vial F dilution	125
H	400	100 of vial G dilution	25
I	400	0	0 = Blank
Dilution Scheme for Enhanced Test Tube Protocol (Working Range = 5–250 µg/mL)			
Vial	**Volume of Diluent (µL)**	**Volume and Source of BSA (µL)**	**Final BSA Concentration (µg/mL)**
A	700	100 of Stock	250
B	400	400 of vial A dilution	125
C	450	300 of vial B dilution	50
D	400	400 of vial C dilution	25
E	400	100 of vial D dilution	5
F	400	0	0 = Blank

For Research Use Only. Not for use in diagnostic procedures.

30 January 2020

ThermoFisher SCIENTIFIC

Table 9.5 Preparation of diluted albumin (BSA) standards

Preparation of the BCA working reagent (WR)

Use the following formula to determine the total volume of WR required:

(# standards + # unknowns) × (# replicates) × (volume of WR per sample)

Prepare WR by mixing 50 parts of BCA Reagent A with 1 part of BCA Reagent B (50:1, Reagent A:B). For the above example, combine 50 mL of Reagent A with 1mL of Reagent B.

Microplate procedure (sample to WR ratio = 1:8)

The samples, which are stored at -80 ° are previously thawed at room temperature. The first two rows of the plate are reserved for the albumin standard to construct the calibration curve. In each remaining well of the plate, 3 µl of sample, 27 µl of water and 270 µl of BCA solution (bicinconinic acid) prepared a little in excess are placed. In the wells reserved for the blank, only 30 µl of water is added and then the WR is added. The plate has to be covered and incubated at 37°C for 30 minutes. Therefore, in order to quantify the concentration of proteins in the sample, the absorbance of the colored product is measured using a UV spectrophotometer, then the plate is moved to the appropriate VICTOR® reading device, which represents an absorbance reading at 562 nm whose value is proportional to the concentration of proteins present in each sample. The average 562 nm absorbance measurement of the Blank standard replicates has to be substract from the 562 nm measurements of all other individual standard and unknown sample replicates. Finally, a standard curve is prepared by plotting the average Blank–corrected 562 nm measurement for each BSA standard vs. its concentration in µg/mL.

In this way it is possible use the standard curve to determine the protein concentration of each unknown sample, and so loading inside the gel the same concentration of proteins of different samples.

9.6.2. Western blot analysis

Western Blot (or Immunofixation or Immunoblot) is a biochemical technique that allows the identification of a specific protein within a complex mixture, through the use of a specific antibody directed to a specific domain of the protein (Figure 9.5).

Western Blot allows to monitor the expression or phosphorylation of a specific protein within a cell, thus establishing the presence, quantity and molecular weight of a specific protein.

At the basis of this qualitative and semi-quantitative evaluation there is an initial separation of the proteins according to their molecular weight, thanks to an electrophoretic run on polyacrylamide gel.

The proteins are subsequently transferred onto a support such as a polyvinylidene difluoride (PVDF) membrane, which allows their detection.

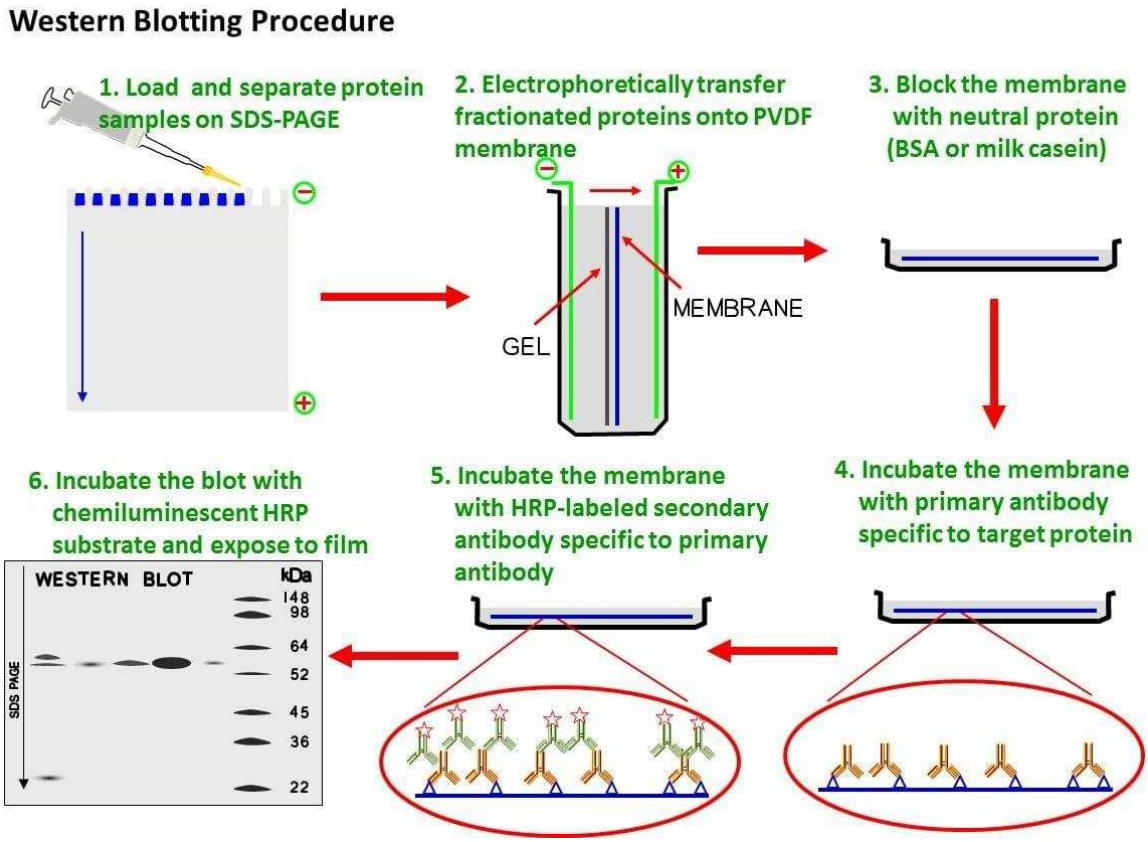

Figure 9.5 Western Blot summary scheme

Taken and modified from www.microbeonline.com)

The previously prepared samples are subjected to SDS-PAGE (Sodium Dodecyl Sulfate-

PolyAcrilAmideGel Electrophoresis). SDS is an anionic detergent which has a negative charge and which has the function of going to denature proteins, thus giving each protein the same charge-mass ratio. In this way the protein separation will take place solely on the basis of their different molecular weight. At the end of the electrophoretic run, the proteins are transferred from the gel to a PVDF membrane. This membrane will be incubated first with a specific primary antibody and subsequently with a secondary antibody which will allow the detection of the proteins of interest.

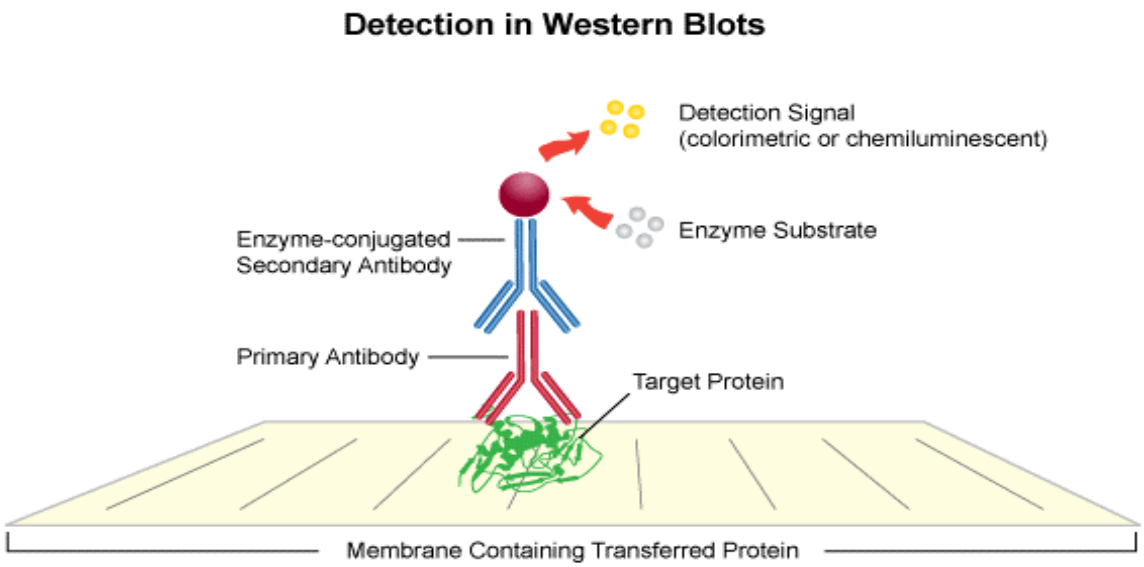

Figure 9.6 Summary scheme of the interaction between antibody and protein of interest in the Western Blot

Source: www.microbeonline.com

Gels preparation

After sample preparation it is necessary to set up the gels in which the electrophoretic run will take place (Figure 9.7).

This gel is in turn divided into two types of gel characterized by different function and composition:

Stacking gel (or packing gel): represents the upper portion of the gel and the wells inside which the samples are loaded are obtained, to ensure that the proteins present start migrating from the same starting point. It is a wide-meshed gel in which, at the flow of the current, depending on the pH of the buffer, an isotacophoresis condition is created which has the purpose of packing the samples into thinner bands, in order to start the run from the same band.

Running gel (or separation gel): it constitutes the lower part of the gel in which the separation of proteins takes place according to the molecular weight. Based on the operator's assessments regarding the size of the protein sought, this gel can have more or less wide meshes.

The two types of gel are made up of the same components, but in different quantities and

with different pH. In particular, the quantity of acrylamide which is the determining factor for the size of the pores of the gel varies: higher concentrations allow the formation of smaller pores and vice versa. The polymerization of the gel (1 mm thick) takes place between two slides, mounted on a special support. Initially the Running gel is prepared which is poured between the two slides and immediately after this operation a 0.1% SDS solution is added on the top edge of the gel, to prevent dehydration of the latter. Then it is left to cure in a cold environment.

Once the polymerization has taken place, the SDS 0.1% is removed and the preparation of the Stacking gel is started. The latter, once poured over the running gel, allows the formation of wells thanks to the insertion of a special comb. The number of wells to be created is chosen according to the number of samples to be loaded, for this reason there are wells of different sizes. Once polymerization is complete, it is necessary to gently remove the comb and check that all the wells are intact.

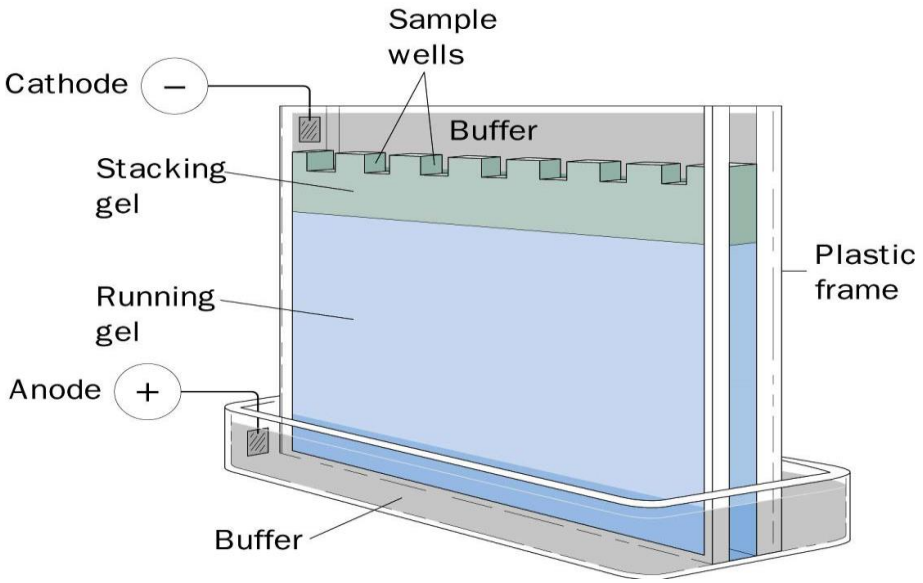

Figure 9.7 SDS-PAGE schematic

Taken from www.siumed.edu and modified

Loading of samples and electrophoretic run

In each well a volume of sample and Milli-Q water equal to the quantity determined by the protein count are loaded, so as to obtain the same concentration of the various samples (Figure 9.8). The total volume of these two components is 12 µl, and 4 µl si of Sample Buffer 5X are added to this quantity, so as to obtain a total of 16 µl per well.

A well is reserved for loading the reference molecular weights (BIO-RAD Precision Plus ProteinTMWesternCTMStandards) consisting of proteins of known weight and marked with dyes. The dyes are bound to proteins through covalent bonds, so as not to dissociate during migration and blotting procedures. Any empty wells are filled with Sample Buffer 5X, after loading the samples. After loading, the samples are run with the use of a special electrophoretic apparatus (BIO-RAD Mini_PROTEAN ® Tetra System) in a RUNNING BUFFER 1X

solution at a current intensity of 200 V for a period of time between 30 and 40 minutes.

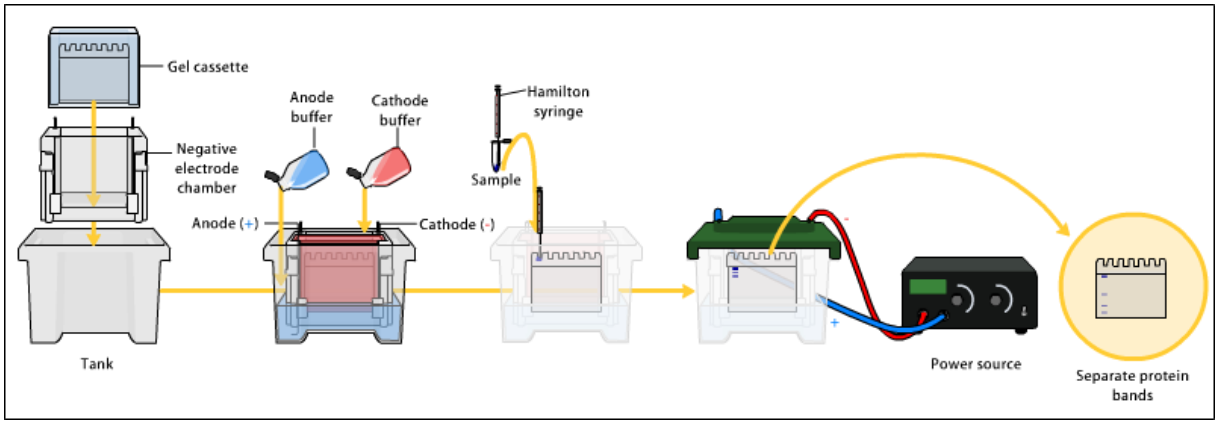

Figure 9.8 Electrophoretic loading and stroke

Taken and modified https: // it.wikipedia.org/wiki/Western_blot

Immunoblotting

At the end of the electrophoretic run, the proteins, separated in the gel according to the molecular weight, are transferred onto a PVDF (Immobilon®) membrane of suitable dimensions (5.5 cm x 8.5 cm) and previously activated in methanol for 10 seconds. Then there is the preparation of the so-called "sandwich" using the appropriate support and arranging the various components as illustrated in Figure 9.9.

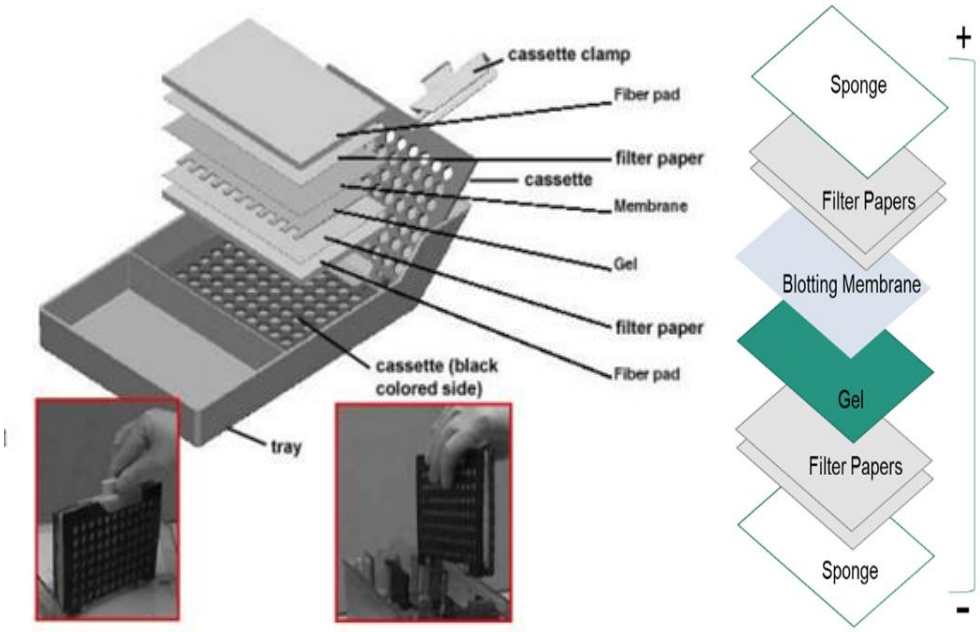

Figure 9.9 Preparation of the Western Blot sandwich

Taken and modified from https://www.creative-proteomics.com

The "sandwiches" are placed inside a tray containing transfer buffer kept agitated by a magnet, and are connected to the electrodes by applying a current intensity of 100V for a time of 70 minutes. The transfer buffer solution in the hours prior to its use must be placed in the refrigerator at -20ºC in order to improve the transfer performance. In fact, at this stage, due to the passage of the current, there is heat production which could interfere with the result of the process. At the end of the transfer, the membrane is incubated for about an hour in a blocking buffer 5% BSA (Bovin Sieric Albumine) solution, necessary to saturate all the non-specific sites present, subsequently this membrane is washed in TBS-1X TWEEN 0.1%. The thus blocked membrane is incubated, under continuous stirring with the primary antibody containing 100 µl of NaN3, as a preservative. Incubation times vary from 2h30 to all night (Over night) depending on the type of antibody or the manufacturer.

About 60 µg of total proteins were loaded for Western blot experiments. Proteins were separated by 8 % sodium dodecyl sulphate-polyacrylamide gel electrophoresis (SDS-PAGE) and transferred to a polyvinyldenedifluoride (PVDF) membrane, which was then incubated with primary antibodies (dilution 1:1000). After incubation with the primary antibody, the membrane is washed with TBS TWEEN 0.1%: 3 washes of 5 minutes. Blots were then incubated, for 30 minutes at RT, with a secondary antibody (anti-mouse, 7076s anti-rabbit 7074s) conjugated with horseradish peroxidase diluted 1: 2000 in a 10 ml solution of TBS 1XAb, containing 0.1g of BSA, to which 0.5µl of molecular weight marker is added (BIO-RAD Precision ProteinTMStepTactin HRP Conjugate).

The secondary antibodies (Cell-Signaling Technology) used are of 2 types:

- ✓ α-Mouse
- ✓ α-Rabbit

Development of chemiluminescence signal

Figure 9.10 ChemiDoc Imaging System, Bio-Rad

After washing with TBS 1X TWEEN, the membrane is inserted inside the dark room of the ChemiDoc ™ Touch Imaging System (Bio-Rad, Figure 9.10). After the correct positioning of the membrane above the appropriate support, about 500 µl of ECL are inserted on the membrane in correspondence with the bands of interest and the detection starts, setting the desired program. The analysis continues until the band of interest appears. ECL is a chemiluminescent detection system based on luminol and hydrogen peroxide (1: 1). It is a non-radioactive light emission method that is used to detect antibodies conjugated with the peroxidase enzyme. The solution of ECL (luminol + hydrogen peroxide) catalyzes the cleavage of hydrogen peroxide in water and superoxide radical, which is able to oxidize the luminol (Figure 9.11). This oxidation brings the luminol to an excited state from which it can decay to the ground state with the emission of photons (light) thus making the signal detectable.

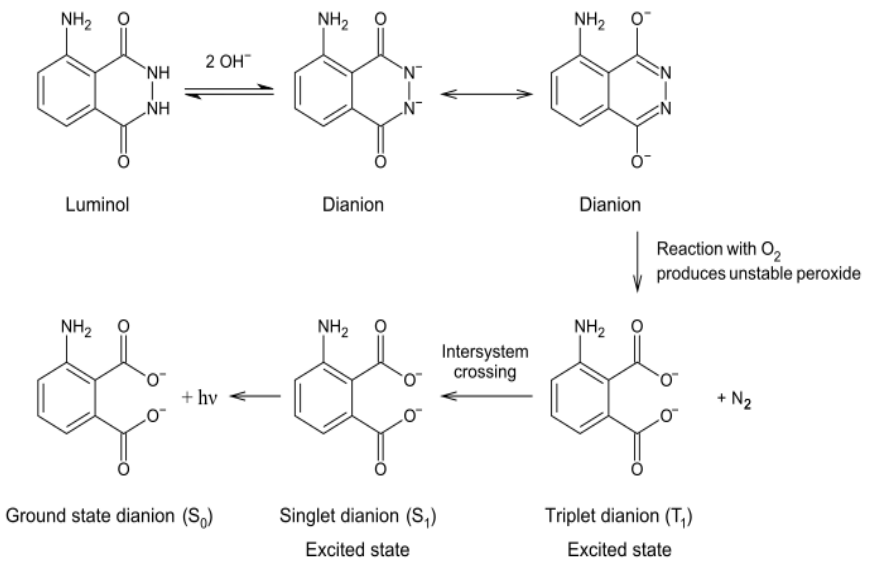

Figure 9.11 Photochemical reaction of luminol

Source www.wikipedia.it and modified

The exposure time of the sheet varies according to the operator's choice, in order to obtain an optimal result from a technical point of view and appreciable with the naked eye.

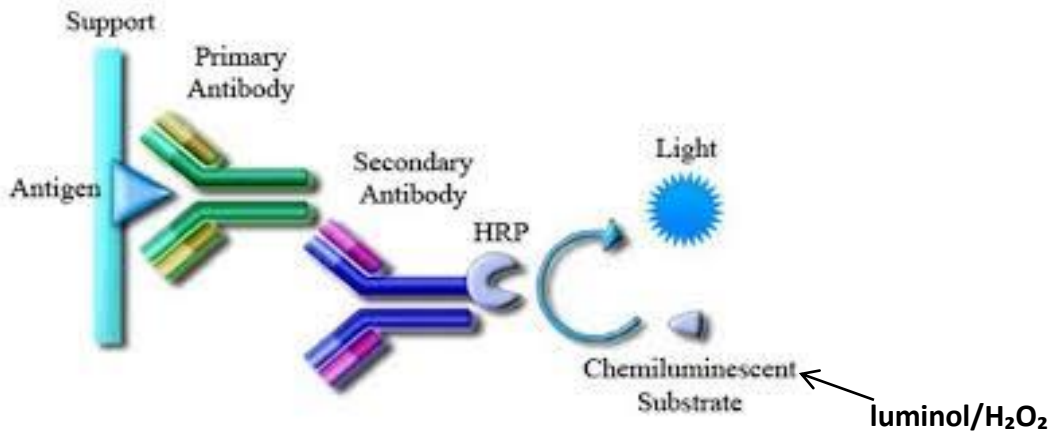

Figure 9.12 Scheme of the chemiluminescence reaction

Source www.wikipedia and modified

Densitometry and Statistical analysis

The results of developments used for the densitometry analysis were expressed as Absolute Optical Density (O.D.). Densitometry analysis allows to obtain the mass or the concentration of an absorbent substance that is directly proportional to the quantity of absorbed light at a precisely wavelength. From the detection of light absorbed quantity is possible to obtain the mass or the concentration of the absorbent substance. The transmittance is the fraction of

incident electromagnetic power that is transmitted through a sample:

T = SPECTRAL RADIANCE TRANSMITTED / SPECTRAL RADIANCE RECEIVED

The transmission is normally expressed as a percentage and the optical density (O.D.) is the inverse logarithm of the transmission: O.D. = Log 1 / T

The O.D. ranges from 0 (100% transmission) to infinity (transmission = 0, for a completely opaque material). Integrated Optical Density (I.O.D.) is defined as the sum of the O.D. individual of each sample of the measured area. This shows that it is possible to calculate the mass or concentration of positive substrate for a given histochemical reaction simply by knowing the area occupied by the substrate. Densitometric calibration concerns various aspects of image acquisition. First, the white calibration must be performed, by choosing an empty area of the preparation and by adjusting the intensity of the light source. Furthermore, it is necessary to eliminate the "background noise" by setting the output signal to zero. Finally, it is necessary to perform a densitometric calibration on the density of a standard image in order to measure any deviations from this on the images in the studio. Data were analyzed by the Bio-Rad Image Lab SoftwareTM 6.0.1 and collected data were bringing to Excel to be normalized with Tubulin or actin and to do the ratio between Phosphorylated protein and the total one, then also normalized for the loading protein. For each group of samples, the average, standard deviation and the average standard error were calculated. One-way ANOVA test followed by Bonferroni post-test was used to analyze the results by GraphPad Prism version 5.0 for Windows (GraphPad Software, San Diego, CA, USA, www.graphpad.com). Data that were analyzed in couple were submitted to t-test (non-parametric) followed by Mann Whitney test (whit Confidence Intervals of 95%). Values with $p < 0.05$ were retained statistically significant.

<u>Solution recipes</u>

- ✓ **Sample buffer 5X**
  - Tris HCl Ph: 6.8 — 70%
  - SDS — 1%
  - Blu di bromofenolo — 0.001%
  - Glicerolo — 30%

- ✓ **TBS 10X (Tris Buffered Saline)**
  - Tris base — 24.4.g
  - NaCl — 80 g

  Add 800 ml of Milli-Q water and Make up to a pH 7.4 with HCl, then make up to a volume of 1L with MILLI Q

- ✓ **TBS 1X Ab**
  - TBS 10X — 50 ml
  - Acqua MilII-Q — 450 ml
  - TWEEN 20 — 0.5 ml

- ✓ **TBS 1X TWEEN (0.1%)**
  - TBS 10X 100 ml
  - TWEEN 20 1 ml

Make up to a volume of 1L with deionized water

- ✓ **Stripping buffer**
  - Restore TM Western Blot Stripping Buffer (THERMO SCIENTIFIC)

- ✓ **Blocking buffer**
  - TBS 1X TWEEN 10 ml
  - BSA (Bovin Serum Albumine) 1 g

- ✓ **Running buffer**
  - Glicina 14.4 g
  - Tris HCl 3.02 g
  - SDS 1 g

Make up to a volume of 1L with MILLI Q water

- ✓ **Tranfer buffer**
  - Glicina 14.4 g
  - Tris base 3.02 g
  - Metanolo 150 ml

Make up to a volume of 1L with MILLI Q

- ✓ **Stacking gel**

Sostanza	Quantità (µl)
H_2O Milli-Q	1350
Tris HCl Ph 6.8	562.5
SDS 10X	22.5
Acril/Bis acrilamide	300
APS 10%	36
TEMED 8%	18

- ✓ **Running gel**

Sostanza	10%	8%
H_2O Milli-Q	2.5 ml	2.9 ml
Tris-HCl Ph 8.8	1.5 ml	1.5 ml
Acril/Bis acrilamide	2 ml	1.6 ml
SDS 10X	60 µl	60 µl
TEMED 8%	20 µl	20 µl
APS 10%	40 µl	40 µl

Chapter 10 – Results

1) Impact of different diet components on pathophysiological mechanism(s) involved in the development of metabolic derangements

10.1. Diet compositions

We first compared the correlations between different dietary components and the caloric intake.

As reported in table 10.1, the diets we have used contained high concentrations of: fat (HFD), fructose (Fr) or both fructose and fat (HFHF), compared to a normocaloric diet (ND).

	ND Formulation Fat 10% Kcal Carbohydrate 70% Kcal Protein 20% Kcal	HFD Formulation Fat 61,6% Kcal Carbohydrate 20,3% Kcal Protein 18,1% Kcal	HFHF Formulation Fat 45% Kcal Carbohydrate 35% Kcal Protein 20% Kcal	Fr Formulation Fat 10% Kcal Carbohydrate 70% Kcal (60% fructose) Protein 20% Kcal
Fat	Soybean Oil, USP 25,00g Lard 20,00g	Soybean Oil 25,00g Lard 250,00g	Soybean Oil 25,00g Lard 177,50g	Soybean Oil, USP 25,00g Lard 20,00g
Carbohydrate	Starch, Corn 550,00g Lodex 10 150,00g Sucrose 4,00g	Maltodextrin 100g Sucrose 104,00g	Corn Starch 72,80g Maltodextrin 10 100,00g Fructose 172,80g	Starch, Corn 94,48g Sucrose 10,30g Fructose 640,00g
Protein	Casein, Lactic, 30 Mesh 200,00g L- Cystein 3,00g	Casein 30 Mesh 179,00g L- Cystein 3,00g	Casein 30 Mesh 200,00g L- Cystein 3,00g	Casein, Lactic, 30 Mesh 200,00g L- Cystein 3,00g
Fiber	Solka Floc, FCC200 50,00g	Cellulose 50,00g	Cellulose, BW200 50,00g	Cellulose, BW200 50,00g
Mineral	S10026B 50,00g Choline Bitartrate 2,00g	Mineral mix S10026 10,00g DiCalcium Phosphate 13,00g DiCalcium Carbonate 5,50g Potassium Citrate, 1 H2O 16,50g Choline Bitartrate 2,00g	Mineral mix S10026 10,00g DiCalcium Phosphate 13,00g DiCalcium Carbonate 5,50g Potassium Citrate, 1 H2O 16,50g Choline Bitartrate 2,00g	S10026B 50,00g
Vitamin	Vitamin mix V10001C 10,00g	Vitamin mix AIN-76 10,00g	Vitamin mix V10001C 10,00g	Vitamin mix V10001C 10,00g
Dye	Dye Blue FD&C #1, Alum. Lake 35-42 %0,03g	FD&C Blue No.1 0,05g	FD&C Red Dye #40 0,05g	FD&C Red Dye #40 0,05g

Table 10.1 Composition of the experimental diets used

10.1.1. Impact of diet composition and kinetics of exposure on Body Weight Gain

Body weight gain, for example, was massive for mice exposed to HFD, but also for HFHF after 12 weeks, conversely for mice exposed to Fr, an increase in body weight was observed only after 24 weeks of dietary manipulation (Figure 10.1). The graph does not show the results of weight gain percentage of HFD and HFHF after 24 weeks, since for these two groups significant results were already obtained at 12 weeks.

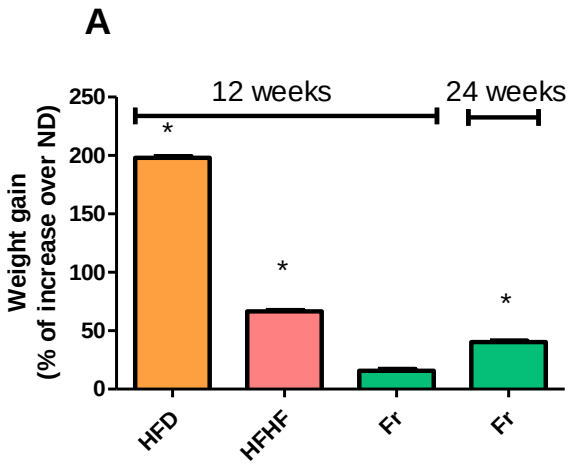

Figure 10.1 Body weight on mice exposed to HFD, HFHF and Fr

Effects of HFD, HFHF and Fr administration on mouse body weight. All data are expressed as mean ± SEM for n number of observations. $*p < 0.05$ vs ND.

Focusing on mice exposed to the sugar diet, we described how the kinetics of exposure and the concentrations and formulations may affect the increase in body weight of the animals.

We demonstrated that there is no difference in the body weight gain compared to the normocaloric diet, for a regime of 12 weeks of fructose diet, neither changing the administration at different concentrations, 30% and 60%, or at different formulation, liquid (L-Fr syrup was prepared dissolving 60% of fructose in water with 3,5% citric acid as preservative) and solid (Figure 10.2A). Instead 24 weeks of 30% fructose diet induced increase in body weight (Figure 10.2B) of about 15% compared to the corresponding formulations of Fr at 12 weeks.

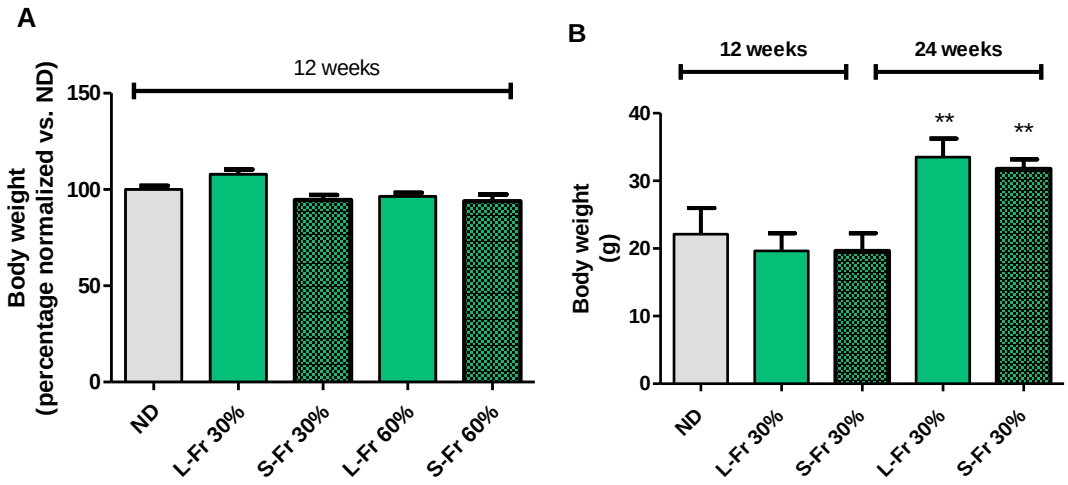

Figure 10.2 Body weight on mice exposed to a fructose diet

Body weight after 12 and 24 weeks in mice subjected to 12 weeks of a 30% and 60% liquid fructose diet (A). Body weight, normalized with respect to the ND group, measured after 12 and 24 weeks of food regimen enriched with 30% fructose, in liquid and solid formulation (B). The analyzed data are expressed as mean ± SEM on n = 8-10 per group. The statistical analysis was carried out using one-way ANOVA and post-test Bonferroni. **p<0,01 vs the corresponding formulations of Fr

10.1.2. Impact of diet composition and kinetics on Insulin Sensitivity and Insulin Signaling Pathway

As a result of the evaluation of body weight, it was important to go into greater detail on how the diet impacted the system's glycemic profile of the animals. The figure 10.3 shows fasting blood glucose values in order to monitor the amount of glucose in the blood.

Data obtained with HFD and HFHF show a significant worsening in glycemic profile with an increase in plasma fasting glucose, if compared to ND. Also it is possible to observe significant statistical diffence in Fr fed mice after 12 weeks.

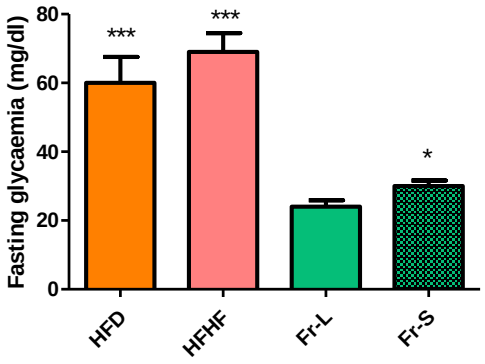

Figure 10.3 Fasting glycemia on mice exposed to HFD, HFHF and Fr

Effects of HFD, HFHF and Fr administration on mouse fasting glycemia. All data are expressed as mean ± SEM for n number of observations. $*p < 0.05$ vs ND; ***p<0,01 vs ND

10.2. Effects of AGEs on the Cross-Talk Mechanisms Linking Microbiota to Metabolic Inflammation

The data previously showed demonstrate that the high chemical reactivity of fructose substantially contributes to the massive formation of intracellular Advanced Glycation End Products. In our experiments (Paper 4 on Discussion section) we show also that this accumulation evokes marked cellular alterations and organ dysfunction, thus supporting the hypothesis that AGEs play a pivotal role on the development of metabolic derangement.

Diet is the major source of AGEs *in vivo*, because they can be produced endogenously from a diet with a high content of simple sugars, especially fructose. Modern diets are also largely heat-processed and as a result contain high levels of AGEs. In order to deeply investigate their pathogenic role in diet-related metabolic derangements we explored the impact of chronic exposure to exogenous AGEs. Our investigation using chronic administration of exogenous AGEs did not show to significantly affect metabolic parameters: body weight, lipid profile and fasting blood sugar, despite the increase in insulin plasma level and the impairment in glucose tolerance test, compared with those obtained in mice exposed to the control diet (Table 10.2).

	Control Diet (n=24)	AGE DIET (n=20)
Body weight (g)	29.30 ± 2.38	27.51 ± 2.13
Food Intake (g/day)	3.60 ± 0.36	3.30 ± 0.25
Water Intake (ml/day)	4.81 ± 0.15	4.82 ± 0.20
Caloric Intake (Cal/day)	13.87± 1.38	11.91 ± 0.96
Triglycerides (mg/dl)	75 ± 5	75 ± 2
Total cholesterol (mg/dl)	110 ± 6	108 ± 4
HDL cholesterol (mg/dl)	63 ± 10	60 ± 3
Insulin (pg/ml)	2659,9 ± 226	3521,1 ± 384*
Blood glucose (mg/dl)	95,83 ± 3,48	91,9 ± 2,57
AUC of Oral Glucose Tolerance Test	18162,5 ± 382,12	19195,77 ± 306,84*

Table 10.2 Effects on mice body weight and systemic lipid/glucose profile at 22 weeks of the AGE-D in comparison to the ND. AUC: Area under curve represents glucose concentration over time.

On a molecular point of view, the insulin pathway was worsened, in fact in skeletal muscle of mice fed a normocaloric diet enriched in AGEs was registered, compared to mice fed a normocaloric diet, an increase in the degree of phosphorylation on serine 307 of insulin substrate receptor-1 resulting in a reduction in phosphorylation of downstream mediators protein kinase B Akt on serine 473 and glycogen synthase kinase-3β (Figure 10.4).

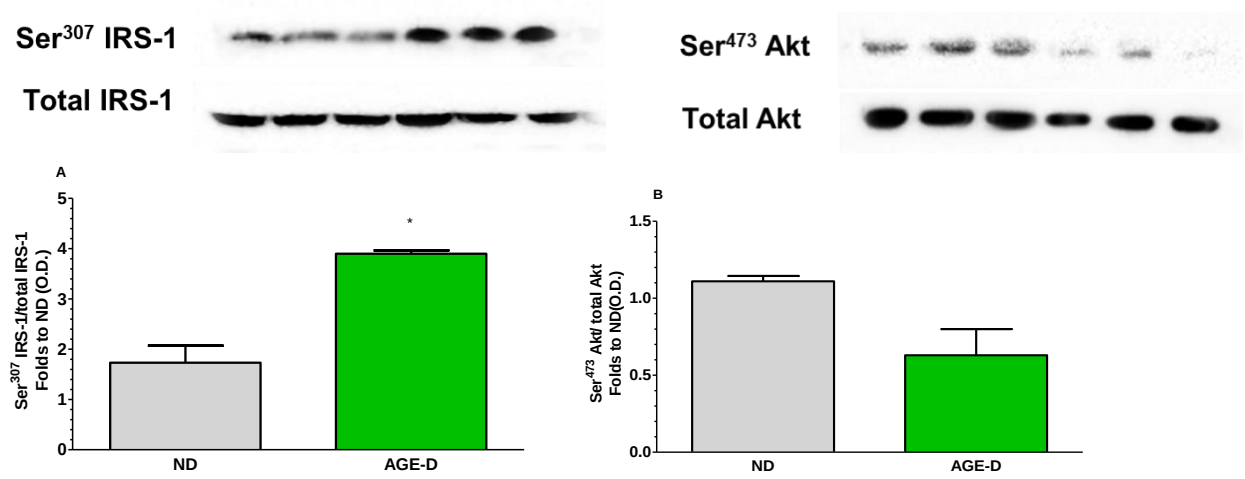

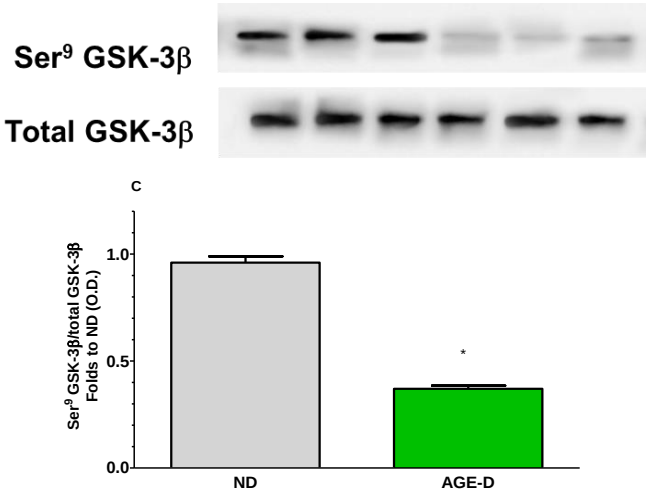

Figure 10.4: Evaluation of the phosphorylation of IRS-1, Akt and GSK-3β in muscle tissue

Representation of the phosphorylation of IRS-1, Akt and GSK-3β in the muscle tissue of mice subjected to ND or AGE-D, during 22 weeks. The results were obtained by the Western Blot technique, expressed as mean ± SEM on n = 6 per group. The densitometric analysis of the bands is expressed as the relative optical density (D.O.) of: phosphorylated IRS-1 (p-Ser1101) corrected with the corresponding total (IRS-1 Tot); Phosphorylated Akt (p-Akt473) corrected with the corresponding total (Akt Tot) and GSK-3β phosphorylated (p-Ser9) corrected with the corresponding total (GSK-3β Tot). The values were corrected with the corresponding tubulin and normalized with respect to the values of the ND group. The statistical analysis was carried out using T test *p < 0.05 vs ND

On the other hand, it is interesting to note how the diet enriched in AGEs has caused a significant reduction in the blood levels of incretins, GIP and GLP-1, which are known to exert insulin sensitivity effects, and which, according to what has emerged from recent studies, are also able to modulate inflammation, oxidative stress and apoptosis. In physiological conditions incretins are able to reduce hyperglycemia and proinflammatory cytokines [63]. Our data confirm the correlation between systemic levels of incretin and the levels of inflammatory markers, demonstrating that in the presence of an enriched diet in AGEs there is a simultaneous reduction in systemic levels of incretins which is associated with an increase in the systemic inflammatory profile (Figure 10.5).

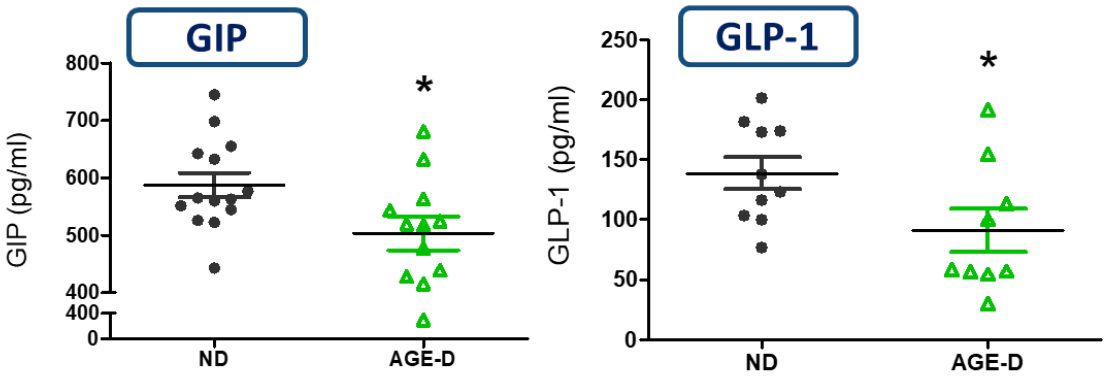

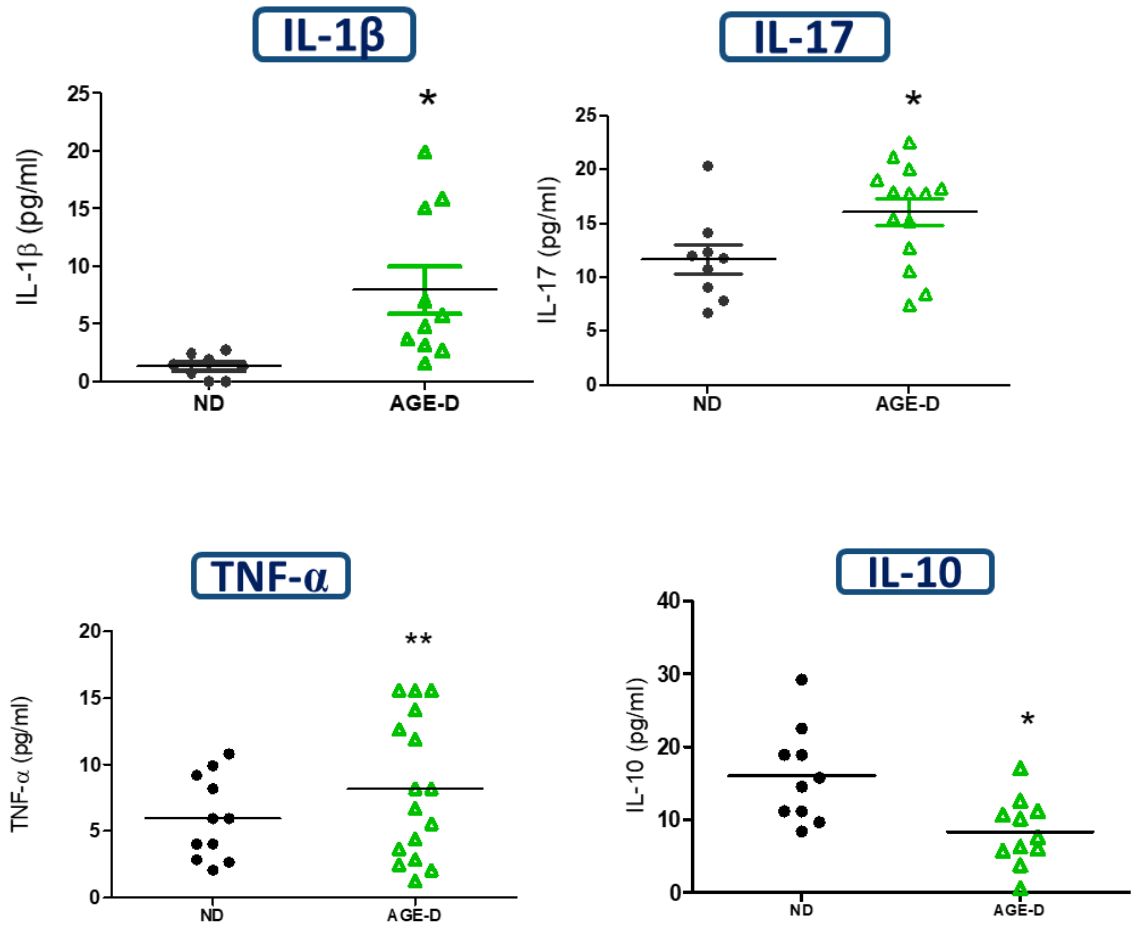

Figure 10.5 Effects of AGEs-enriched diet (AGE-D) on systemic levels of incretins and cytokines

Plasma levels of GLP-1, GIP, il-1β, IL-17, TNF-α and IL-10 in CD and AGE-D mice were measured by luminex suspension bead-based multiplexed Bio-Plex 3D system. Data are means ± S.E.M. (n = 15 per group). Statistical significance: ** $p < 0.01$, * $p < 0.05$ vs. CD.

AGEs can mediate their effects via specific receptors, such as RAGE, activating diverse signal transduction cascades and downstream pathways, including also the generation of reactive oxygen species (ROS). Oxidative stress occurs as a result of the imbalance between ROS production and antioxidant defenses. The accumulation of ROS results in turn, leading to a vicious cycle, in the induction of lipid peroxidation and glycoxidation reactions, which contributes to the elevated endogenous production of reactive aldehydes and their derivatives giving rise to advanced lipoxidation (ALEs) and glycation (AGEs), in turn facilitating protein cross-linking and aggregation resulting in an alteration in cell signaling and functioning, which causes cell damage. During the training at the laboratory of Professor Rosa Maria Saiz Menendez, at the University of Oviedo (Institute of Oncology "Principado de Asturias", Oviedo, Spain) I have evaluated the antioxidant capacity of the samples. For this purpose, I have used a method based on the free radical 2, 2-azinobis (ABTS). The reduction of ABTS, that occurs when antioxidants are present in the sample, produces a color desaturation of the solution and this reduction is measured by suppressing its characteristic wavelength. In figure 10.6 the antioxidant capacity of the samples is expressed in ascorbic acid equivalents. This data show that the simple addition of AGEs to a normocaloric diet determines a reduction in antioxidant capacity.

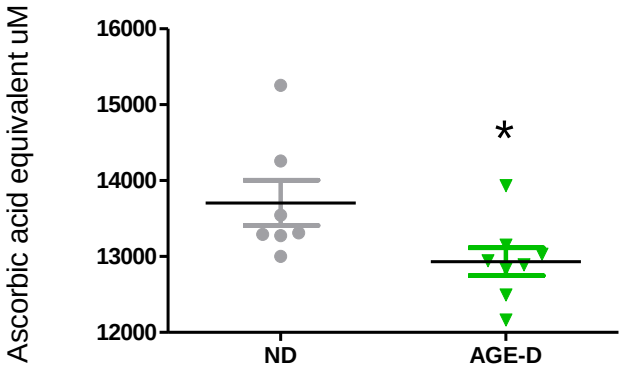

Figure 10.6 Effect of AGEs-enriched diet (AGE-D) on systemic levels of oxidatative stress

The antioxidant capacity of the samples is expressed in ascorbic acid equivalents. Data analyses by T test *p < 0.05 vs ND

Again at a systemic level, thanks to the collaboration of the research group of Professor Lokesk Joshi of the University of Galway in Ireland, we were able to document an effect on the glycomic component. Glycosylation is the most versatile and one of the most abundant protein modifications. It has a structural role as well as diverse functional roles in many specific biological functions. The formation of AGEs depends on a non-enzymatic glycation process, but their presence in biological molecules modifies their biomechanical and functional properties. Proteins, lipids and nucleic acids can be targets of advanced glycation end products, modifying enzyme-substrate interactions, protein-DNA interactions, protein-protein interactions, DNA regulation and epigenetic modulation, thus interfering with numerous physiological functions of the organism. The glycobiology research is limited by the lack of a technology for rapid analysis of glycan composition of glycoproteins. Currently used methods for glycoanalysis are complex, typically requiring high levels of expertise and days to provide answers and are not readily available to all researchers. The method is based on binding of an intact glycoprotein to the arrayed lectins, resulting in a characteristic fingerprint that is highly sensitive to changes in the protein's glycan composition. The large number of lectins, each with its specific recognition pattern, ensures high sensitivity to changes in the glycosylation pattern. A set of proprietary algorithms automatically interpret the fingerprint signals to provide a comprehensive glycan profile output. During my training at the University of Galway I have carried out the experiments using a 52 lectin microarray platform, in order to investigated the changes in terms of glycosylation on the plasma samples. In figure 10.7, are showed the graphs represent the binding fluorescence intensity of the samples with lectins, combining the results of experiments carried out in triplicate, as well as the clustering result.

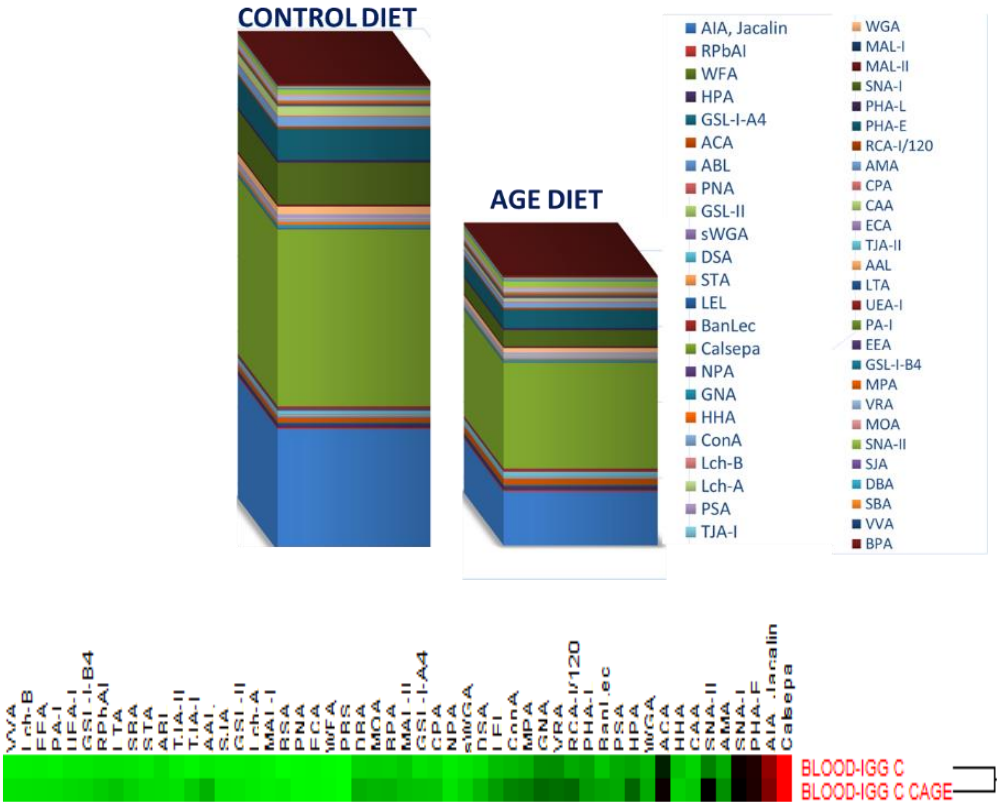

Figure 10.7 Effect of AGEs-enriched diet (AGE-D) on plasma proteins glycosylation profile

Clustering of lectin microarray profiles for fluorescently-labelled samples, based on their glycosylation profile. Red indicated high binding and green low binding.

Specifically, plasma samples were fractionated into two components, IgG and IgG-depleted fractions (DP) and fluorescently labelled. Similar structures were present in both fractions, albeit with diverse distribution, suggesting different glycosylation profiles between IgG and DP fractions (Figure 10.8). Binding on AIA, WGA, and SNA-I with labelled IgG fractions was significantly increased in the AGE-D group, suggesting an increase in galactose (AIA binding), presence of N-acetylglucosamine residues (WGA binding) and sialylation which would most likely be terminal α-(2,6) linked sialic acid (WGA and SNA-I binding). On the other hand, binding on AIA and PHA-E was significantly decreased in the AGE-D group in the DP fractions, implying a decrease in galactose (AIA binding) and N-linked complex type structures with β-linked Gal or Gal-β-(1,4)GlcNAc termini, with or without bisecting GlcNAc (PHA-E binding).

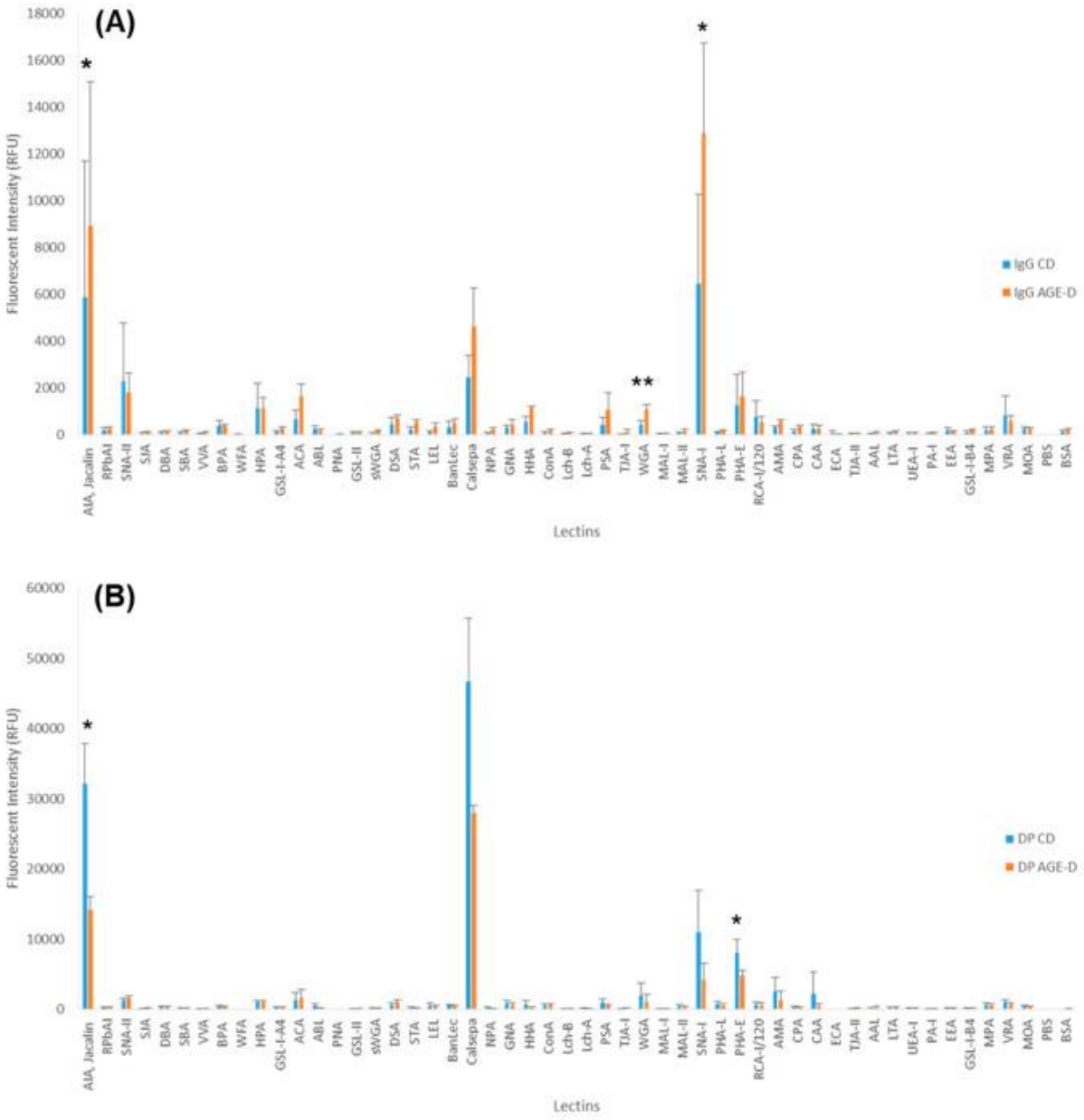

Figure 10.8 Chronic AGEs Exposure Evokes Changes in Plasma Glycosylation

Glycosylation profiles of (**A**) immunoglobulin fractions, control diet (IgG CD) and control diet enriched in AGEs (IgG AGE-D) and (**B**) plasma glycoproteins depleted from IgG fractions, control diet (DP CD) and control diet enriched in AGEs (DP AGE-D). Bars represent the average binding intensity of fluorescently labelled samples from three technical replicate experiments and error bars represent +/- standard deviation. Statistical significance: ** $p < 0.01$, * $p < 0.05$ vs. CD, determined by two-tailed, paired Student's t-test.

IgG glycosylation is known to be altered by environmental and *in vivo* status, and, in turn, to influence the immune response, acting therefore as a potential dynamic biomarker for disease or therapeutics [64]. Significant increase in galactosylation and IgG sialylation, most likely α-(2,6)-linked, were observed in mice fed with AGE-enriched diet compared to the control group. Level of sialylation is known to correlate to level of galactosylation [65]. Our feeding study showed an increase in circulatory pro-inflammatory cytokines; therefore, suggesting an activation of inflammation transcription factors. Decrease in sialylation and galactosylation is often associated with poor metabolic health [66] and with chronic inflammatory disease [67].

Whereas the opposite has been shown to be linked with anti-inflammatory response, with α-(2,6)-linked sialylation playing a key role in mediating the response [68]. However, in agreement with the cytokine profile here evoked by the AGE-D, it has been reported that the sialylated IgG fraction reduces phagocytosis by monocytes and induces a switch of the cytokine profile from IL-6/IL-8 to TNF-α/IL-1β [69]. We could thus hypothesize that in the acute body response to the AGE-D, the IgG glycosylation is altered in an attempt to counteract or attenuate the effect of the circulatory proinflammatory cytokines.

Using immunochemistry analysis, we also documented that the AGE-enriched diet evoked CML accumulation and increased RAGE expression in both submandibular salivary glands and the ileum tract of intestine. Specifically, in the submandibular salivary glands of AGE-D mice, we detected increased CML immunopositivity in the extracellular spaces among serous and mucous acini and in the cytoplasm of duct cells, while RAGE was mainly expressed in the ducts of myoepithelial cells and basal lamina, compared to the CD mice. Similarly, CML accumulation was higher in the villi epithelium of the ileum of AGE-D mice when compared to CD mice and RAGE expression was maximally expressed at the basal membrane and muscularis mucosae of AGE-D mice (Figure 10.9)

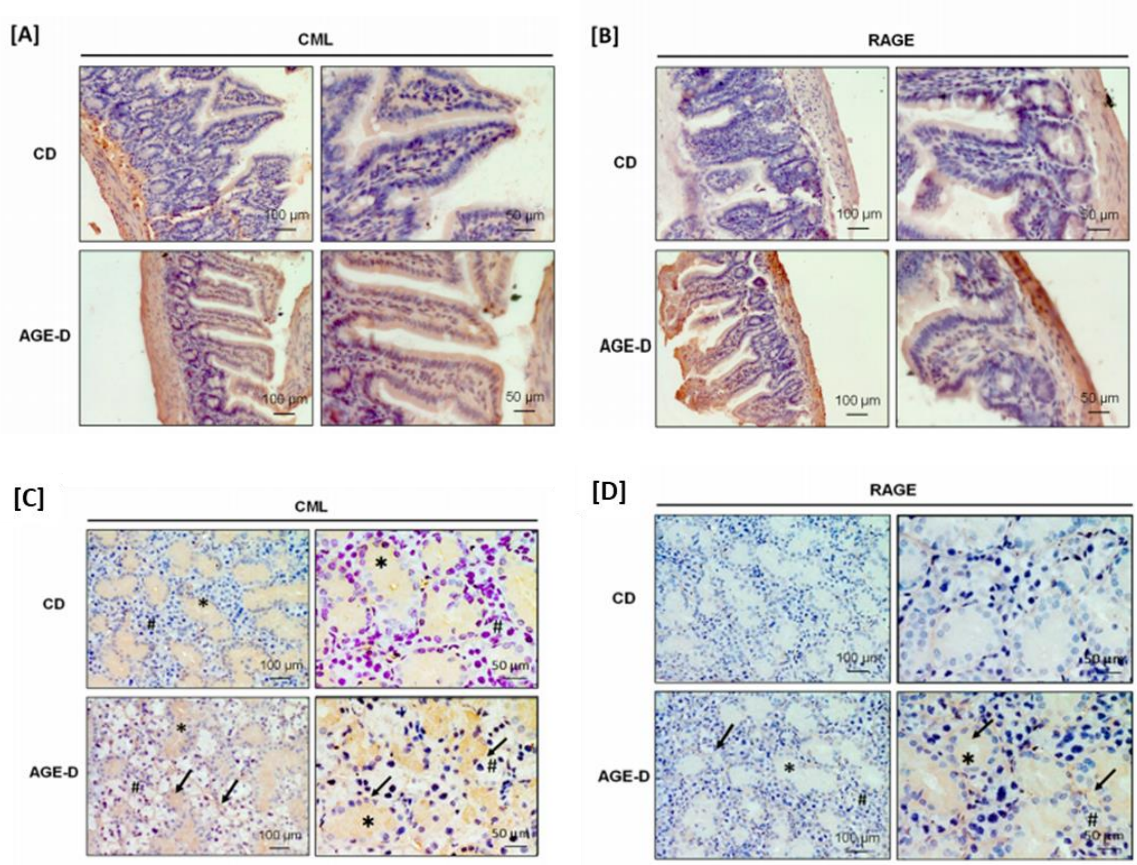

Figure 10.9 Effect of AGEs-enriched diet (AGE-D) on plasma proteins glycosylation profile

Immunohistochemistry performed on paraffin-embedded submandibular salivary glands (A-B) and ileum portion of intestine (C-D). (A)Photomicrographs at 20× and 40× magnification for carboxymethyllysine (CML) immunopositivity, showing increased amounts in acini (#) and ducts (∗), as indicated by arrows, of the AGE-D mice. (B) Photomicrographs at 20× and 40× magnification for receptor for AGEs (RAGE) immunopositivity, which was increased in the myoepithelial and basal lamina of ducts as indicating by arrows. (C) Photomicrographs at 20× and 40× magnification for CML immunopositivity, showing

increased amounts in villi epithelium of the AGE-D mice. (D) Photomicrographs at 20× and 40× magnification for RAGE immunopositivity, mostly increased in the basal membra

We finally have also documented the effect of AGEs at intestinal microbiota profile. The data obtained in collaboration with the research group of Professor Kieran Tuohy of the University of Trento is presented here. The exogenous AGEs introduced with the diet have determined a dysbiosis (Figure 10.10). Interestingly, a positive correlation was identified between the s24-7 family, the prevotella gene and the lactabacillus gene with GIP and GLP-1 and a negative correlation with Il-1β and Il-17. This correlation was also confirmed by the fact that the ruminococcus gene of lachospiracea, the oscillospira gene and the parabacterroides gene correlate positively with Il-1β and Il-17 and negatively with incretins (Figure 10.11).

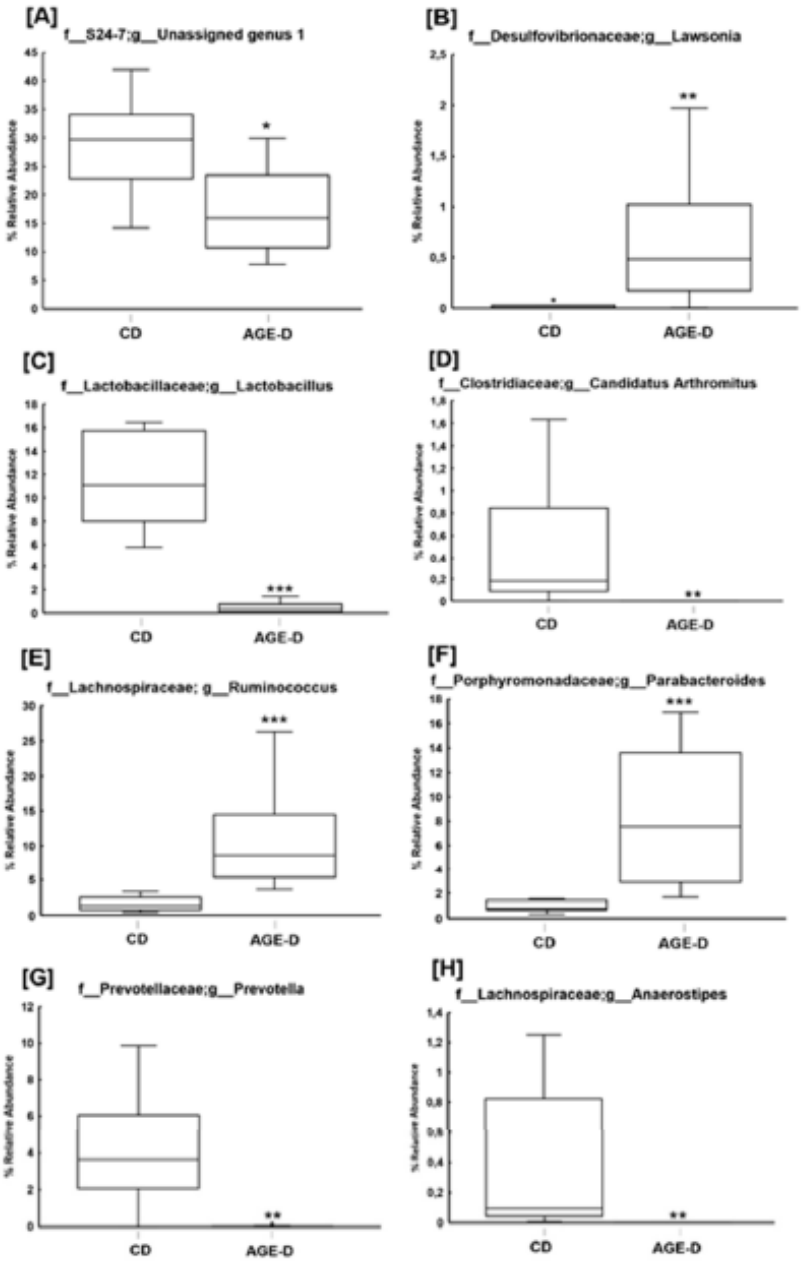

Figure 10.10 Exogenous AGEs affect gut microbiota composition

(A–H) Boxplots of percentage relative abundance of fecal microbial genera in CD (n = 8) and AGE-D (n = 10) mice at 22 weeks (T22) of dietary intervention after 16SrRNA sequencing using V3-V4 targeted primers. “Unidentified genus 1”: a genus within the Family S 24-7 which could not be assigned at a percentage sequence homology of at least 95% to any existing genera within the reference database (http://greengenes.lbl.gov).

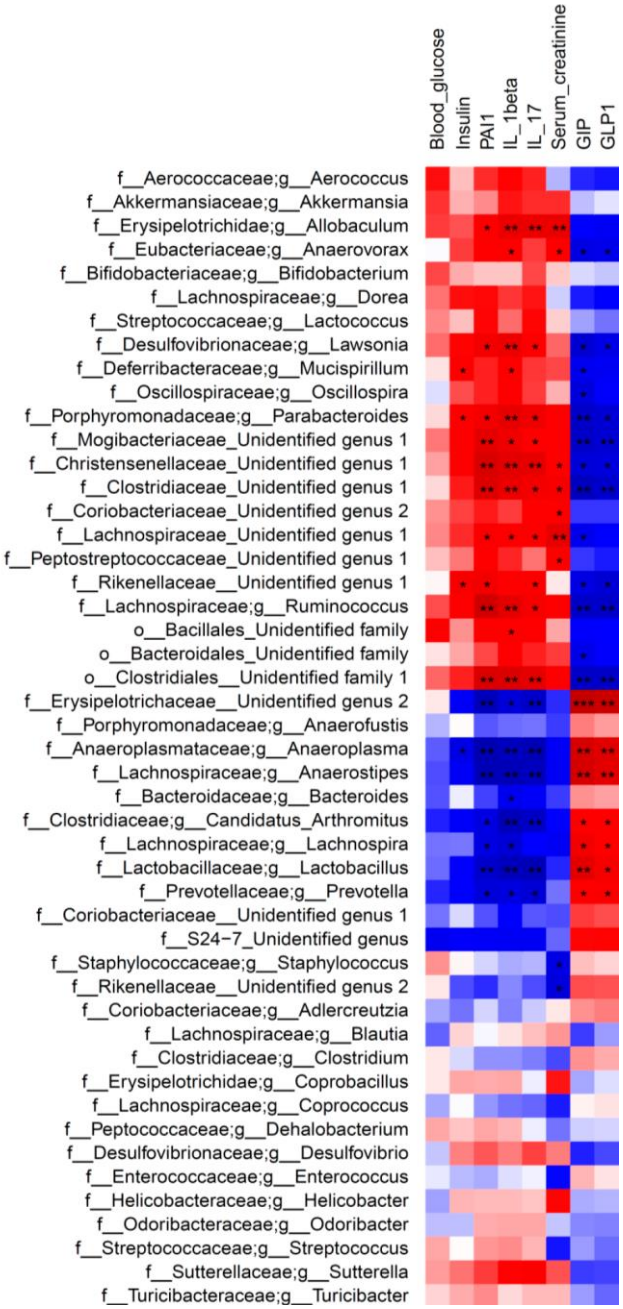

Figure 10.11 Heatmap of Spearman’s correlation between the fecal bacteria genera and systemic measurements in CD and AGE-D groups

Dark red indicates positive correlation, while dark blue represents negative correlation. Statistical significance: * $p < 0.05$, ** $p < 0.01$. Genera and familieswere reported as “Unidentified” when they could not be assigned to any genera/family within a given family/order at a percentage sequence homology of 95% and 90%, respectively, to existing genera and families in the reference database (http://greengenes.lbl.gov).

10.3. Tagatose reduced Susceptibility to Sugar-Induced Metabolic Derangements when Compared to Fructose

In order to counteract the state of development of chronic diseases caused by excessive consumption of fructose, new sweeteners have taken on great importance, with the aim of reducing calorie consumption. Among the alternative sugars, one of the most promising is D-tagatose, an epimer of fructose that has good sweetening properties and a low calorie content. [70]. This natural ketohexose is proved to be a potential replacement to sucrose-like high-calorie bulk sweeteners as food additives, thanks to its poor absorption and metabolization within the human body [71]. Unlike fructose that has high glycation capacity and promotes lipogenesis, D-tagatose has a lower glycation index [72]. In human subjects, D-tagatose lowered postprandial blood glucose and insulin response allegedly through inhibiting intestinal disaccharides as like as glucose transport. In addition, the results of a phase 3 clinical trial illustrated the potential for D-tagatose, which effectively lowered HbA1c levels in type 2 diabetic patients compared to placebo [73].

Thus, the aim was to determine if and how D-tagatose alters lipid and sugar metabolism in comparison to the results obtained with fructose, well known for its glycative and lipogenic potential.

Four-week-old male C57Bl/6j mice (Charles River Laboratories, Calco, Italy, n = 30) were housed in a temperature-controlled environment with a 12 h light/dark cycle, were randomly allocated into the following dietary regimens: a group fed a normocaloric diet and drinking tap water (ND group, n=6), a group fed a ND and drinking a 30% fructose syrup (L-Fr group, n=6), a group fed with 30% fructose solid diet and drinking tap water (S-Fr group, n=6), a group fed a ND and drinking a 30% D-tagatose syrup (L-Tg group, n=6), and a group fed with 30% D-tagatose solid diet and drinking tap water (S-Tg group, n=6) during 24 weeks. All groups received drink and food *ad libitum*.

As shown in Table 10.3, chronic exposure to Fr diet evoked a two-fold increase in body weight gain, when compared to ND at 24 weeks of dietary manipulation. In contrast, body weight gain recorded in mice exposed to D-tagatose was similar to that recorded in control mice. Furthermore, while solid and liquid fructose feeding led to increased abnormal systemic glucose homeostasis (Figure 10.12), altered lipid profile (Figure 10.13) and renal function parameters (Figure 10.14), none of these metabolic abnormalities were detected when mice were fed with both the solid and liquid D-tagatose diets. These data documented that the metabolic abnormalities caused by exposure to an unhealthy diet containing high concentrations of fructose were not recorded when fructose was replaced by D-tagatose, thus demonstrating that the proposed change in nutrient composition favorably affected metabolic homeostasis.

Group	ND	L-Fr	S-Fr	L-Tg	S-Tg
Body weight gain (g)	3,52 ± 0,26	6,00 ±0,26**°°	6,32 ±0,50**°°	2,64±0,43	2,38±0,27

Table 10.3 Effects of fructose and tagatose on body weight gain after 24 weeks of dietary manipulation
Data are means ± S.E.M. **p<0,01 vs ND; °°P<0,01 VS tagatose

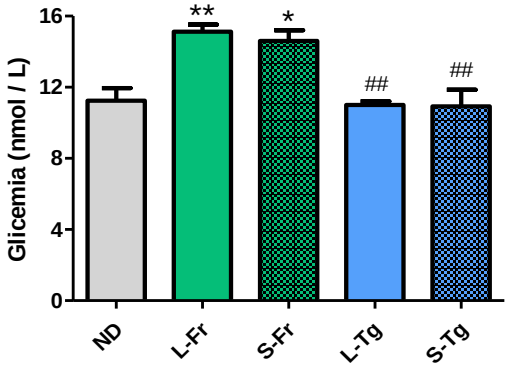

Figure 10.12 Effects of fructose and tagatose on the glycemic profile.

Representation of the concentration of glucose in the blood of mice subjected to a different diet, during 24 weeks. The results are expressed as the mean ± SEM on n = 6 per group. Statistical analysis was used via one-way ANOVA followed by the correction performed using the Bonferroni post test: ** p <0.01 compared to a ND; * p <0.05 compared to a ND; ## p <0.01 compared to the corresponding formulations of Fr

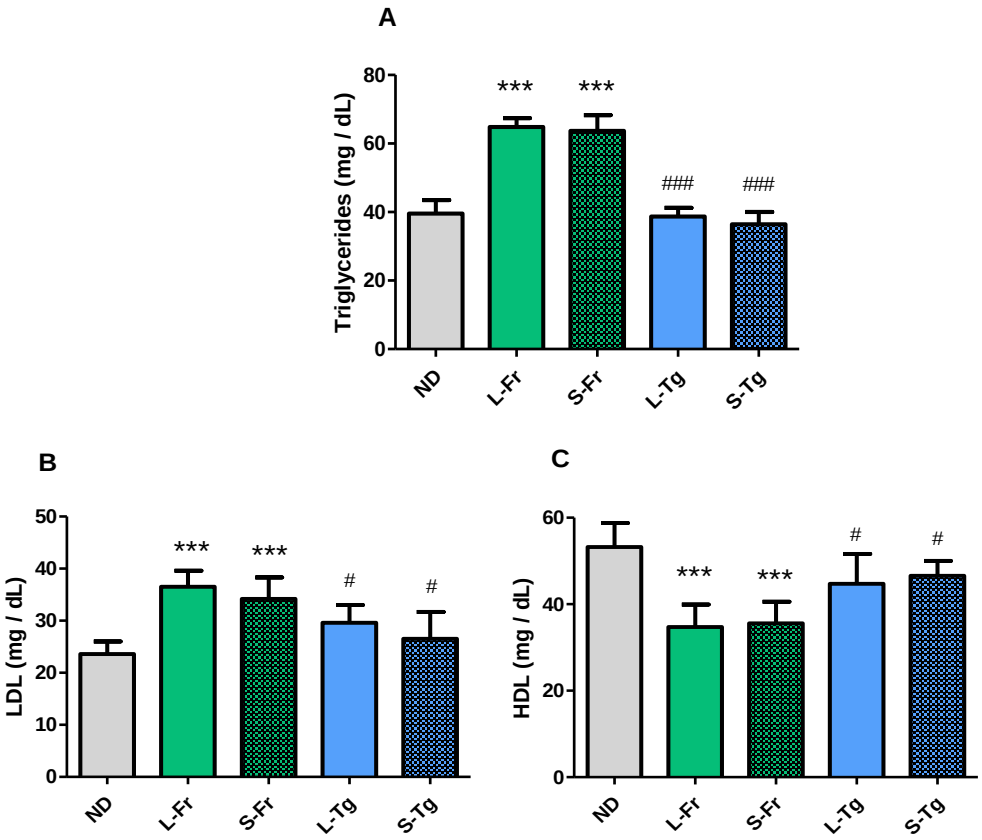

Figure 10.13 Effects of fructose and tagatose on the lipid profile.

Representation of plasma triglyceride (A), LDL (B) and HDL (C) levels of mice subjected to different diet regimens, during 24 weeks. The results were expressed as mean ± D.S. on n = 6 per group. The statistical analysis was carried out using ANOVA One-way followed by the correction made using the Bonferroni post test: *** p <0.001 compared to ND; ###p < 0,001 compared to the corresponding formulations of Fr; #p < 0,05 compared to the corresponding formulations of Fr.

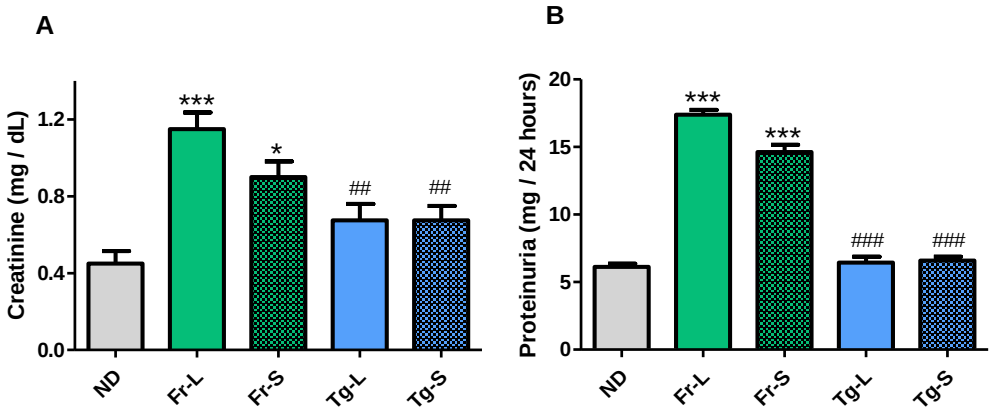

Figure 10.14 Effects of fructose and tagatose on renal function parameters.

Representation of plasma creatinine (A) and proteinuria (B) levels of mice subjected to different diet, during 24 weeks. The experimental groups were divided as follows: ND (n = 6); Fr-L (n = 6); Fr-S (n = 6); Tg-L (n = 6) and Tg-S (n = 6). The results are expressed as the mean ± SEM on n = 6 per group. Statistical analysis was used using one-way ANOVA followed by the correction performed using the Bonferroni post test. *** p <0.001 with respect to ND; * p <0.05 with respect to ND: ### p <0.001 with respect to the associated formations of Fr; ## p <0.01 with respect to the formative instructions of Fr.

Interestingly, fructose formulations led to significant AGEs accumulation in mouse hearts, as well as a robust increase in myocardial AGE receptor (RAGE), as expected, instead Western blot analysis demonstrated that D-tagatose feeding was associated with a significantly lower AGEs accumulation and RAGE hyperexpression when compared to those recorded in the Fr group (Figure 10.15).

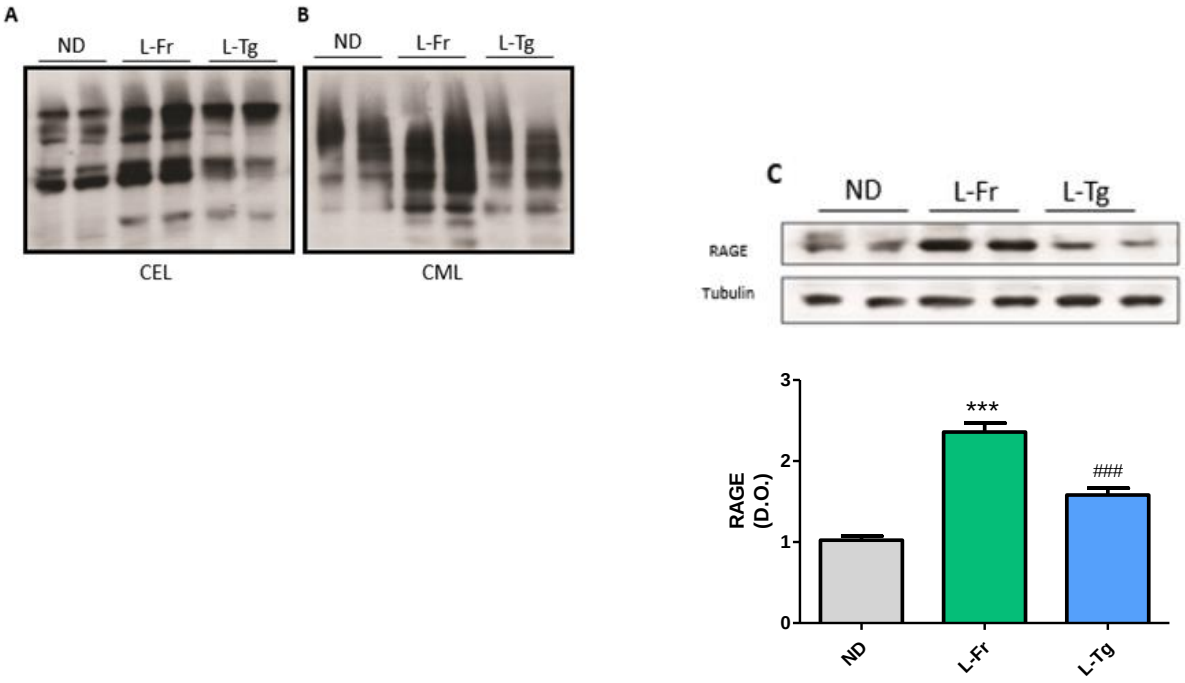

Figure 10.15 Effects of liquid sugars feeding on myocardial accumulation of AGE and expression of RAGE.

Representative Western blotting and relative densitometric analysis of CEL- and CML-glycated proteins (A and B, respectively) and RAGE expression (C) in the heart of mice fed for 24 weeks with a ND or L-Fr/ L-Tg. Values are represented as means ± S.E.M. of 6 animals per group. ***p<001 vs. ND. ### p<001 vs. L-Fr diet.

Our data demonstrate significant qualitative and quantitative sugar dependent differences in early markers of organ injury, due to selective interference of fructose with the AGEs/RAGE cascade, not recorded when mice were fed with D-tagatose, confirming the pivotal role of accumulation of AGEs in metabolic derangements. We offered also for the first time, the experimental evidence of the lower chemical reactivity of D-tagatose when compared to its epimer fructose. Thus, we can state that slight differences in the position of the hydroxyl group at carbon atom 4 may result in significant differences in sugar reactivity and sugar metabolism. Thanks to its very low caloric value and organoleptic similarities with fructose, the rare sugar D-tagatose may represent a safer paradigm of sweeteners with limited toxicological impact on obesity and associated metabolic disorders.

10.4. Effects of Pyridoxamine administration as AGEs scavenger for dietary intervention

As consequence of the results showing a crucial role of AGEs in evoking marked cellular alterations and organ dysfunction, one of the most current challenging topics was to identify pharmacological treatments that prevent this accumulation, and in particular with focus on preventing the onset of diabetic nephropathy by acting on the initial stages of diabetes related renal dysfunction. One of the most recently proposed pharmacological tools is Pyridoxamine, a structural analog of vitamin B6 that exerts antiglycative effects. However, so far, the potential beneficial effects of pharmacological modulation of AGEs production in the context of diet-related kidney dysfunction have been poorly investigated. To our knowledge, nephroprotective effects of pyridoxamine supplementation have been tested only in strains of mice genetically programmed to develop diabetic nephropathy, with limited insights on molecular mechanisms [74]. Our study aims to investigate whether oral administration of pyridoxamine (1 g/L, the equivalent of about 150mg/kg/day) prevents the onset of diet related kidney dysfunction, affecting selective inflammatory and profibrotic signaling pathways in a nongenetic animal model of diet-induced metabolic disease.

Four-week-old male C57Bl/6j mice were randomly allocated into the following dietary regimens: normocaloric diet (ND, n=15) and a high-fat high fructose diet (HFHF, n=20) for 12 weeks. After three weeks of dietary manipulation, two subgroups of ND and HFHF began pyridoxamine supplementation in the drinking water for the remaining nine weeks (ND + P, n=5; HFHF + P, n=10).

Our experiments demonstrated that despite the body weight gain was not significantly reduced by pyridoxamine, the concentration of fasting serum glucose was significantly reduced by daily administration of pyridoxamine remaining still higher than that recorded in the ND group. Chronic exposure to HFHF strongly increased serum levels of triglycerides and total cholesterol. Most notably, pyridoxamine treatment significantly normalized the changes in triglycerides contents and trendily reduced the levels of total cholesterol (Table 10.4).

	SD (n=10)	ND+P (n=5)	HFHF (n=10)	HFHF+P (n=10)
Body weight (g)	25,4 ± 1,3	26,6 ± 3,0	32,8 ± 1,7*	34,7 ± 3,6*

Blood glucose (mg/dl)	72,8 ± 18,9	61,8 ± 16,2	138,8 ± 12,7*	104,6 ± 9,7*°
Plasma triglycerides (mg/dl)	37,1 ± 7,6	29,3 ± 5,5	50,5 ± 9,2*	34,7 ± 4,7°
Plasma cholesterol (mg/dl)	77,2 ± 6,1	84,8 ± 16,4	97,2 ± 8,2*	87,2 ± 2,2

Table 10.4: Effects of HFHF and pyridoxamine administration on mouse body and blood chemistry at 12 weeks of dietary manipulation

Values are mean ± SEM. $*p < 0.05$versus ND; $°p < 0.05$ versus HFHF.

Mice fed with the HFHF exhibited a severe degree of vacuolar degeneration, as well as a complete loss of the brush border integrity. Damage was observed in S1-S2 and S3 parts of the tubule. Pyridoxamine administration prevented the diet induced morphological alterations. Kidneys from groups fed with ND showed proximal tubules with a normal well preserved histoarchitecture (Figure 10.16A-B). The HFHF-induced renal pathology correlated with decline in kidney function, as shown by increased levels of serum creatinine, which was significantly reduced by pyridoxamine administration (Figure 10.16C). Similarly, albumin levels were increased in the HFHF group compared with the control group and slightly reduced by pyridoxamine treatment, without reaching a statistical significance (Figure 10.16D).

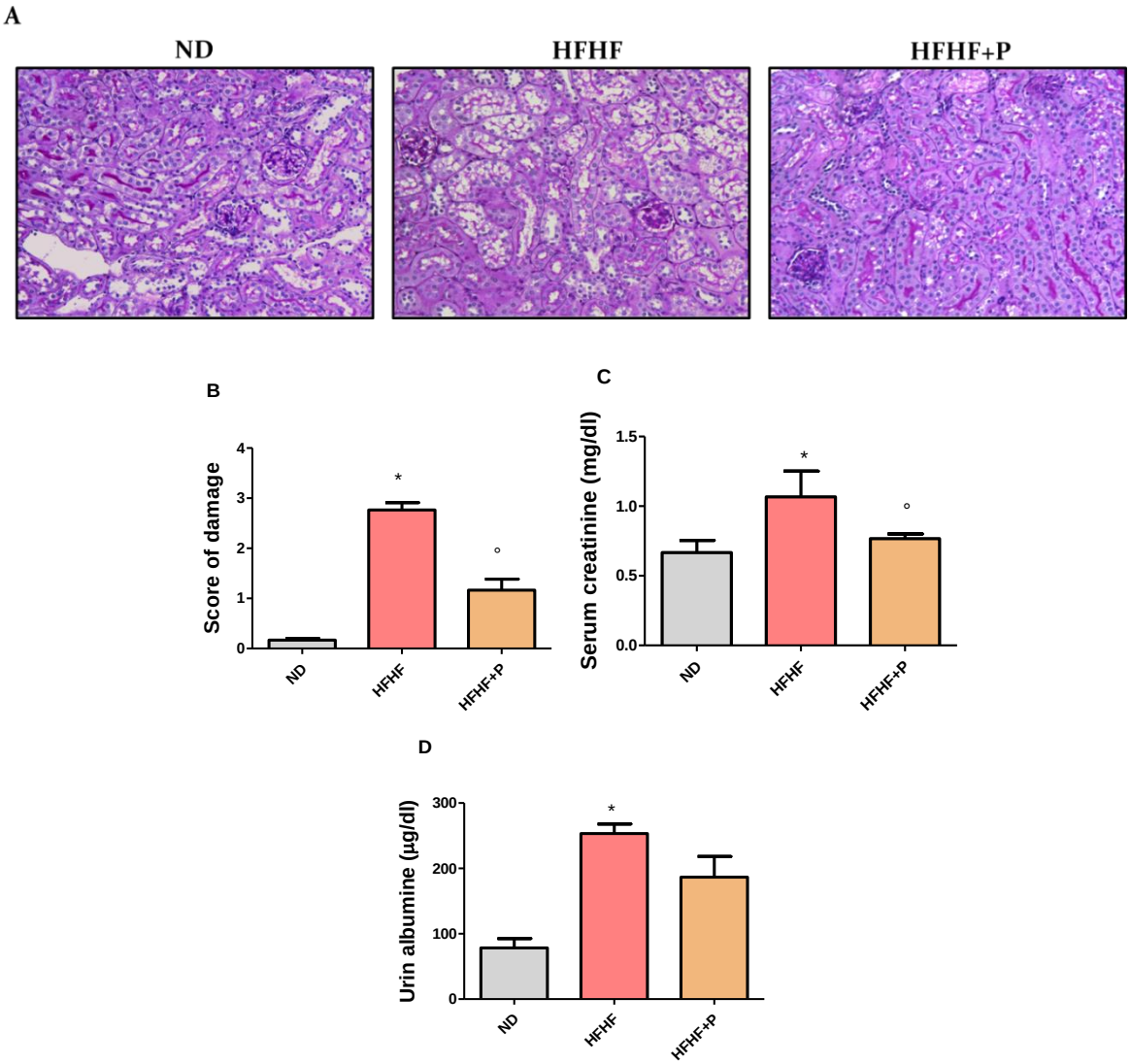

Figure 10.16: Effects of HFHF and pyridoxamine administration on kidney structure

Representative kidney section from the experimental group stained with PAS (A) 20X, score quantification (B), Serum creatinine (C) and urinary albumin (D) levels. Values are mean ± SEM of five animals per group $*p < 0.05$ vs ND; §$p < 0.05$ vs HFHF.

These modulatory effects of pyridoxamine, that I have analyzes from a mechanistic point of view, demonstrate that this antiglycative compound exerts nephroprotective effects by at least in part, reducing the local accumulation of AGEs (Figure 10.17).

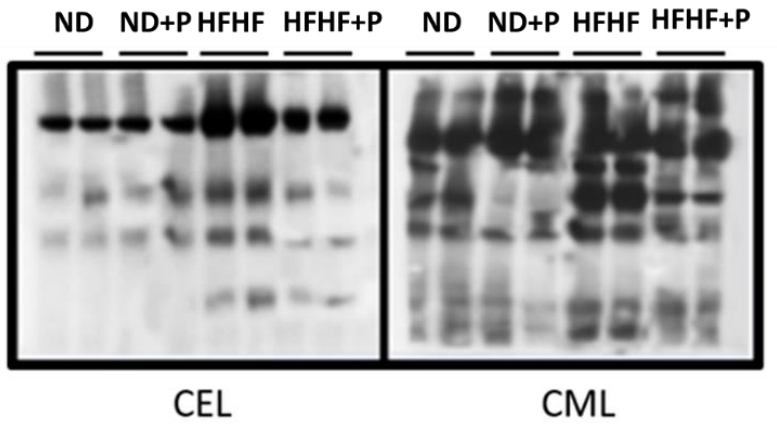

Figure 10.17 Effects of HFHF and pyridoxamine administration on kidney AGE expression

CEL- and CML- glycated proteins were analyzed by western blot on kidney homogenates obtained from mice exposed to ND or HFHF with or without pyridoxamine administration.

2) study the effects of the pharmacological modulation of selective pro- and anti inflammatory pathways of metaflammation in experimental models of cardiometabolic diseases.

10.5. Impact of hypercaloric diets on metaflammation development

Metabolically driven, chronic, low-grade inflammation has a crucial role in the pathogenesis of obesity and type 2 diabetes, and multiple stress-signaling cascades link insulin resistance and the immune response [75]. Enhanced serum concentrations of proinflammatory cytokines play a key role in the development of metabolic derangements [76].

NF-κB (p65) one of the main transcription factors implicated in the inflammatory process, it is responsible for the expression of a large amount of inflammatory factors such as cytokines, chemokines and adhesion proteins. HFD, but more HFHF and Fr cause an activation of this pathway in kidney and myocardium (Figure 10.18).

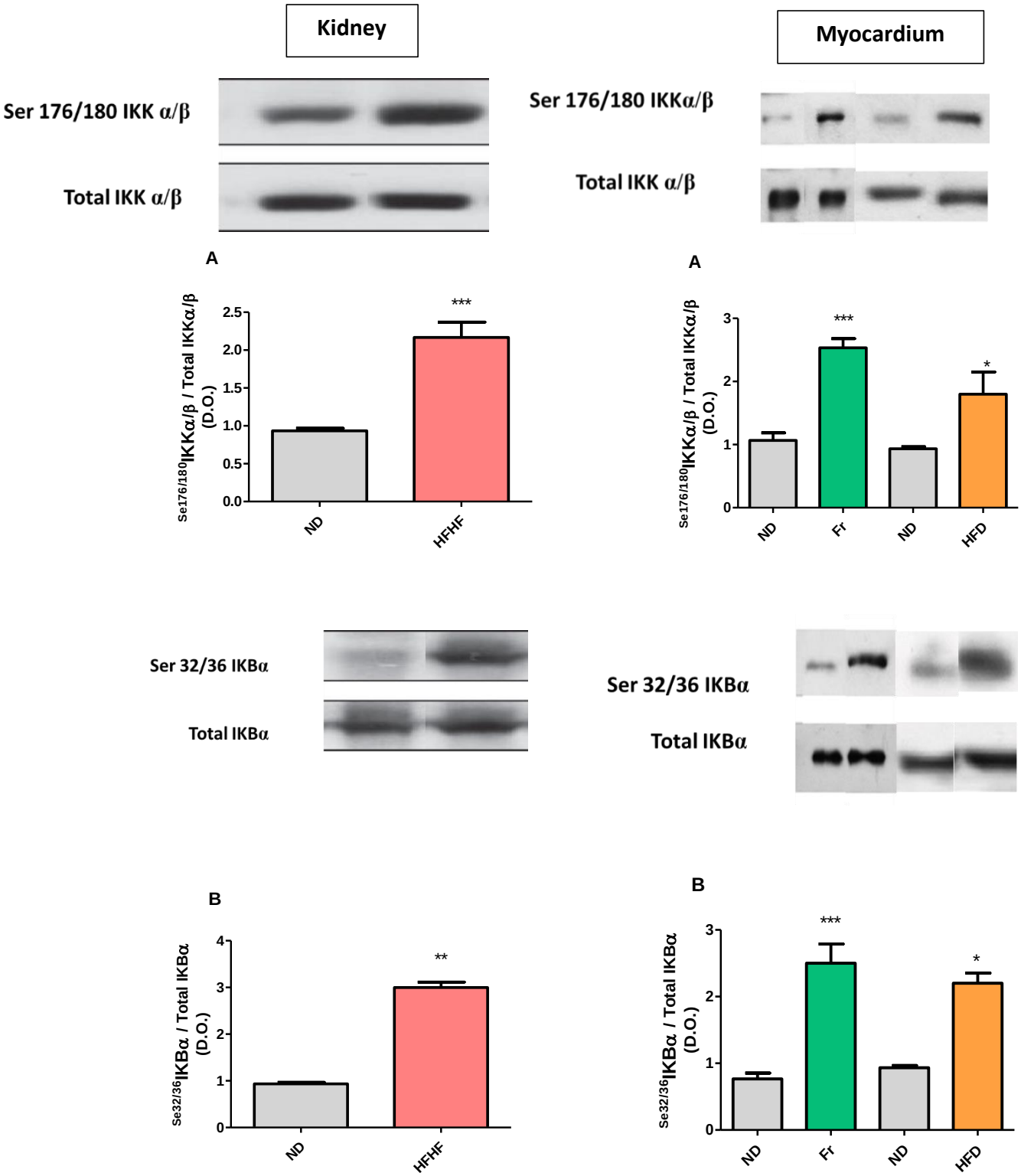
Kidney
Myocardium
Ser 176/180 IKK α/β
Total IKK α/β
Ser 176/180 IKKα/β
Total IKK α/β
A
A
Se176/180IKKα/β / Total IKKα/β (D.O.)
***
2.5
2.0
1.5
1.0
0.5
0.0
ND
HFHF
Se176/180IKKα/β / Total IKKα/β (D.O.)
***
*
3
2
1
0
ND
Fr
ND
HFD
Ser 32/36 IKBα
Total IKBα
Ser 32/36 IKBα
Total IKBα
B
B
Se32/36IKBα / Total IKBα (D.O.)
**
4
3
2
1
0
ND
HFHF
Se32/36IKBα / Total IKBα (D.O.)
***
*
3
2
1
0
ND
Fr
ND
HFD

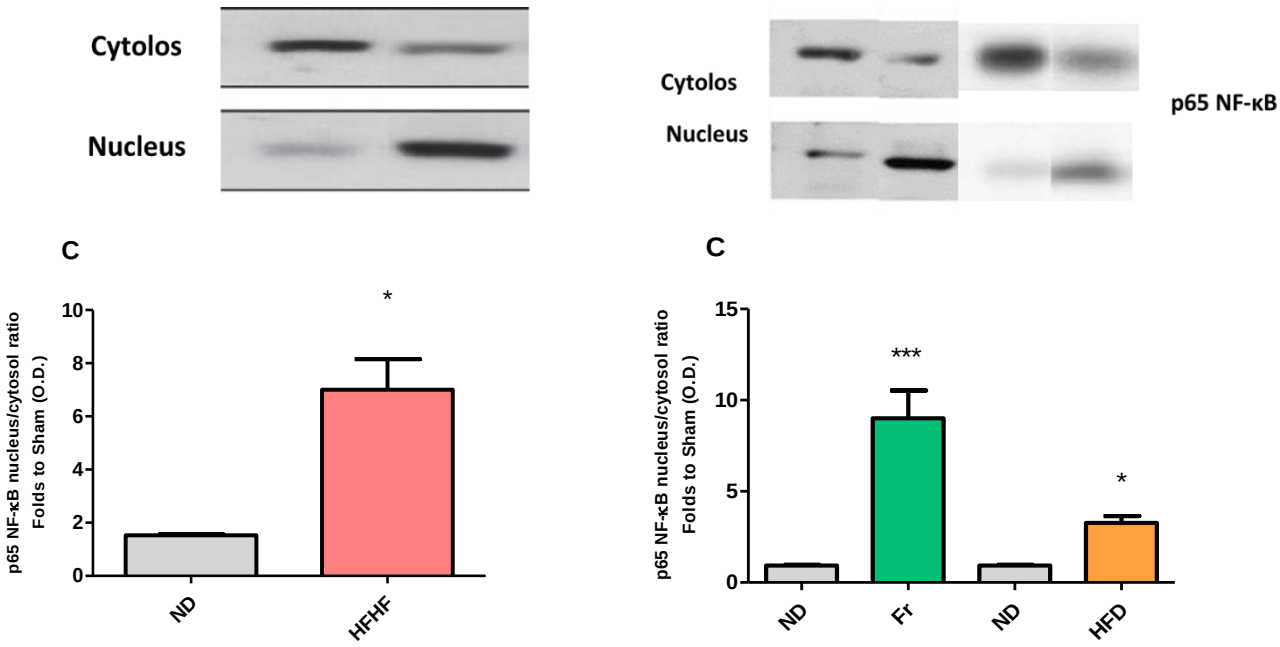

***Figure 10.18 Evaluation* of the activation of the NF-kB signal cascade**

Evaluation of the phosphorylation of IKKα / β (A) and IkBα (B) normalized to IKKα and kBα expression and the translocation of the p65 (C) subunit of NF-kB expressed as the ratio between nucleus and cytoplasm, normalized for the corresponding Tubulin or Histone 3. The data was obtained through the Western Blot technique with homogenates of renal tissue and myocardial tissue from ND, Fr, HFD and HFHF mice. Protein expression is assessed by densitometric analysis (O.D.) normalized for ND. Average values ± SEM on 5-6 samples per group: *** p <0.001 vs ND; ** p <001 vs. ND

One of the most recently identified signaling pathways, whose activation seems to affect many metabolic disorders, is the NLRP3 inflammasome, that integrates multiple exogenous and endogenous danger signals into the immediate secretion of IL-1β and IL-18. Most recent data suggest that activation of the NLRP3 inflammasome complex contributes to the pathophysiological mechanisms that explain the development of visceral obesity and insulin resistance. Thanks to its wide distribution in different tissues and organs, the NLRP3 inflammasome protein complex may represent a crucial signaling pathway that facilitates organ crosstalk and local injury in tissues target of metabolic damage [77]. Previous works of Professor M.Collino's lab had demonstrated the activaction of NLRP3 inflammasome pathway in mice fed with a HFD [78] and HFHF [79]. Here we extended the previous findings on the impact of Fructose-enriched diet on NLRP3 inflammasome expression in the liver (Figure 10.19), that together with the results obtained with caspase1 and IL-1β (Paper 2 on discussion section) confirmed the activation of the NLRP3 inflammasome pathway.

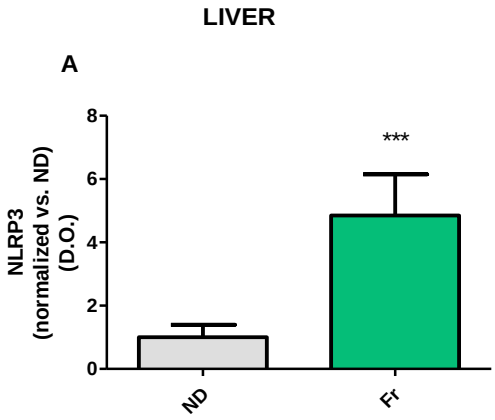

Figure 10.19 NLRP3 expression

NLRP3 in liver, has been evaluated by Western blotting analysis. Data are means ± S.E.M. of 6–10 mice per group. Statistical significance: ***P<0.001, vs. ND.

10.6. Baricitinib counteracts metaflammation, thus protecting against diet-induced metabolic abnormalities in mice

Recent evidence suggests a substantial pathogenic role for the Janus kinase (JAK) / signal transducer and activator of transcription (STAT) pathway as a potential master regulator in the signaling events involving more than 50 cytokines, many of which play a pivotal role in the pathophysiology of metaflammation.

Thus we have investigated the effects of the pharmacological modulation of the JAK cascade with baricitinib a JAK1/2 inhibitor, in an *in vivo* model of diet-induced metabolic alterations.

4-week old male C57BL/6 mice were randomly allocated to three experimental groups (n=15 per group): mice fed with a normocaloric diet (ND group), mice fed with a high fat high sugar diet (HFHF group) for 22 weeks and mice fed with HFHF for 22 weeks and treated with baricitinib (10 mg/kg die, p.o.) for the last 16 weeks (HFHF+B).

In our experiments mice exposed to HFHF showed an excessive development of the expected dysmetabolic phenotype. In fact, they displayed increased levels of serum triglycerides, cholesterol and LDL (Table 10.5), higher body weight, blood glucose levels and an impairment in OGTT, when compared to ND group (Figure 10.20).

	ND *(n = 15)*	**HFHF** *(n = 15)*	**HFHF+B** *(n = 15)*
Triglycerides, *mmol/L*	0.87±0.03	1.07±0.02*	0.98±0.03
Total cholesterol, *mmol/L*	2.77±0.07	3.43±0.07*	2.89±0.03§

LDL, *mmol/L*	0.57±0.06	0.91±0.05*	0.59±0.03§
HDL, *mmol/L*	1.67±0.05	2.01±0.02*	1.71±0.04§
LDL : HDL *ratio*	0.32±0.04	0.43±0.03*	0.32±0.02§

Table 10.5: Effects of HFHF and baricitinib administration on mouse blood lipid profile at 22 weeks of dietary manipulation

With the Baricitinib treatment the metabolic abnormalities were reverted, proving that this JAK1/2 inhibitor protects against the deleterious effects evoked by exposure to a HFHF, when chronic administrated during the last 16 weeks.

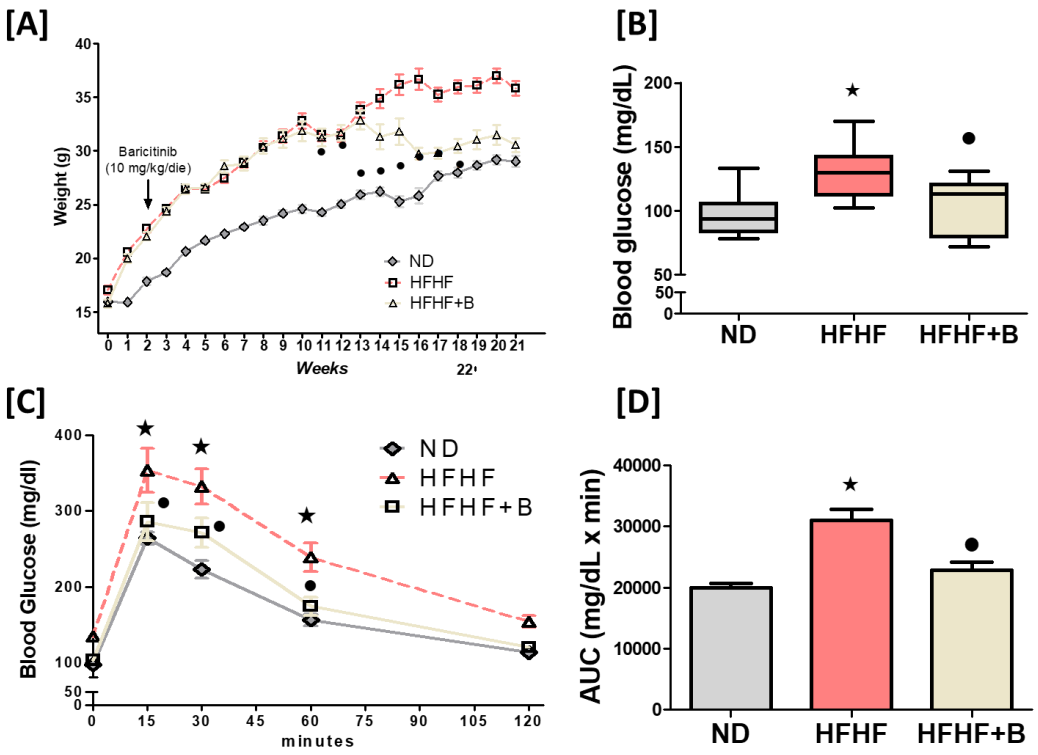

Figure 10.20: Effects of HFHF and baricitinib administration on mouse body weight at 22 weeks of dietary manipulation

(A). Basal non-fasted blood glucose was measured at 22 weeks 6 h prior to harvest via the saphenous vein (n = 6–10/group). (B). Oral glucose tolerance was assessed over 120min at 22 weeks 1 week prior to harvest. (C). The area under curve (AUC) of OGTT was calculated for respective groups and used for statistical analysis (D). All data are expressed as mean ± SEM for n number of observations. $*p < 0.05$ versus ND; $•p < 0.05$ versus HFHF

Also, on a molecular point of view our study provides the first evidence that the improved glucose tolerance evoked by baricitinib administration in HFHF was, at least partially, mediated by enhancing the insulin-related signaling pathway in both liver and skeletal muscle. In fact, the defects in insulin signaling observed with HFHF fed mice were restored by pharmacological inhibition of JAK activity (Figure 10.21).

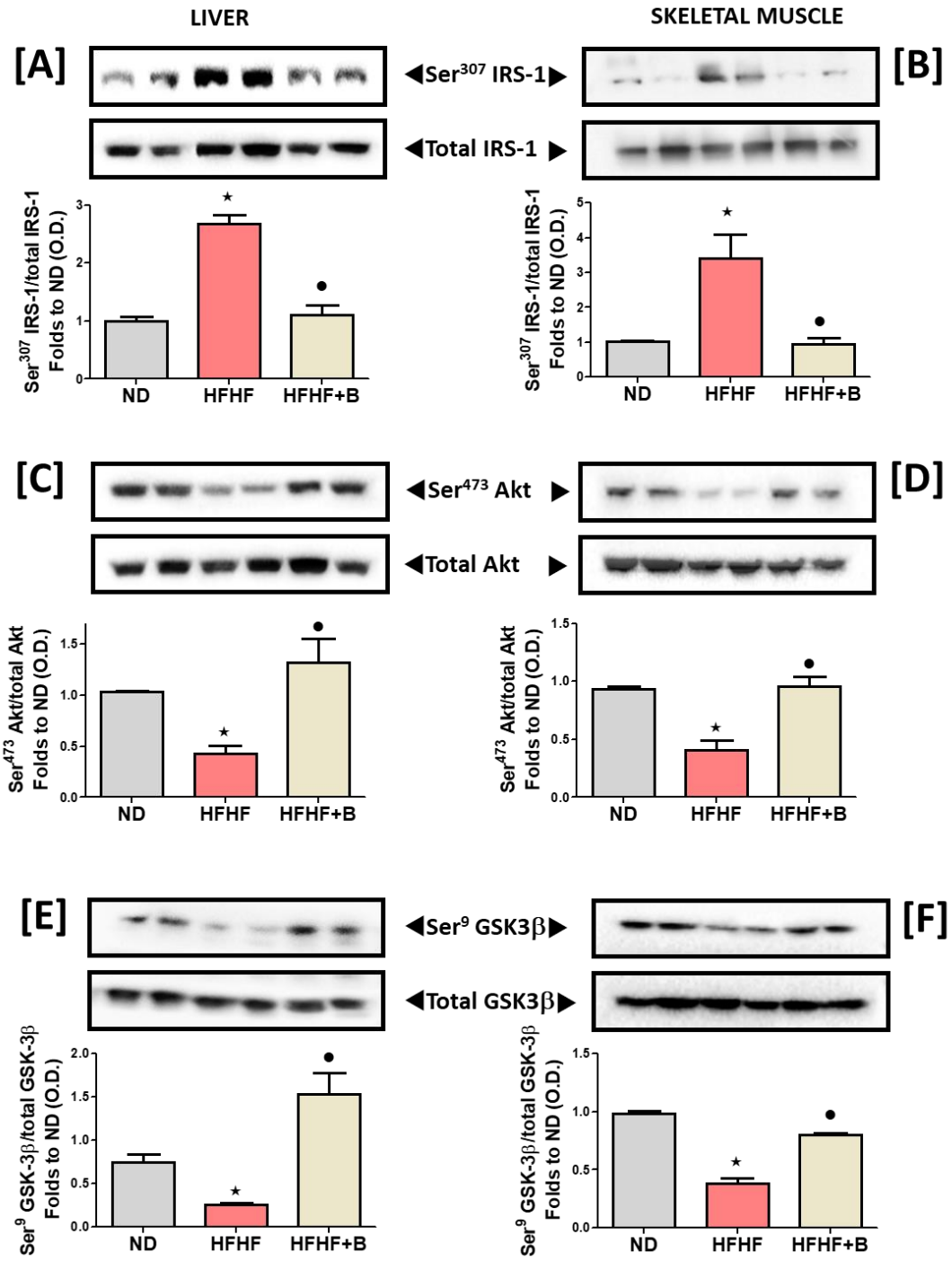

Figure 10.21: Baricitinib attenuates HFHF induced development of peripheral insulin resistance

Western blot analysis for Phosphorylation of Ser307 on IRS-1 in liver (A) and Skeletal muscle (B) and normalized to total IRS-1; for phosphorylation of Ser473 on Akt in liver (C) and the skeletal muscle (D) and normalized to total Akt; for phosphorylation of Ser9 on GSK-3ß in the liver (E) and in the skeletal muscle (F) and normalized to total GSK-3ß. Data are expressed as mean ± SEM for n number of observations. *p < 0.05 vs. ND; •p < 0.05 vs HFHF.

The best characterized activators of the JAK signaling in the context of metabolic disorders, are adipokines, including leptin and resistin, which are known to be involved in the pathogenesis of insulin resistance [80] (Figure 10.22). Treatment with baricitinib also resulted in an increase in the serum levels of GIP and ghrelin, both of which are involved in glucose homeostasis conferring protective effects for metabolic dysfunctions. In fact, beyond its

insulinotropic effects in the pancreas, GIP has been demonstrated to exert important biological actions in many other tissues, with key role in regulating fat metabolism and lipid storage in adipose tissue [81]. Ghrelin signaling has been demonstrated to be another key mediator linking nutrient-sensing signals with adipose inflammation and insulin resistance and ablation of ghrelin has been reported to worsen diet-induced obesity, insulin resistance and adipose inflammation [82].

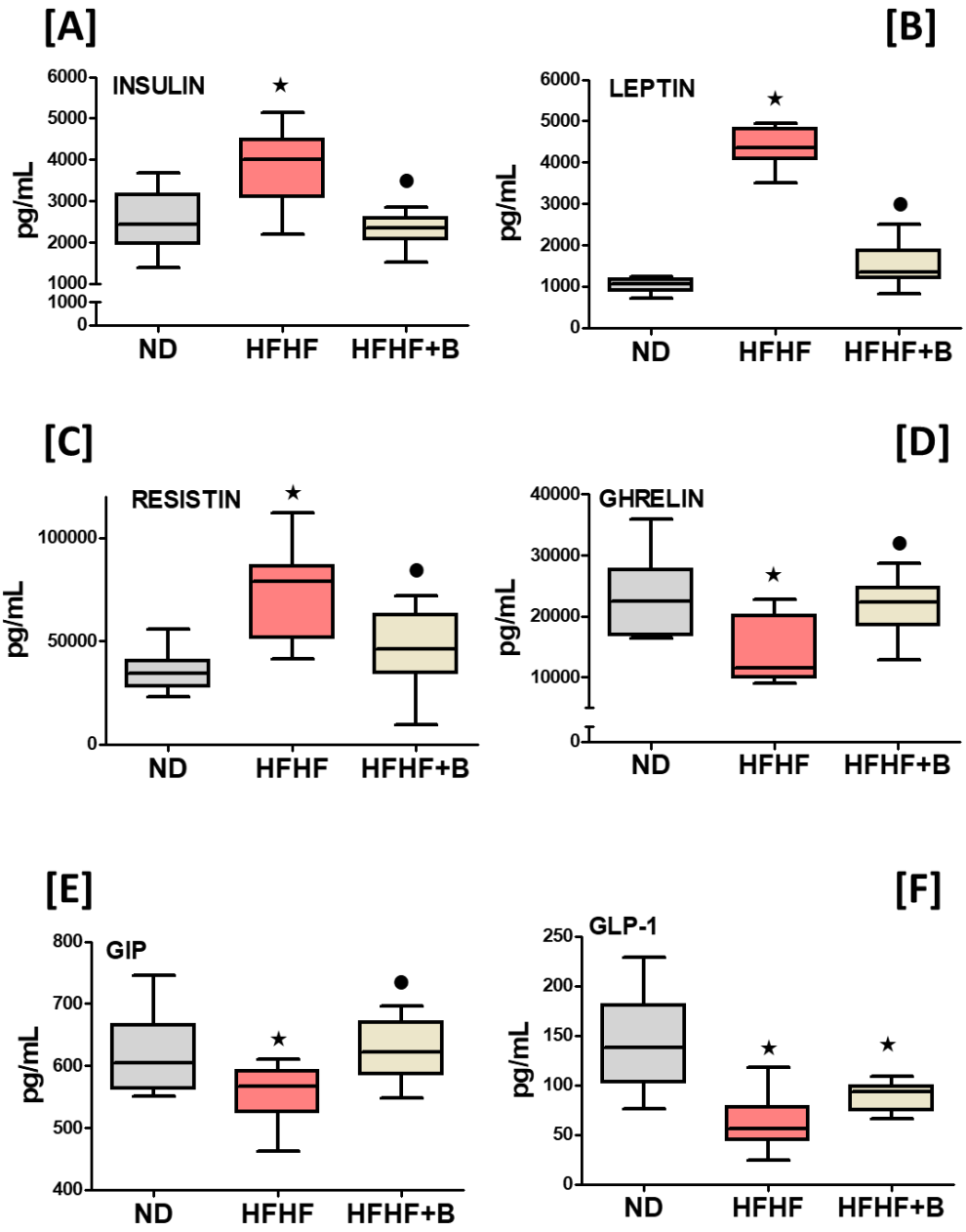

Figure 10.22 Effects of dietary manipulation and baricitinib administration on metabolic parameters

Serum concentration of: Insulin (A), Leptin (B), Resistin (C), Ghrelin (D); GIP (E) and GLP-1 (F). All data are expressed as mean ± SEM for n number of observations. $*p < 0.05$ versus ND; $\bullet p < 0.05$ versus HD

The overactivation of JAK2 was registered in skeletal muscle and kidney of HFHF mice. As shown in Figure 10.23, HFHF has determined a significant increase in the phosphorylation of $Tyr^{1007/1008}$ on JAK2 suggesting increased activation, resulting in a downstream increase in Tyr^{690} phosphorylation of STAT2, demonstrating that JAK2/STAT2 signalling pathway is activated in the skeletal muscle and kidney of mice that show metabolic derangements.

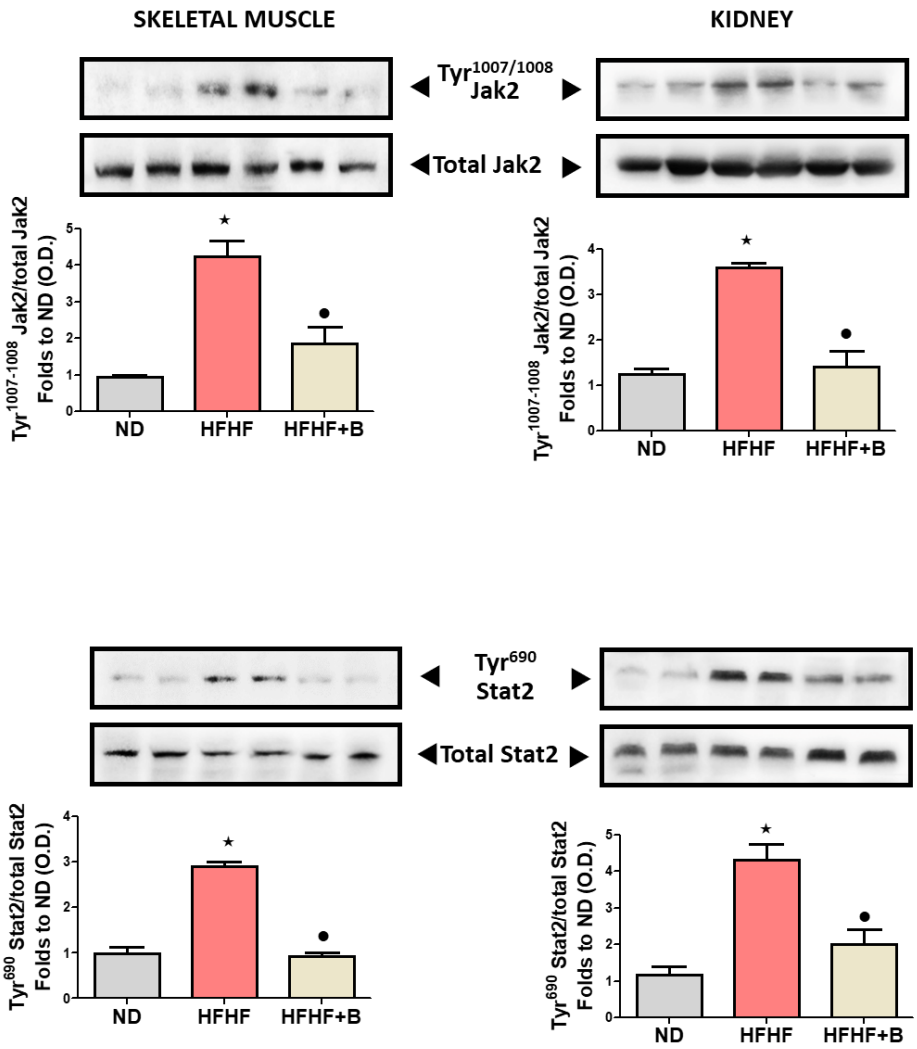

Figure 10.23 Baricitinib attenuates HFHF induced JAK/STAT pathway

Western blot analysis for Phosphorylation of $Tyr^{1007/1008}$ JAK1/2 in Skeletal muscle (A) and Kidney (B) and normalized to total JAK1/2 and for phosphorylation of Tyr^{690} on STAT2 in the skeletal muscle (C) and the kidney (D) and normalized to total STAT2. Data are expressed as mean ± SEM for n number of observations. *p < 0.05 vs. ND; •p < 0.05 vs HFHF.

When activated, JAKs in turn phosphorylates and activates STAT proteins, which themselves dimerize and translocate to the nucleus where they regulate gene transcription, including cytokines production. Here we confirmed that HFHF does drive the phosphorylation of JAK2 and STAT2 and report that the JAK1/2 inhibitor baricitinib attenuates the phosphorylation of both JAK2 and STAT2 in mice with an HFHF. These effects of baricitinib were associated with a significant reduction in the serum concentrations of the JAK-STAT dependent cytokines IL-

1β, TNF-α and INF-γ. In contrast, the anti-inflammatory cytokine IL-10 and IL-6 were upregulated following baricitinib exposure (Figure 10.24).

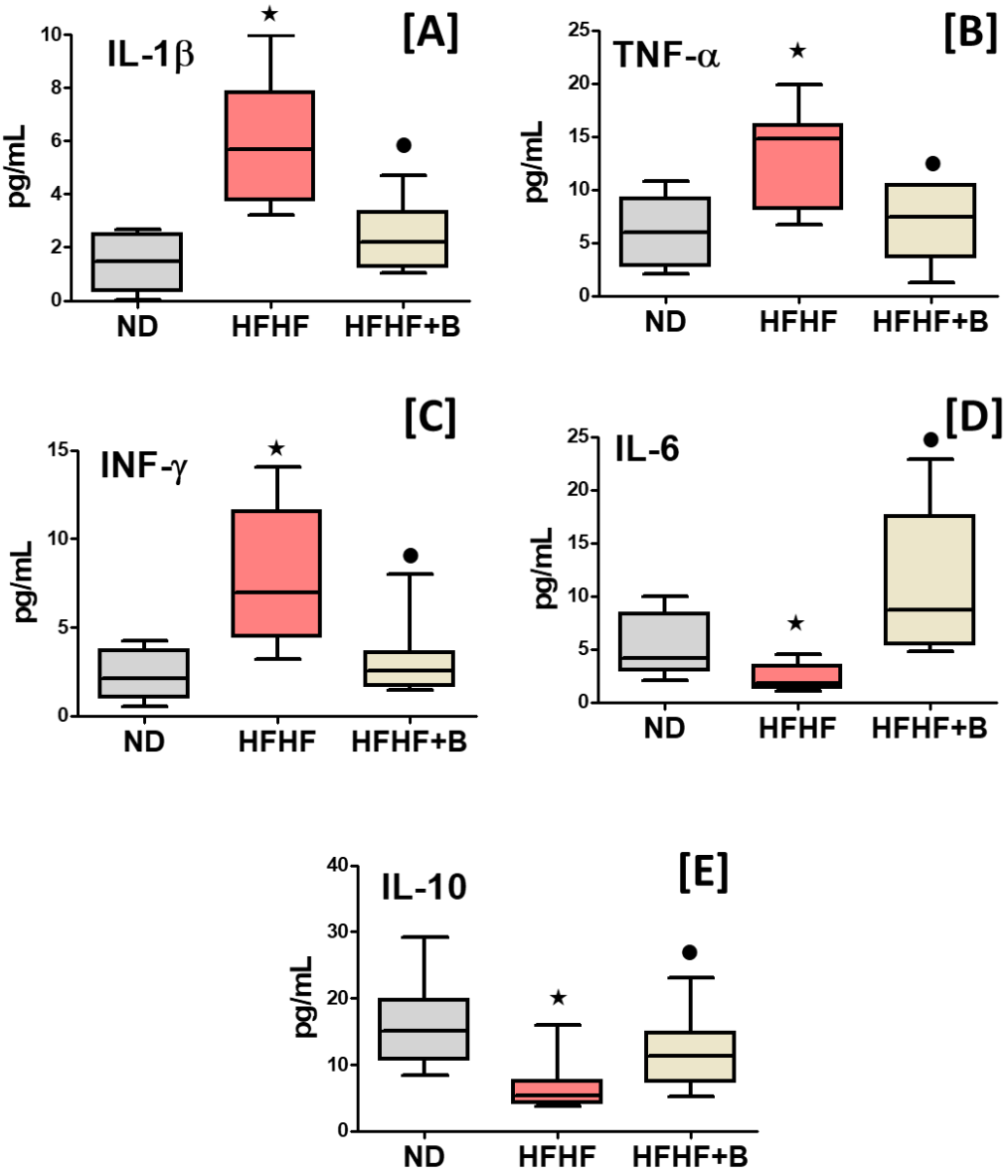

Figure 10.24 Baricitinib reduces systemic inflammatory response

Serum concentration of inflammatory cytokines: Il-1ß (A), TNF-α (B), INF (C), IL-6 (D) and IL-10 (E). All data are expressed as mean ± SEM for n number of observations. $*p < 0.05$ versus ND; $•p < 0.05$ versus hFHF.

It is important to underlying that we documented a significant increase in IL-6 concentrations following baricitinib administration, consistent with a previous study showing that IL6-deficient mice fed HFD develop significant hepatosteatosis and insulin resistance [83]. In fact, IL-6 is not a classical pro-inflammatory cytokine and may exert several anti-inflammatory actions, including downregulation of IFN-γ, IL-1β, and TNF-α [84].

In conclusion, all of our results confirmed that mice exposed to HFHF for 22 weeks showed an excessive production of cytokines and drived the phosphorylation of JAK2 and STAT2 and accompanied by the development of the expected dysmetabolic phenotype. Thus, targeting

metaflammation by inhibiting JAK signaling by baricitinib, makes it really attractive as novel candidate for the treatment of diet-related metabolic derangements.

10.7. Effects of the pharmacological modulation of the in anti-inflammatory pathway in an experimental model of metabolic diseases

Resolution of inflammation is a physiological active process, which is highly coordinated and regulated by several endogenous mediators of protein and lipid nature. In particular, specialized pro-resolving mediators (SPMs), including lipoxins, protectins, maresins and resolvins, do not completely inhibit the inflammatory process, but reprogram the immune response to accelerate resolution of inflammation [85].

Annexin A1 (ANXA1) is an endogenously produced anti-inflammatory protein, which plays an important role in the pathophysiology of diseases associated with chronic inflammation. We demonstrate that patients with type-2 diabetes have increased plasma levels of ANXA1 when compared to normoglycemic subjects. Plasma ANXA1 positively correlated with fatty liver index and elevated plasma cholesterol, suggesting a link between aberrant lipid handling and ANXA1 (Paper 7 on Discussion section). We have investigated (a) the role of endogenous ANXA1 in the pathophysiology of HFHF-induced insulin resistance using ANXA1−/− mice, and (b) the potential use of hrANXA1 as a new therapeutic approach for experimental diabetes and its microvascular complications.

For these purposes the study was carried out on 10 weeks old ANXA1-/-mice and wild-type (WT) C57BL/6 mice randomly assigned either a ND or HFHF diet. After 4 weeks of dietary manipulation mice were randomly assigned to a treatment group receiving either with hrANXA1 (40 µg/kg, i.p.) or vehicle (Hepes 50mM, NaCl 140mM i.p.) 5 days per week for 6 weeks.

Consistent with the observation in patients with T2DM, mice fed an HFHF had elevated levels of circulating ANXA1 (Figure 10.25). When compared to chow-fed mice, WT-mice fed an HFHF gained more weight, had elevated levels of serum insulin, higher (non-fasted) blood glucose levels and a significant impairment in tolerance to oral glucose challenge (Table 10.5).

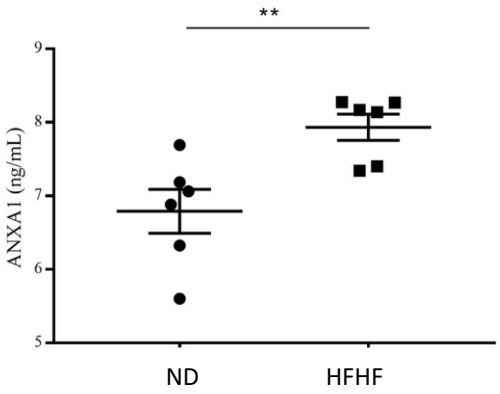

Figure 10.25 ANXA1 attenuates the development of obesity and insulin resistance in HFHF fed mice

ELISA for ANXA1 levels were measured in serum isolated from whole blood at harvest (n=6). Data analysis by a one-way ANOVA followed by a Bonferroni post-hoc test and the mean is expressed mean ± SEM: *p< 0,06; **p<0,01; ***p<0,001; *p<0,0001 vs WT+HFHF; §p<0,05; §§P<0,01; §§§P0,001 vs ANXA1-/- +HFHF.

ANXA1-/- fed an HFHF gained significantly more weight, had higher blood glucose levels and an even more severely impaired OGTT when compared to ND fed ANXA1-/-mice. HFHF-fed WT-mice treated with hrANXA1 had lower serum insulin levels, lower (non-fasted) blood glucose levels and an improved OGTT when compared to HFHF-fed WT-mice. Administration hrANXA1 to ANXA1-/- mice (rescue experiment) resulted in significantly lower serum insulin levels, blood glucose levels, a reduction in weight gain and an improvement in OGTT; suggesting that endogenous ANXA1 is a key mediator of glucose homeostasis. (Table 10.6).

	Wild Type				ANXA1 -/-		
	ND	ND+ ANXA1	HFHF	HFHF+ ANXA1	ND	HFHF	HFHF+ANXA1
Body weight (g)	9,790±0,602*	9,857±0,674*	16,81±0,479	12,87±0,455*	4,550±0,276°	13,89±0,772	7,00±0,447°
Blood glucose (mmol/L)	8,438±0,542*	7,682±0,29*	13,86±0,6621	9,088±0,442*	8,650±0,493°	19,56±1,224	8,483±0,541°
Serum Insulin (mmol/L)	6,694±1,282*	7,110±1,06*1	18,73±2,454	7,860±0,697*	5,321±0,238°	20,54±1,271	13,47±0,817°
OGTT (AUC)	84,42±4,506*	84,96±3,659*	110,7±3,659	89,42±0,999*	87,65±4,716°	127,6±3,767	99,93±3,560°

Table 10.6 Animal biochemistry

Body weight gain from baseline, blood glucose, serum insulin, and OGTT AUC were measured in wild type (WT) C57BL/6 or ANXA1−/− mice fed a standard diet (chow) or a high-fat diet (HFD) for 10 weeks. HFD-mice were treated with either vehicle or human recombinant (hr) ANXA1 (40 µg/kg, i.p.) five times per weeks between weeks 4 and 10. Data are expressed as mean± SEM of 7–10 mice per group. Data were analyzed by a one-way ANOVA followed by a Bonferroni post-hoc test, *p < 0.05 vs. WT HFHF or °p < 0.05 vs. ANXA1-/- HFHF

As endogenous ANXA1 protected against the development of experimental diabetes and treatment with hrAXNXA1 improved the diabetic phenotype of HFHF-fed mice, we next investigated the potential mechanisms underlying the observed beneficial effects of both hrANXA1 and endogenous ANXA1. When compared to WT-mice fed a ND, WT-mice fed a HFHF exhibited an increase in the degree of IRS-1 on Ser^{307} in liver (Figure 10.26) as well as a decrease in the phosphorylation of downstream effectors of the insulin signaling pathway,

AKT on Ser^{473} and GSK-3β on Ser^{9}. All of the above findings suggest that WT-mice fed a HFHF had developed peripheral insulin resistance. ANXA1-/-mice fed a HFHF exhibited a further significant increase in the degree of phosphorylation of IRS- 1 on Ser^{307} resulting in a decrease in the phosphorylation of AKT on Ser^{473} and glycogen synthase kinase-3β (GSK-3β) on Ser^{9}. These data, obtained also in the skeletal muscle, are consistent with the more severe diabetic phenotype observed in ANXA1−/− mice fed a HFHF.

Treatment of WT-mice fed a HFHF with hrANXA1 attenuated the increase in phosphorylation of IRS-1 on Ser^{307}, and the subsequent decrease in phosphorylation of AKT on Ser^{473} and GSK-3β on Ser^{9}. Additionally, when hrANXA1 was given to ANXA1−/− mice all abnormal signaling events were restored to that of mice fed a ND and highlighting of ANXA1 as a signaling molecule in the IRS-1 signal transduction pathway.

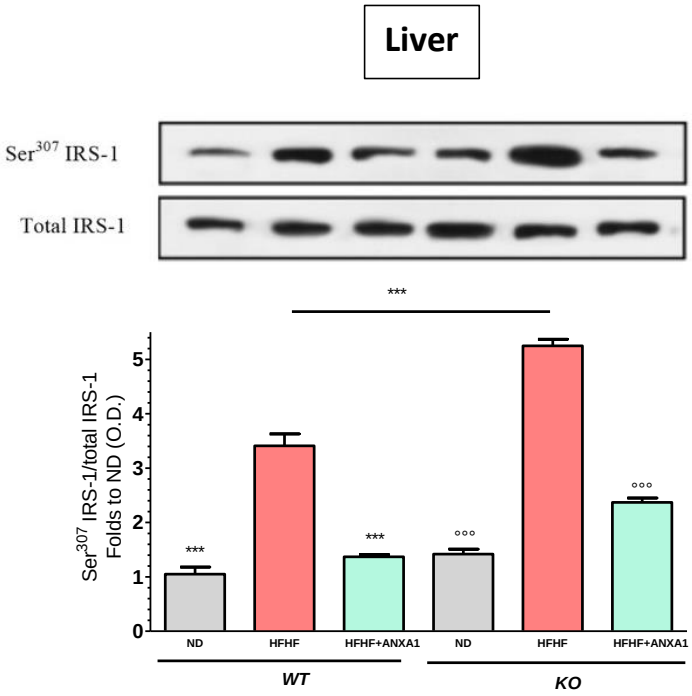

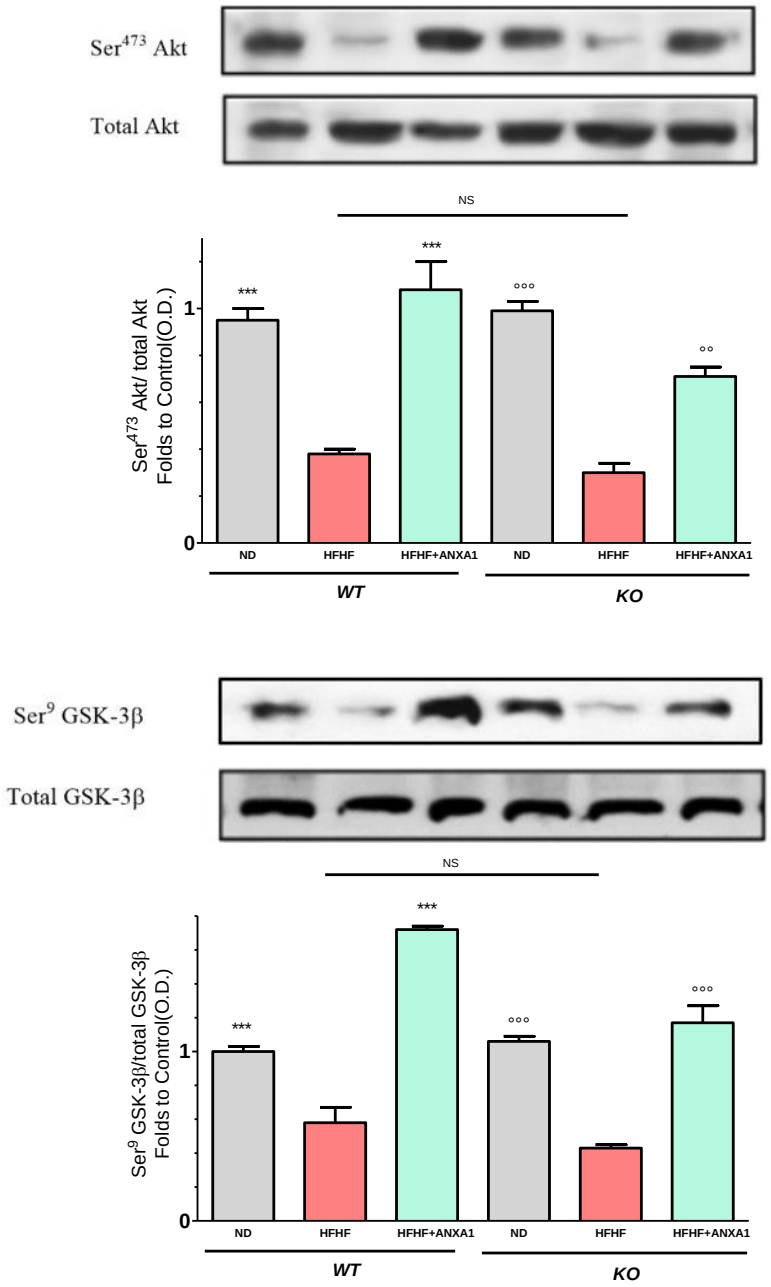

Figure 10.26 ANXA1 attenuates HFHF induced development of peripheral insulin resistance

Western blot analysis for Phosphorylation of Ser307 on IRS-1 in liver and normalized to total IRS-1; for phosphorylation of Ser473 on Akt in liver and normalized to total Akt; for phosphorylation of Ser9 on GSK-3b in the skeletal muscle and normalized to total GSK-3b. Data were analyzed by a one-way ANOVA followed by a Bonferroni post-hoc test and the mean is expressed mean ± SEM., ***p < 0.001 vs WT HFHF; °°p < 0.01, °°°p < 0.001 vs. ANXA1−/− HFHF. NS: no significant

We also demonstrate, for the first time, that ANXA1−/− mice have constitutively activated RhoA (Figure 10.27), in kidney and skeletal muscle. Interestingly, diabetic mice, which have reduced tissue expression of ANXA1, also have activated RhoA. Treatment of HFHF-mice with hrANXA1 restored tissue levels of ANXA1 that attenuates the downstream effector MYPT1 in liver and inhibited RhoA activity, which, in turn, resulted in restoration of the activities of AKT, GSK-3β secondary to re-sensitization of IRS-1 signaling.

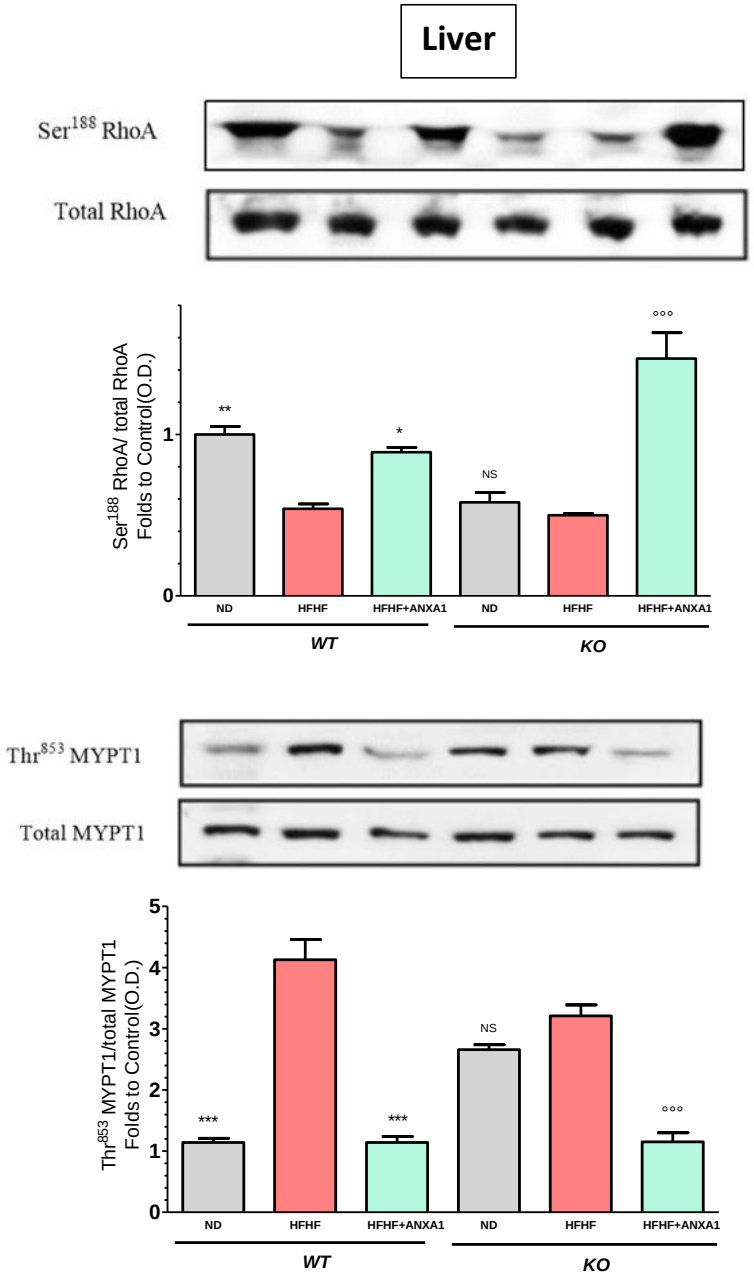

Figure 10.27 ANXA1 attenuates RhoA induction in mice fed a HFHF

Phosphorylation of Ser188 on RhoA was normalized to total RhoA in skeletal muscle (A). Phosphorylation of Thr853 on MYPT1 was normalized to total MYPT1 liver (B). A representative blot is shown for each protein and densitometry quantification of n = 3 experiments represented in the histograms. Data were analyzed by a one-way ANOVA followed by a Bonferroni post-hoc test and the mean is expressed mean ± SEM., *p < 0.05, **p < 0.01, ***p <0.001, vs. WT HFD; °°°p < 0.001 vs. ANXA1−/− HFHF. NS: no significant

In summary our data suggest that ANXA1 is a key regulator of RhoA activity, which restores IRS-1 signal transduction showing a new biological function of ANXA1 beyond those of as an anti-inflammatory mediator. Thus, recombinant human ANXA1 may represent a novel candidate for the treatment of T2DM and its complications.

3) Targeting metaflammation as new pharmacological strategy for cardio-metabolic diseases

10.8. Effects of the pharmacological modulation of IKK-16 in an experimental model of cardiometabolic disease

During my research another aim was to investigate the molecular links between metabolic and cardiovascular diseases, so we focused on highlighting the role of specific inflammatory pathways in the crosstalk between these two pathological conditions.

In a context of cardiometabolic damage, the pharmacological modulation of inflammatory signalling pathways allows decreasing the metabolic damage induced by insulin resistance associated inflammation, and, at the same time, reducing the incidence of cardiovascular injury related. These findings may open new prospective in the pharmacological treatment of CMD.

In particular, in the Paper 8 of discussion section, we show, for the first time, that a pre-existing diabetic phenotype worsens the cardiac (organ) dysfunction associated with CLP-sepsis in mice. It also shows that activation of the NF-κB pathway is a key driver of cardiac dysfunction in mice with T2DM/sepsis. Therefore, targeting NF-κB activation may be a potential strategy to treat the excessive inflammation and cardiac dysfunction in patients with T2DM and sepsis.

In fact, T2DM alone resulted in a small degree of NF-κB activation in the heart. However, sepsis in diabetic mice resulted in a dramatic increase in the serum concentrations of proinflammatory cytokines and a further increase in NF-κB activation in the heart. Most notably, inhibition of NF-kB, with a potent and selective IKK inhibitor, IKK16 treatment (1 mg/kg i.v.) reduces the organ dysfunction/injury associated with sepsis in mice with pre-existing T2DM (Figure 10.28).

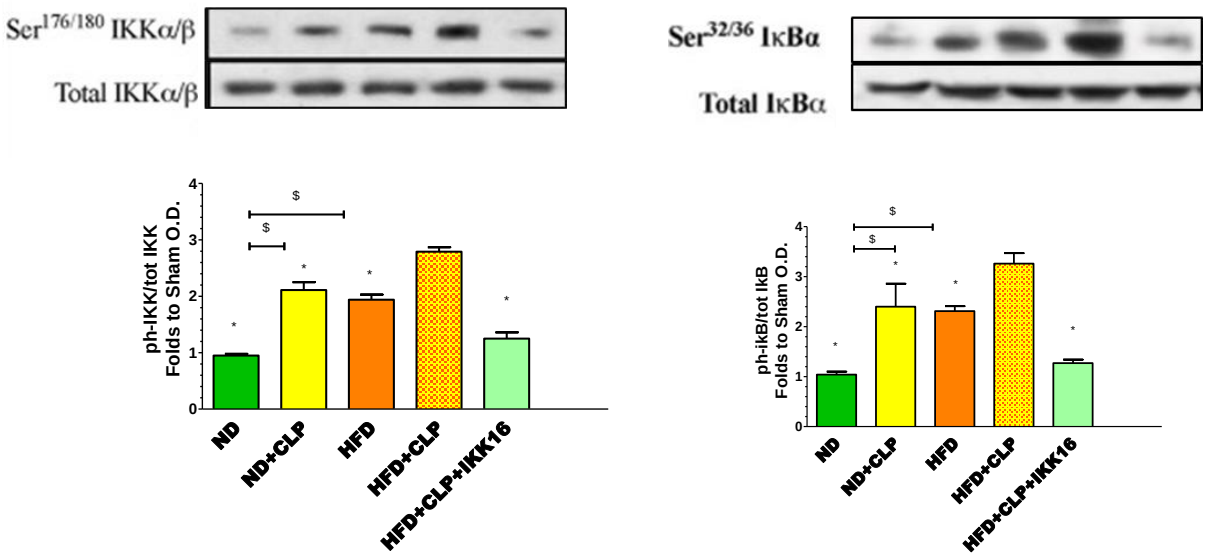

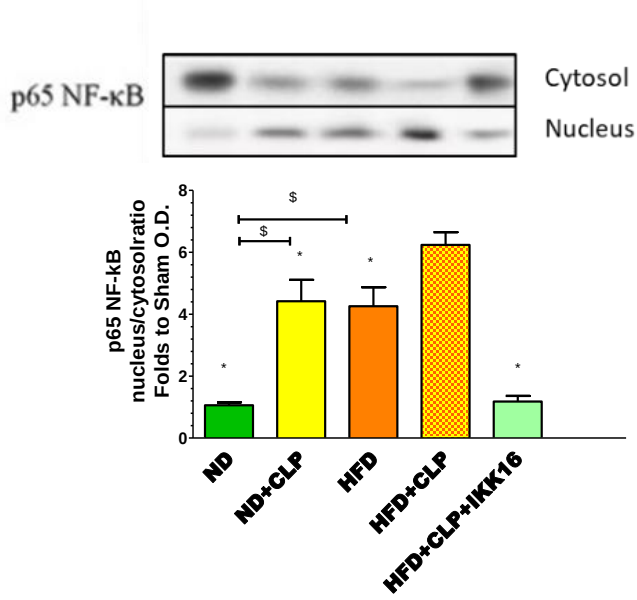

Figure 10.28 Effects of CLP and IKK-16 post treatment on NF-κB signaling pathway in the heart of mice with pre-existing T2DM.

Densitometry analysis of the bands are expressed as relative optical density of (A) IKKα/β phosphorylation on Ser178/180 corrected to the corresponding total IKKα/β content and normalized using the related sham band; (B) IκBα phosphorylation on Ser32/36 corrected to the corresponding total IκBα content and normalized using the related sham band; (C) NF-κB p65 subunit levels in both, cytosolic and nuclear fractions expressed as a nucleus/cytosol ratio normalized using the related sham bands. Data was analyzed using one-way ANOVA followed by Bonferroni's post-hoc test and expressed as mean ± SEM.*P < 0.05 compared to HFD+CLP group, $P < 0.05. (n = 4–6 per group).

10.9. Repurposed drugs as innovative pharmacological tools in cardiometabolic disorders

During my research we have repurposed drugs, already involved in the proposed inflammatory pathways, as innovative pharmacological targets in cardiometabolic disorders.

The potential protective effects of the impairment of the crosstalk between DDP-4 and NF-kB activation in sepsis-induced multiorgan dysfunction have never been tested in animal models of diet-induced diabetes, which is known to be characterized by an increase in baseline NF-kB activity. The aim was to evaluate whether the administration treatment of a DPP-4 inhibitor, especially linagliptin, in a sepsis condition, could play a protective role, beyond its mechanism with a positive effect on modulation of insulin resistance, which appears only following a chronic administration of the drug.
Treatment of mice on HFD with linagliptin, at 1 h after CLP, resulted in significant reduction in IKK α/β and IkBα phosphorylation and p65 translocation when compared to mice on HFD subjected to CLP and treated with vehicle ($P < 0.05$; Figure 10.29).

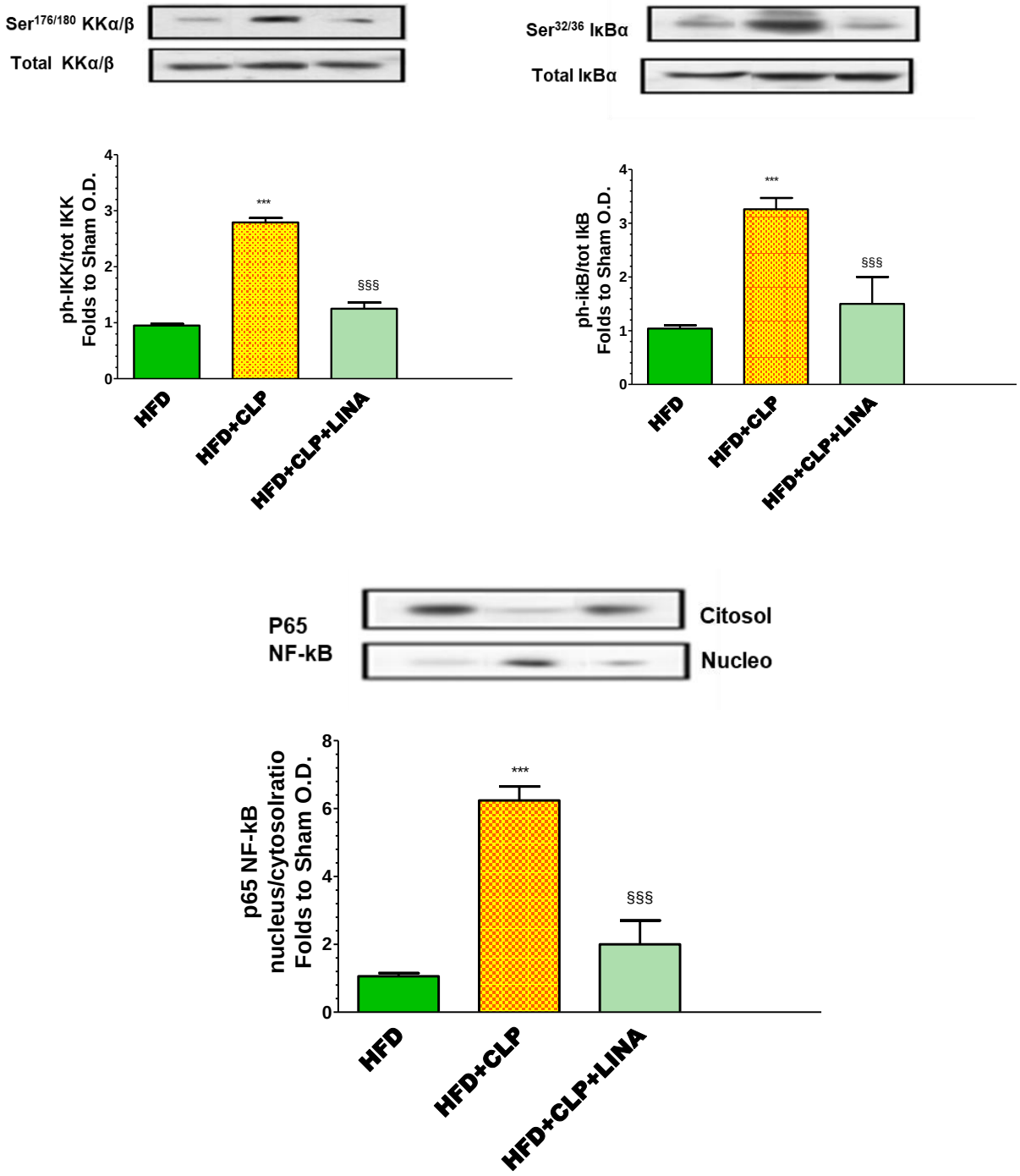

Figure 10.29 Effects of CLP and Linagliptin post treatment on NF-κB signaling pathway in the heart of mice with pre-existing T2DM.

Densitometry analysis of the bands are expressed as relative optical density of (A) IKKα/β phosphorylation on Ser178/180 corrected to the corresponding total IKKα/β content and normalized using the related sham band; (B) IκBα phosphorylation on Ser32/36 corrected to the corresponding total IκBα content and normalized using the related sham band; (C) NF-κB p65 subunit levels in both, cytosolic and nuclear fractions expressed as a nucleus/cytosol ratio normalized using the related sham bands. Data was analyzed using one-way ANOVA followed by Bonferroni's post-hoc test and expressed as mean ± SEM.*P < 0.05 compared to sham group, §P < 0.05. (n = 4–6 per group) vs HFD+CLP.

We cannot exclude that other effects associated with DPP-4 inhibition (that do not involve NF-kB inhibition) may have contributed to the observed beneficial effects of Linagliptin. However,

our data demonstrating that the magnitude of the effect of the inhibition of NF-kB with IKK-16 is similar to the one observed with Linagliptin and this observation supports the view that inhibition of NF-kB is central in the observed beneficial effects of both treatments. Thus, with these data we indicate that linagliptin may be “repurposed” for the use in sepsis and/or other conditions that are associated with local or systemic inflammation driven by the excessive activation of NF-kB.

Regarding the modulation of another inflammatory pathway, JAK/STAT, involved in the development of cardiometabolic disorders [86], as mentioned above we used a JAK inhibitor, already approved for rheumatoid arthritis, to prove that it can be used as promising treatment option in the clinical context of metabolic diseases. In fact, the use of the JAK 1/2 inhibitor baricitinib, which was administered for the last 16 weeks of the 22 weeks-dietary manipulation, exerted multi-organ protection against the deleterious effects of HFHF exposure.

Interestingly, targeting metaflammation by inhibiting JAK signaling by small molecules such as baricitinib might offer several advantages when compared with a therapeutic strategy centered on targeting cytokines with biologics, including better pharmacokinetics and cost effectiveness, fewer immunosuppressive effects and wider simultaneous targeting of multiple pathogenic pathways, thus making them really attractive and potentially suitable for drug repurposing.

Chapter 11 – Discussion

The first aim of my thesis was to set up *in vivo* models to study the pathophysiological mechanism(s) involved in the development of diet-induced metabolic derangements.

As documented in detail in the below mentioned published papers, we demonstrated a key role for the overaccumulation of AGEs following exposure to reactive sugars, mainly fructose, in affecting the mechanisms of insulin resistance and exacerbating the metaflammation.

We deepened the impact of sugar exposure in AGEs accumulation demonstrating that the charactheristics of the sugar may evoke different effects on AGEs-related metabolic derangements. Specifically, for the first time, we provide evidence that D-tagatose, which shows lower chemical reactivity in evoking AGEs than fructose, does not exert the same deleterious metabolic derangements evoked by its epimer fructose. In fact, we documented that the metabolic abnormalities (increased body weight, impairments of systemic glucose and lipid profiles, as well as renal disfunction) caused by exposure to an unhealthy diet containing high concentrations of fructose were not recorded when fructose was replaced by D-tagatose, either at the systemic or at the local level (Paper 2 see below).

We further extended our investigation to the potential impact of different formulations of the same sugar on AGEs accumulation and related metabolic dysfunction. We in fact, have demonstrated that both fructose formulations, solid and liquid, affect its absorption by the small intestine, leading to different outcomes in liver metabolism. Liquid fructose is more rapidly absorbed by intestine and, thus, rapidly metabolized by the liver, leading to lipogenesis, hepatosteatosis and increased levels of markers of fibrosis. Differently solid fructose formulation is higher accumulated in the enterocytes and lower rate of blood transfer, leading to AGEs accumulation and affecting gut barrier integrity in the ileum intestinal mucosa, with the following hepatic activation of the NLRP3 inflammasome pathway (Paper 1 see below).

To confirm the key role of AGEs in mediating metabolic derangements we used a pharmacological approach based on the chronic administration of pyridoxamine (150mg/kg/die), a structural analog of vitamin B6 that exerts antiglycative effect. Pyridoxamine is in fact, an "Amadorin" that principally blocks the conversion of Amadori intermediates into AGE-carboxymethyllysine, the inhibitory mechanism interfering with the catalytic role of the redox metal ions essential for the glycoxidation reaction. In our experiments, kidney morphology of HFHF fed mice showed strong vacuolar degeneration and loss of tubule brush border, associated with a drastic increase in AGEs and RAGE. These effects were significantly counteracted by piridoxamine administration resulting in a significant reduction in the accumulation of CEL and CML (the two most studied AGEs) within the kidney, paralleled by improvement in kidney function and morphology (Paper 3 see below).

All these observations suggest a complex interplay between AGEs formation and metabolic complications: the accumulation of AGEs is not an isolated process, but part of a range of oxidative chemical modifications of tissue proteins that increase in metabolic diseases.

The design of drugs to inhibit AGEs formation and thereby to protect against diabetic complications could represent a novel approach not focused on specific molecular target (such as a protein, an enzyme or a receptor, in a specific tissue). In fact, AGEs inhibitors must trap a

wide range of reactive intermediates, also intercepting them in the presence of much higher concentrations of reactive functional groups on proteins.

Diet is the major source of AGEs *in vivo*, because they can be produced endogenously from a diet with a high content of simple sugars, especially fructose. Modern diets are also largely heat-processed and as a result contain high levels of AGEs. In order to deeply investigate their pathogenic role in diet-related metabolic derangements we explored the impact of chronic exposure to exogenous AGEs.

Our data suggest that chronic exposure to exogenous AGEs introduced in a normal calorie diet causes a significant imbalance in the incretin axis and a systemic increase in pro-inflammatory cytokines and ROS, accompanied by an upregulation of RAGE expression. These effects are associated with alterations in the insulin signal, changes in the intestinal microbiota and a different glycosylation profile. In general, AGEs can be considered early biomarkers and triggers of metabolic damage related to food.

The results of this investigation led to the publication of the following articles:

1 Mastrocola R, Ferrocino I, Liberto E, Chiazza F, Cento AS, Collotta D, QuerioG, Nigro D, Bitonto V, Cutrin JC, Rantsiou, Durante M, Masini E, Aragno M, Cordero C, Cocolin L, Collino M. **Fructose liquid and solid formulations differently affect gut integrity, microbiota composition and related liver toxicity: a comparative in vivo study**. *Journal of Nutritional Biochemistry 55 (2018) 185–199*

2 D. Collotta, L. Lucarini, F. Chiazza, A. S. Cento, M. Durante, S. Sgambellone, J. Chini, F. Baratta, M. Aragno, R. Mastrocola, E. Masini and M. Collino. **Reduced Susceptibility to Sugar-Induced Metabolic Derangements and Impairments of Myocardial Redox Signaling in Mice Chronically Fed with D-Tagatose when Compared to Fructose.** *Hindawi Oxidative Medicine and Cellular Longevity Volume2018, Article ID5042428,11pages*

3 *F. Chiazza, A. S. Cento, D. Collotta, D. Nigro, G. Rosa, F. Baratta, V. Bitonto, J. C. Cutrin, M. Aragno, R. Mastrocola and M. Collino.* ***Protective Effects of Pyridoxamine Supplementation in the Early Stages of Diet-Induced Kidney Dysfunction.*** *Hindawi BioMed Research International Volume 2017, Article ID 2682861, 12 pages*

4 *Mastrocola R, Collotta D, Gaudioso G, Le Berre M, Cento AS, Ferreira Alves G, Chiazza F, Verta R, Bertocchi I, Manig F, Hellwig M, Fava F, Cifani C, Aragno M, Henle T, Joshi L, Tuohy K, Collino M.* ***Effects of Exogenous Dietary Advanced Glycation End Products on the Cross-Talk Mechanisms Linking Microbiota to Metabolic Inflammation.*** *Nutrients. 2020 Aug 19;12(9):E2497.*

The second aim was to study the effects of the pharmacological modulation of selective pro- and anti inflammatory pathways of metaflammation in experimental models of cardiometabolic diseases.

Specifically, we tested the effects evoked by the administration of a selective inhibitor of the pro-inflammatory cascade Janus kinase/signal transducer and activator of transcription (JAK-STAT) as well as the effects evoked by either pharmacological and genetic modulation of the anti-inflammatory annexin A1 pathway.

In both experimental protocols, mice exposed to HFHF showed the development of the expected dysmetabolic phenotype with increased body weight, blood glucose levels and an impairment in OGTT, compared to the control group.

ANXA1$^{-/-}$ mice fed a HFHF developed a more severe diabetic phenotype. So we have used hrAXNXA1 with the aim to restore its normal tissue level and protecting against the deleterious effects of HFHF (Paper 7 see below).

On the contrary, JAK2 deficiency confers resistance to diet-induced metabolic stress and protects against diet-induced metaflammation and insulin resistance. So we have demonstrated that chronic administration of baricitinib, an oral JAK1/2 inhibitor protects against the deleterious effects evoked by exposure to a high-fat diet combined with an overconsumption of sugars.

Applying two different strategies, pharmacological inhibition of the proinflammatory JAK/STAT pathway (using baricitinib 10 mg/kg die, p.o. for the last 16 weeks) and pharmacological activation of the anti-inflammatory ANXA1 cascade (using hrANXA1 (40 µg/kg, i.p. 5 days per week for 6 weeks.) we confirmed that ANXA1 and the JAK/STAT pathways are key mediators of glucose homeostasis, in fact, both treatments attenuated the increase in phosphorylation of IRS-1 on Ser^{307} and the subsequent decrease in phosphorylation of Akt on Ser^{473} and GSK-3β on Ser^{9} in skeletal muscle (Papers 6 and 7 see below).

Our results confirm and further extend previous findings on the importance of a correct balance between pro- and anti-inflammatory endogenous mechanism to reduce the incidence of diet-related metabolic derangements.

Another pathway I focused my attention on was NLRP3 inflammasome, to which, I dedicated a revision work of the literature data to summarize published data confirming its crucial role as pharmacological target for metaflammation (Paper 5 see below).

The results of this investigation led to the publication of the following articles:

5 *D. Collotta, BSc; M. Collino, PhD.* ***NLRP3 Inflammasome Signaling Platform as New Pharmacological Target for Metaflammation.*** *Diabetes Research Openventio J. 2016; 2(3): e14-e16*

6 D.Collotta, W.Hull R.Mastrocola, F.Chiazza, A.S.Cento, C.Murphy, R.Verta, G.F.Alves, G.Gaudioso, F.Fava, M.Aragno, K.Tuohy, C.Thiemermann M.Collino. **Baricitinib counteracts metaflammation thus protecting against diet-induced metabolic abnormalities in mice.** Molecular Metabolism 13 May 2020, 101009

7 G *S.D. Purvis, M. Collino, R.A. Loiola, A. Baragetti, F. Chiazza, M. Brovelli, M. H. Sheikh, D. Collotta, A. Cento, R. Mastrocola, M. Aragno, J. C. Cutrin, C. Reutelingsperger, L. Grigore, A. L. Catapano, M. M. Yaqoob, G. Danilo Norata, E. Solito and Christoph Thiemermann.* ***Identification of AnnexinA1 as an Endogenous Regulator of RhoA and Its Role in the Pathophysiology and Experimental Therapy of Type-2 Diabetes*** *Front. Immunol., 27 March 201*9

We also tried to combine together the models of diet-induced metabolic disorders with those of cardiovascular injury in order to prove cross-talk mechanisms of inflammation that can be

addressed to counteract the development of cardiometabolic diseases. Here we decided to test the impact of linagliptin in an experimental model of sepsis in mice with pre-existing diet-induced metabolic disease. It has been shown that the DPP-4 signaling cascade is involved in pathogenesis of sepsis, mainly due to a selective cross-talk between DPP-4 and the pathway of the nuclear transcription factor NF-κB. The aim was to evaluate whether the administration treatment of a DPP-4 inhibitor, especially linagliptin, in a sepsis condition, could play a protective role, beyond its mechanism with a positive effect on modulation of insulin resistance, which appears only following a chronic administration of the drug. Treatment of mice on HFD with linagliptin, 1 h after CLP, resulted in significant reduction in NF-κB activation when compared to mice on HFD subjected to CLP and treated with vehicle ($P < 0.05$). Although we cannot exclude that other effects associated with DPP-4 inhibition (that do not involve NFkB inhibition) may have contributed to the observed beneficial effects of linagliptin, our data demonstrating that the magnitude of the effect of the inhibition of NF-kB with IKK-16 is similar to the one observed with linagliptin supports the view that inhibition of the activation of NF-kB is at the heart of the observed beneficial effects of both linagliptin and IKK-16.

The results of these investigations have led to the publication of the following article

8 Al Zoubi S, Chen J, Murphy C, Martin L, Chiazza F, Collotta D, Yaqoob MM, Collino M, Thiemermann C. **Linagliptin Attenuates the Cardiac Dysfunction Associated with Experimental Sepsis in Mice with Pre –existing Type 2 Diabetes by Inhibiting NF-κB** Front Immunol. 2018 Dec 18;9:2996.

Chapter 12 – Conclusion and future prespectives

Taken together the results here reported show that immune fuction and metabolic regulation are highly integrated and the proper function of each is dependent on the other. Since the metabolic inflammation has a central impact on whole-body homeostasis, an unbalance between pro- and anti-inflammatory mechanisms may contribute to the development of a cluster of chronic metabolic disorders, particularly obesity, type 2 diabetes and cardiovascular diseases. Thus, the modulation of metabolic inflammation may represent an innovative pharmacological strategy for effective therapeutic intervention on cardiometabolic disorders.

As documented in the Thesis, effective pharmacological approaches are not only the interventions aimed to decrease proinflammatory mediators, but also those aimed to increase resolution of inflammation intermediaries, like Annexine A1 that powerfully contributes to reduce the abnormalities in cardiometabolic disorders.

For the pharmacological targeting of the metabolic inflammation, when possible, we tried to use pharmacological tools that are already approved drugs in other clinical contexts. For instance, we decided to test the effect of baricitinib, the JAK inhibitor already approved for rheumatoid arthritis in a model of diet induced metabolic deragment, and the antidiabetic drug linagliptin in an experimental model of septic shock in a pre-existing type 2 diabetes. The approaches used were able to counteract the demages evoked thanks to the reduction of activation of pathways involved in the exacerbated inflammatory response. Besides, all the proposed pharmacological approaches are small molecules, which may offer several advantages when compared with a therapeutic strategy centered on targeting cytokines with biologics, including better pharmacokinetics and cost effectiveness, fewer immunosuppressive effects, thus making them really attractive and potentially suitable for drug repurposing.

We are however conscius that our experimental approaches are designed to easily allows us to perform comparative studies, in a strictly controlled environment, and that also, the lack of pharmacokinetics, hemodynamic, functional data as well as the impossibility to distinguish between the redox and inflammatory effects related to sugar exposure limit the pharmacological interpretation of the effects recorded and their potential clinical relevance. Another point that it can be considered as a limitation of the studies conducted is the lack of equipment needed to evaluate functional parameter (like functional photoacoustic microscopy of diabetic vasculature) or the absence of behavioral assays as well as the absence of methodologhy, besides the ones performed in order to confirm data, especially related to the interaction assays (like binding receptor assays).

Overall, the purpose of the present PhD project was to identify the cross-talk mechanisms involved in cardiometabolic disease and test the effects of their pharmacological modulation. The data here reported demonstrate that cardiometabolic disorders are a spectrum of interconnected pathological alterations in organs involved in metabolic and cardiovascular functions. The identification of common mechanisms involved in metaflammation in these clinical contexts offers important insights for an effective pharmacological targeting of key prossimal drivers of metaflammation needed to improve the dramatic impact of cardiometabolic diseases.

Highlights

-We demonstrated differences in terms of intensity and kinetics of development of systemic metabolic derangements (body weight gain, glucose and lipid profiles) when mice were fed with diet enriched with different components. Specifically, diets enriched in fat or in a combination of fat and fructose evoked significant increases in body weight and glucose plasma level at 12 weeks of dietary manipulation, whereas longer kinetics (24 weeks) are needed to obtain similar metabolic derangements with diets enriched in fructose only.

-Liquid and solid fructose lead to different outcomes in liver injury. Liquid fructose is more rapidly absorbed by intestine and, thus, rapidly metabolized by the liver, leading to lipogenesis, hepatosteatosis and increased levels of markers of fibrosis. Differently solid fructose formulation is higher accumulated in the enterocytes and lower rate of blood transfer, leading to AGEs accumulation and affecting gut barrier integrity in the ileum intestinal mucosa, with the following hepatic activation of the NLRP3 inflammasome pathway.

-The overaccumulation of AGEs and the expression of RAGE in intestine, heart, kidney and salivary glands, following exposure to reactive sugar (fructose vs tagatose), affects the mechanisms of insulin resistance and exacerbates the metaflammation, evoking marked cellular alterations and organ dysfunction.

-The addition of exogenous AGEs in a normocaloric diet evokes significant imbalance in the incretin axis and a systemic increase in pro-inflammatory cytokines and ROS, accompanied by an upregulation of RAGE expression. These effects are associated with alterations in the insulin signal, changes in the intestinal microbiota and a different glycosylation profile.

-We identified selective pro- (NF-κB, NLRP3 inflammasome, JAK/STAT cascades) and anti-inflammatory (Annexine A1) pathways involved in the pathogenesis of cardiometabolic disorders.

-We demonstrated that the pharmacological modulation of the above mentioned inflammatory pathways may counteract the diet-induced cardiometabolic derangements in mice.

-Our data suggest that drugs affecting the activity of the above mentioned inflammatory pathways, already used for other therapeutic purposes, could be repurposed as innovative pharmacological targets in cardiometabolic disorders. We specifically focused on the potential repurposing of Linagliptin in sepsis, when associated with metabolic derangements, and Baricitinib in the context of metabolic diseases.

List of publications

-D. Collotta, BSc; M. Collino, PhD *NLRP3 Inflammasome Signaling Platform as New Pharmacological Target for Metaflammation* Diabetes Research Openventio J. 2016; 2(3): e14-e16.

-D. Collotta, L. Lucarini, F. Chiazza, A. S. Cento, M. Durante, S. Sgambellone, J. Chini, F. Baratta, M. Aragno, R. Mastrocola, E. Masini and M. Collino *Reduced Susceptibility to Sugar-Induced Metabolic Derangements and Impairments of Myocardial Redox Signaling in Mice Chronically Fed with D-Tagatose when Compared to Fructose* Hindawi Oxidative Medicine and Cellular Longevity Volume2018, Article ID5042428,11pages

-D. Collotta, W. Hull R. Mastrocola, F. Chiazza, A. S. Cento, C. Murphy, R. Verta, G. Ferreira Alves, G. Gaudioso, F. Fava, M. Aragno, K. Tuohy, C. Thiemermann M. Collino *Baricitinib counteracts metaflammation thus protecting against diet-induced metabolic abnormalities in mice.* Molecolar metabolism 2020

-Mastrocola R, Collotta D, Gaudioso G, Le Berre M, Cento AS, Ferreira Alves G, Chiazza F, Verta R, Bertocchi I, Manig F, Hellwig M, Fava F, Cifani C, Aragno M, Henle T, Joshi L, Tuohy K, Collino M. *Effects of Exogenous Dietary Advanced Glycation End Products on the Cross-Talk Mechanisms Linking Microbiota to Metabolic Inflammation.* Nutrients. 2020 Aug 19;12(9):E2497.

-R. Mastrocola, C. Penna, F. Tullio, S. Femminò, D. Nigro, F. Chiazza, L. Serpe, D. Collotta, G. Alloatti, M. Cocco, M. Bertinaria, P. Pagliaro, M. Aragno and M. Collino *Pharmacological Inhibitionof NLRP3 Inflammasome Attenuates Myocardial Ischemia/Reperfusion Injury by Activation of RISK and Mitochondrial Pathways* Hindawi Publishing Corporation Oxidative Medicine and Cellular Longevity Volume 2016, Article ID 5271251, 11 pages

-F. Chiazza, A. S. Cento, D. Collotta, D. Nigro, G. Rosa, F. Baratta, V. Bitonto, J. C. Cutrin, M. Aragno, R. Mastrocola and M. Collino *Protective Effects of Pyridoxamine Supplementation in the Early Stages of Diet-Induced Kidney Dysfunction* Hindawi BioMed Research International Volume 2017, Article ID 2682861, 12 pages

-Mastrocola R, Ferrocino I, Liberto E, Chiazza F, Cento AS, Collotta D, QuerioG, Nigro D, Bitonto V, Cutrin JC, Rantsiou, Durante M, Masini E, Aragno M, Cordero C, Cocolin L, Collino M. *Fructose liquid and solid formulations differently affect gut integrity, microbiota composition and related liver toxicity: a comparative in vivo study* Journal of Nutritional Biochemistry 55 (2018) 185–199

-Al Zoubi S, Chen J, Murphy C, Martin L, Chiazza F, Collotta D, Yaqoob MM, Collino M, Thiemermann C*. Linagliptin Attenuates the Cardiac Dysfunction Associated with Experimental Sepsis in Mice with Pre –existing Type 2 Diabetes by Inhibiting NF-κB* Front Immunol. 2018 Dec 18;9:2996.

-G. S.D. Purvis, M. Collino, R.A. Loiola, A. Baragetti, F. Chiazza, M. Brovelli, M. H. Sheikh, D. Collotta, A. Cento, R. Mastrocola, M. Aragno, J. C. Cutrin, C. Reutelingsperger, L. Grigore, A. L. Catapano, M. M. Yaqoob, G. Danilo Norata, E. Solito and Christoph Thiemermann *Identification of AnnexinA1 as an Endogenous Regulator of RhoA and Its Role in the*

Pathophysiology and Experimental Therapy of Type-2 Diabetes Front. Immunol., 27 March 2019

-Sordi R, Chiazza F, Collotta D, Migliaretti G, Colas RA, Vulliamy P, BrohiK, Dalli J, Collino M, Thiemermann C. *Resolvin D1 Attenuates the Organ Injury Associated with Experimental Hemorrhagic Shock.* Ann Surg. 2019 Jun7.

-O'Riordan CE, Purvis GSD, Collotta D, Chiazza F, WisCollino M, Thiemermann C *Bruton's Tyrosine Kinase Inhibition Attenuates the Cardiac Dysfunction Caused by Cecal Ligation and Puncture in Mice. Front Immunol.*suwa B, Al Zoubi S, Stiehler L, Martin L, Coldewey SM, *2019 Sep 6;10:2129.*

-C. Penna, M. Aragno, A. Cento, S. Femmino', I. Russo, F. Dal Bello, F. Chiazza, D. Collotta, G. Ferreira Alves, M. Bertinaria, E. Zicola, V. Mercurio, M. Collino and P. Pagliaro. *Ticagrelor Conditioning Effects Are Not Additive to Cardioprotection Induced by Direct NLRP3 Inflammasome Inhibition: role of RISK, NLRP3 and Redox cascades.* Oxidative Medicine and Cellular Longevity 2020

-Zechendorf E, O'Riordan CE, Stiehler L, Wischmeyer N, Chiazza F, Collotta D, Denecke B, Ernst S, Müller-Newen G, Coldewey SM, Wissuwa B, Collino M, Simon TP, Schuerholz T, Stoppe C, Marx G, Thiemermann C, Martin L. *Ribonuclease 1 attenuates septic cardiomyopathy and cardiac apoptosis in a murine model of polymicrobial sepsis*. JCI Insight. 2020 Apr 23;5(8). pii: 131571.

-J. Chen, G. S.D. Purvis, D. Collotta, S. Al Zoubi, M.A. Sugimoto, A. Cacace, L. Martin, R.A. Colas, M. Collino, J. Dalli, Christoph Thiemermann, *RvE1 attenuates polymicrobial sepsis-induced cardiac dysfunction and enhances bacterial clearance*. Cardiovascular Research

-A. Ferrigno, L. G. Di Pasqua, G. Palladini, C. Berardo, R. Verta, P. Richelmi, S. Perlini, D. Collotta, Ma. Collino and M. Vairetti. *Transient Expression of Reck Under Hepatic Ischemia/Reperfusion Conditions Is Associated with Mapk Signaling Pathways. Biomolecules 2020*

-Ilaria Bertocchi, Federica Foglietta, Debora Collotta, Carola Eva, Vincenzo Brancaleone, Christoph Thiemermann, Massimo Collino. *The hidden role of NLRP3 inflammasome in obesity-related COVID-19 exacerbations: lessons for drug repurposing*. Br J Pharmacol. 2020 Aug 9

-Gareth S.D.Purvis, Massimo Collino, Haidee Aranda-Tavio, Fausto Chiazza, Caroline E. O'Riordan, Lynda Zeboudj , Shireen Mohammad, Debora Collotta, Roberta Verta, Nicolas E.S. Guisot, Peter Bunyard, Magdi M. Yaqoob, David R. Greaves, Christoph Thiemermann *Inhibition of Bruton's TK regulates macrophage NF-κB and NLRP3 inflammasome activation in metabolic inflammation*. British Journal of Pharmacology 2020

-Caroline E. O'Riordan, Gareth S. D. Purvis, Debora Collotta, Nadine Krieg, Bianka Wissuwa, Madeeha H. Sheikh, Gustavo Ferreira Alves, Shireen Mohammad, Lauren A. Callender, Sina M. Coldewey, Massimo Collino, David R. Greaves and Christoph Thiemermann. X-Linked Immunodeficient Mice with No Functional Bruton's Tyrosine Kinase Are Protected from Sepsis-Induced Multiple Organ Failure. Front. Immunol., 07 October 2020

- Collaboration on the drafting on the manual “L’Esame di Stato per Farmacisti – Tracce svolte e prove pratiche” ISBN: 9788833190167 Edition: I/2018 Publisher: EDISES.

-Collaboration to the SIF Magazine (Italian Pharmacological Society) - featured drugs - Medical Devices section.

Congress & projects

-38th National Cogress of the Italian Society of pharmacology (SIF). "Farmaci, Salute e Qualità della Vita". Rimini 24-28 October 2017

Poster1: *The AGEs Inhibitor pyridoxamine prevent kidney injury and dysfunction in mice fed high-fructose diet*.

Poster2: *Toxicological impact of high fructose intake on gut microbiota and liver/intestine integrity: any differences between solid and liquid formulations?*

-XXI Seminar of the National Congress of the Italian Society of Pharmacology - PhD Students, Fellows, Post Doc and Specialist Trainees. Bresso 19-20 September 2018

Poster: *Role of high sugar exposure in metabolic inflammation: a comparative in vivo study on fructose and its epimer tagatose in both liquid and solid formulations.*

-39th National Cogress of the Italian Society of pharmacology (SIF). Florence 20-23 November 2019

Presentation1: *Role of exogenous dietary advanced glycation end products (AGEs) in the cross-talk mechanisms linking diet, microbiota and metabolic inflammation*.

Poster1: *Salivary advanced glycation end products (AGEs) as novel biomarkers in evaluation of risk factors for diet-related diseases: results from the european network salivages.*

-19th National Cogress of the Italian Society of toxicology (SITOX). Bologna 11-12 February 2020

Poster: *Role of exogenous dietary advanced glycation end products (AGEs) in the cross-talk mechanisms linking diet, microbiota and metabolic inflammation*.

-56th annual meeting, Virtual EASD Annual Meeting. 21-25 september 2020.

Poster: *Baricitinib counteracts metaflammation thus protecting against diet-induced metabolic abnormalities in mice*

European project in which I was involved:

- *ERA HDHL: Salivages – Biomarkers for Nutrition and Health*

Project Title: Innovative Technological Approaches for validation of Salivary AGEs as novel biomarkers in evaluation of risk factors in diet-related diseases

- *ERA HDHL: Carb-Q-4-Health - Impact of Diet, Food Components and Food Processing on Body Weight Regulation and Related Metabolic Diseases*

Project Title: Tailored Carbohydrate Quality for Personalized Weight Management and Metabolic Health

References

[1] Sims EA, Danforth E Jr, Horton ES, Bray GA, Glennon JA, Salans LB. Endocrine and metabolic effects of experimental obesity in man. Recent Prog Horm Res. 1973;29:457-96. doi: 10.1016/b978-0-12-571129-6.50016-6. PMID: 4750591.

[2] Farag YM, Gaballa MR. Diabesity: an overview of a rising epidemic. Nephrol Dial Transplant. 2011 Jan;26(1):28-35. doi: 10.1093/ndt/gfq576. Epub 2010 Nov 2. PMID: 21045078.

[3] Saltiel AR, Kahn CR. Insulin signalling and the regulation of glucose and lipid metabolism. Nature. 2001 Dec 13;414(6865):799-806. doi: 10.1038/414799a. PMID: 11742412.

[4] Rydén L, Grant PJ, Anker SD, Berne C et al. (2013). ESC Guidelines on diabetes, pre-diabetes, and cardiovascular diseases developed in collaboration with the EASD: the Task Force on diabetes, pre-diabetes, and cardiovascular diseases of the European Society of Cardiology (ESC) and developed in collaboration with the European Association for the Study of Diabetes (EASD). Eur Heart J. 2013 Oct;34(39):3035-87. doi: 10.1093/eurheartj/eht108. Epub 2013 Aug 30. Erratum in: Eur Heart J. 2014 Jul 14;35(27):1824. PMID: 23996285.

[5] Van Obberghen et al. Surfing the insulin signaling web. Eur J Clin Invest. 2001 Nov;31(11):966-77. doi: 10.1046/j.1365-2362.2001.00896.x. PMID: 11737239.

[6] Lizcano JM, Alessi DR. The insulin signalling pathway. Curr Biol. 2002 Apr 2;12(7):R236-8. doi: 10.1016/s0960-9822(02)00777-7. PMID: 11937037.

[7] Horie T, et al. Oxidative stress induces GLUT4 translocation by activation of PI3-K/Akt and dual AMPK kinase in cardiac myocytes. J Cell Physiol. 2008 Jun;215(3):733-42. doi: 10.1002/jcp.21353. PMID: 18163380.

[8] Shimomura et al. Insulin selectively increases SREBP-1c mRNA in the livers of rats with streptozotocin-induced diabetes. Proc Natl Acad Sci U S A. 1999 Nov 23;96(24):13656-61. doi: 10.1073/pnas.96.24.13656. PMID: 10570128; PMCID: PMC24120.

[9] Wellen KE, Hotamisligil GS. Inflammation, stress, and diabetes. J Clin Invest. 2005 May;115(5):1111-9. doi: 10.1172/JCI25102. PMID: 15864338; PMCID: PMC1087185.

[10] Hotamisligil GS. Inflammation and metabolic disorders. Nature. 2006 Dec 14;444(7121):860-7. doi: 10.1038/nature05485. PMID: 17167474.

[11] Sawaki, D. et al. Visceral Adipose Tissue Drives Cardiac Aging Through Modulation of Fibroblast Senescence by Osteopontin Production. Circulation. 2018 Aug 21;138(8):809-822. doi: 10.1161/CIRCULATIONAHA.117.031358. PMID: 29500246.

[12] Neeland IJ, Poirier P, Després JP. Cardiovascular and Metabolic Heterogeneity of Obesity: Clinical Challenges and Implications for Management. Circulation. 2018 Mar 27;137(13):1391-1406. doi: 10.1161/CIRCULATIONAHA.117.029617. PMID: 29581366; PMCID: PMC5875734.

[13] Alberti KG et al. International Diabetes Federation Task Force on Epidemiology and Prevention; Hational Heart, Lung, and Blood Institute; American Heart Association; World Heart Federation; International Atherosclerosis Society; International Association for the Study of Obesity. Harmonizing the metabolic syndrome: a joint interim statement of the

International Diabetes Federation Task Force on Epidemiology and Prevention; National Heart, Lung, and Blood Institute; American Heart Association; World Heart Federation; International Atherosclerosis Society; and International Association for the Study of Obesity. Circulation. 2009 Oct 20;120(16):1640-5. doi: 10.1161/CIRCULATIONAHA.109.192644. Epub 2009 Oct 5. PMID: 19805654.

[14] Ahrens W.,et al. Prevalence of overweight and obesity in European children below the age of 10. Int J Obes (Lond). 2014 Sep;38 Suppl 2:S99-107. doi: 10.1038/ijo.2014.140. PMID: 25376223.

[15] International Diabetes Federation: the IDF consensus worldwide definition of the metabolic syndrome. https://www.idf.org/e-library/consensus-statements.html

[16] Hakker G. D, et al. Increased myocardial susceptibility to repetitive ischemia with high-fat diet-induced obesity. Obesity (Silver Spring). 2008 Dec;16(12):2593-600. doi: 10.1038/oby.2008.414. Epub 2008 Oct 2. PMID: 18833212; PMCID: PMC3049112.

[17] Mastrocola R, Collino M, Penna C, et al. Maladaptive Modulations of NLRP3 Inflammasome and Cardioprotective Pathways Are Involved in Diet-Induced Exacerbation of Myocardial Ischemia/Reperfusion Injury in Mice. Oxid Med Cell Longev. 2016;2016:3480637. doi: 10.1155/2016/3480637. Epub 2015 Dec 14. PMID: 26788246; PMCID: PMC4691622.

[18] Mezzaroma E., et al. The inflammasome promotes adverse cardiac remodeling following acute myocardial infarction in the mouse. Proc Natl Acad Sci U S A. 2011 Dec 6;108(49):19725-30. doi: 10.1073/pnas.1108586108. Epub 2011 Nov 21. PMID: 22106299; PMCID: PMC3241791.

[19] Benetti E, Chiazza F, Patel NS, Collino M. The NLRP3 Inflammasome as a novel player of the intercellular crosstalk in metabolic disorders. Mediators Inflamm. 2013;2013:678627. doi: 10.1155/2013/678627. Epub 2013 Jun 13. PMID: 23843683; PMCID: PMC3697790.

[20] Lee H.M., et al. Upregulated NLRP3 inflammasome activation in patients with type 2 diabetes. Diabetes. 2013 Jan;62(1):194-204. doi: 10.2337/db12-0420. Epub 2012 Oct 18. PMID: 23086037; PMCID: PMC3526026.

[21] Landecho MF, Tuero C, Valentí V, Bilbao I, de la Higuera M, Frühbeck G. Relevance of Leptin and Other Adipokines in Obesity-Associated Cardiovascular Risk. Nutrients. 2019 Nov 5;11(11):2664. doi: 10.3390/nu11112664. PMID: 31694146; PMCID: PMC6893824.

[22] Van Gaal LF, Mertens IL, De Block CE. Mechanisms linking obesity with cardiovascular disease. Nature. 2006 Dec 14;444(7121):875-80. doi: 10.1038/nature05487. PMID: 17167476.

[23] Williams JW, Huang LH, Randolph GJ. Cytokine Circuits in Cardiovascular Disease. Immunity. 2019 Apr 16;50(4):941-954. doi: 10.1016/j.immuni.2019.03.007. PMID: 30995508; PMCID: PMC6924925.

[24] Goldin A, Beckman JA, Schmidt AM, Creager MA. Advanced glycation end products: sparking the development of diabetic vascular injury. Circulation. 2006 Aug 8;114(6):597-605. doi: 10.1161/CIRCULATIONAHA.106.621854. PMID: 16894049.

[25] Basta G., et all. At least 2 distinct pathways generating reactive oxygen species mediate vascular cell adhesion molecule-1 induction by advanced glycation end products. Arterioscler Thromb Vasc Biol. 2005 Jul;25(7):1401-7. doi: 10.1161/01.ATV.0000167522.48370.5e. Epub 2005 Apr 21. PMID: 15845907.

[26] Boyer, F., et al. Oxidative Stress and Adipocyte Biology: Focus on the Role of AGEs. Oxid Med Cell Longev. 2015;2015:534873. doi: 10.1155/2015/534873. Epub 2015 Mar 23. PMID: 25878764; PMCID: PMC4386674.

[27] Lander, H.M., et al. Redox regulation of cell signalling. Nature. 1996 May 30;381(6581):380-1. doi: 10.1038/381380a0. PMID: 8632794.

[28] Lander, H.M, et al Activation of the Receptor for Advanced Glycation End Products Triggers a p21 ras -dependent Mitogen-activated Protein Kinase Pathway Regulated by Oxidant Stress J Biol Chem. 1997 Jul 11;272(28):17810-4. doi: 10.1074/jbc.272.28.17810. PMID: 9211935.

[29] Lan, A., et al. Inhibition of ROS-activated p38MAPK pathway is involved in the protective e_ect of H2S against chemical hypoxia-induced inflammation in PC12 cells. Neurochem Res. 2013 Jul;38(7):1454-66. doi: 10.1007/s11064-013-1044-x. Epub 2013 Apr 27. PMID: 23624824; PMCID: PMC3671109.

[30] Kamata, H., et al. Reactive oxygen species promote TNF_-induced death and sustained JNK activation by inhibiting MAP kinase phosphatases. Cell. 2005 Mar 11;120(5):649-61. doi: 10.1016/j.cell.2004.12.041. PMID: 15766528.

[31] Cohen, M.P., et al. Glycated albumin increases oxidative stress, activates NF-κB and extracellular signal-regulated kinase (ERK), and stimulates erk-dependent transforming growth factor-1 production in macrophage RAW cells. J. Lab. Clin. Med. 2003, 141, 242–249

[32] Martinon F., et al. The inflammasome: A molecular platform triggering activation of inflammatory caspases and processing of proIL1β. Mol Cell. 2002 Aug;10(2):417-26. doi: 10.1016/s1097-2765(02)00599-3. PMID: 12191486.

[33] Nakahira et al. Autophagy proteins regulate innate immune responses by inhibiting the release of mitochondrial DNA mediated by the NALP3 inflammasome. Nat Immunol. 2011 Mar;12(3):222-30. doi: 10.1038/ni.1980. Epub 2010 Dec 12. PMID: 21151103; PMCID: PMC3079381.

[34] Halle et al. The NALP3 inflammasome is involved in the innate immune response to amyloid-beta. Nat Immunol. 2008 Aug;9(8):857-65. doi: 10.1038/ni.1636. Epub 2008 Jul 11. PMID: 18604209; PMCID: PMC3101478.

[35] Vajjhala, et al. Identification of multifaceted binding modes for pyrin and ASC pyrin domains gives insights into pyrin inflammasome assembly. J Biol Chem. 2014 Aug 22;289(34):23504-19. doi: 10.1074/jbc.M114.553305. Epub 2014 Jul 8. PMID: 25006247; PMCID: PMC4156052.

[36] Senftleben et al. Activation by IKKalpha of a second, evolutionary conserved, NF-kappa B signaling pathway. Science. 2001 Aug 24;293(5534):1495-9. doi: 10.1126/science.1062677. PMID: 11520989.

[37] Rawlings JS, Rosler KM, Harrison DA. The JAK/STAT signaling pathway. J Cell Sci. 2004 Mar 15;117(Pt 8):1281-3. doi: 10.1242/jcs.00963. PMID: 15020666.

[38] Schindler, C., et al. JAK-STAT signaling: from interferons to cytokines. J Biol Chem. 2007 Jul 13;282(28):20059-63. doi: 10.1074/jbc.R700016200. Epub 2007 May 14. PMID: 17502367.

[39] Dodington DW, Desai HR, Woo M. JAK/STAT - Emerging Players in Metabolism. Trends Endocrinol Metab. 2018 Jan;29(1):55-65. doi: 10.1016/j.tem.2017.11.001. Epub 2017 Nov 27. PMID: 29191719.

[40] Haan C, Kreis S, Margue C, Behrmann I. Jaks and cytokine receptors--an intimate relationship. Biochem Pharmacol. 2006 Nov 30;72(11):1538-46. doi: 10.1016/j.bcp.2006.04.013. Epub 2006 Apr 27. PMID: 16750817.

[41] Giorgetti-Peraldi S, Peyrade F, Baron V, Van Obberghen E. Involvement of Janus kinases in the insulin signaling pathway. Eur J Biochem. 1995 Dec 1;234(2):656-60. doi: 10.1111/j.1432-1033.1995.656_b.x. PMID: 8536716.

[42] Saad MJ, Carvalho CR, Thirone AC, Velloso LA. Insulin induces tyrosine phosphorylation of JAK2 in insulin-sensitive tissues of the intact rat. J Biol Chem. 1996 Sep 6;271(36):22100-4. doi: 10.1074/jbc.271.36.22100. PMID: 8703019.

[43] Thirone, A.C., et al., Opposite effect of JAK2 on insulin-dependent activation of mitogen-activated protein kinases and Akt in muscle cells: possible target to ameliorate insulin resistance. Diabetes. 2006 Apr;55(4):942-51. doi: 10.2337/diabetes.55.04.06.db05-1265. PMID: 16567515.

[44] Bako HY, Ibrahim MA, Isah MS, Ibrahim S. Inhibition of JAK-STAT and NF-κB signalling systems could be a novel therapeutic target against insulin resistance and type 2 diabetes. Life Sci. 2019 Dec 15;239:117045. doi: 10.1016/j.lfs.2019.117045. Epub 2019 Nov 12. PMID: 31730866.

[45] Mishra J, Verma RK, Alpini G, Meng F, Kumar N. Role of Janus Kinase 3 in Predisposition to Obesity-associated Metabolic Syndrome. J Biol Chem. 2015 Dec 4;290(49):29301-12. doi: 10.1074/jbc.M115.670331. Epub 2015 Oct 8. PMID: 26451047; PMCID: PMC4705936.

[46] Yu Shi, S., García Martin, R., Duncan, R.E., Choi, D., Lu, S.Y., Schroer, S.A., et al., 2012. Hepatocyte-specific deletion of Janus kinase 2 (JAK2) protects against diet-induced steatohepatitis and glucose intolerance. J Biol Chem. 2012 Mar 23;287(13):10277-88. doi: 10.1074/jbc.M111.317453. Epub 2012 Jan 24. PMID: 22275361; PMCID: PMC3323042.

[47] Corbit, K.C., Camporez, J.P.G., Tran, J.L., Wilson, C.G., Lowe, D.A.,Nordstrom, S.M., et al., 2017. Adipocyte JAK2 mediates growth hormoneinduced hepatic insulin resistance. JCI Insight. 2017 Feb 9;2(3):e91001. doi: 10.1172/jci.insight.91001. PMID: 28194444; PMCID: PMC5291741.

[48] C. Nathan, et al. Points of control in inflammation. Nature. 2002 Dec 19-26;420(6917):846-52. doi: 10.1038/nature01320. PMID: 12490957.

[49] C. N. Serhan, et al. Pro-resolving lipid mediators are leads for resolution physiology. Nature. 2014 Jun 5;510(7503):92-101. doi: 10.1038/nature13479. PMID: 24899309; PMCID: PMC4263681.

[50] A. Recchiuti, et al. Resolvin D1 and its GPCRs in resolution circuits of inflammation. Prostaglandins Other Lipid Mediat. 2013 Dec;107:64-76. doi: 10.1016/j.prostaglandins.2013.02.004. Epub 2013 Mar 15. PMID: 23500003.

[51] V. Gerke et al. Annexins: linking Ca2+ signalling to membrane dynamics. Nat Rev Mol Cell Biol. 2005 Jun;6(6):449-61. doi: 10.1038/nrm1661. PMID: 15928709.

[52] G. Cirino et al. Pepinsky. Recombinant human lipocortin 1 inhibits thromboxane release from guinea-pig isolated perfused lung. Nature. 1987 Jul 16-22;328(6127):270-2. doi: 10.1038/328270a0. PMID: 2955229.

[53] M. Perretti et al. Exploiting the Annexin A1 pathway for the development of novel anti-inflammatory therapeutics. Br J Pharmacol. 2009 Oct;158(4):936-46. doi: 10.1111/j.1476-5381.2009.00483.x. PMID: 19845684; PMCID: PMC2785517.

[54] L. Vong et al. Annexin 1 cleavage in activated neutrophils: a pivotal role for proteinase 3. J Biol Chem. 2007 Oct 12;282(41):29998-30004. doi: 10.1074/jbc.M702876200. Epub 2007 Aug 6. PMID: 17681950; PMCID: PMC2772024.

[55] Michelle Amantéa Sugimoto et al. Annexin A1 and the Resolution of Inflammation: Modulation of Neutrophil Recruitment, Apoptosis, and Clearance. J Immunol Res. 2016;2016:8239258. doi: 10.1155/2016/8239258. Epub 2016 Jan 13. PMID: 26885535; PMCID: PMC4738713.

[56] R. D. Ye, et al. International union of basic and clinical pharmacology. LXXIII. Nomenclature for the formyl peptide receptor (FPR) family. Pharmacol Rev. 2009 Jun;61(2):119-61. doi: 10.1124/pr.109.001578. Epub 2009 Jun 4. PMID: 19498085; PMCID: PMC2745437.

[57] Y. Li et al. Pleiotropic regulation of macrophage polarization and tumorigenesis by formyl peptide receptor-2. Oncogene. 2011 Sep 8;30(36):3887-99. doi: 10.1038/onc.2011.112. Epub 2011 Apr 18. Erratum in: Oncogene. 2011 Oct 20;30(42):4373-4. PMID: 21499310.

[58] S. Bena et al. Annexin A1 interaction with the FPR2/ALX receptor: identification of distinct domains and downstream associated signaling. J Biol Chem. 2012 Jul 13;287(29):24690-7. doi: 10.1074/jbc.M112.377101. Epub 2012 May 18. PMID: 22610094; PMCID: PMC3397896.

[59] D. G. Souza et al. The required role of endogenously produced lipoxin A4 and annexin-1 for the production of IL-10 and inflammatory hyporesponsiveness in mice. J Immunol. 2007 Dec 15;179(12):8533-43. doi: 10.4049/jimmunol.179.12.8533. PMID: 18056401.

[60] Chan EC, et al. Global urinary metabolic profiling procedures using gas chromatography-mass spectrometry. Nat Protoc. 2011 Sep 8;6(10):1483-99. doi: 10.1038/nprot.2011.375. PMID: 21959233.

[61] Reichenbach SE, et al. Alignment for comprehensive two-dimensional gas chromatography with dual secondary columns and detectors. Anal Chem. 2015 Oct 6;87(19):10056-63. doi: 10.1021/acs.analchem.5b02718. Epub 2015 Sep 30. PMID: 26349029.

[62] Kleiner DE, et al. Design and validation of a histological scoring system for nonalcoholic fatty liver disease. Hepatology. 2005 Jun;41(6):1313-21. doi: 10.1002/hep.20701. PMID: 15915461.

[63] Kim W, Egan JM. The role of incretins in glucose homeostasis and diabetes treatment. Pharmacol Rev. 2008 Dec;60(4):470-512. doi: 10.1124/pr.108.000604. Epub 2008 Dec 12. PMID: 19074620; PMCID: PMC2696340.

[64] Russell, A.; Adua, E.; Ugrina, I.; Laws, S.; Wang, W. Unravelling Immunoglobulin G Fc N-Glycosylation:A Dynamic Marker Potentiating Predictive, Preventive and Personalised Medicine. Int J Mol Sci. 2018 Jan 29;19(2):390. doi: 10.3390/ijms19020390. PMID: 29382131; PMCID: PMC5855612.

[65] Plomp, R.; Ruhaak, L.R.; Uh, H.W.; Reiding, K.R.; Selman, M.; Houwing-Duistermaat, J.J.; Slagboom, P.E.; Beekman, M.;Wuhrer, M. Subclass-specific IgG glycosylation is associated with markers of inflammation and metabolic health. Sci Rep. 2017 Sep 26;7(1):12325. doi: 10.1038/s41598-017-12495-0. PMID: 28951559; PMCID: PMC5615071.

[66] Reily, C.; Stewart, T.J.; Renfrow, M.B.; Novak, J. Glycosylation in health and disease. Nat Rev Nephrol. 2019 Jun;15(6):346-366. doi: 10.1038/s41581-019-0129-4. PMID: 30858582; PMCID: PMC6590709.

[67] Arnold, J.N.; Saldova, R.; Hamid, U.M.; Rudd, P.M. Evaluation of the serum N-linked glycome for the diagnosis of cancer and chronic inflammation. Proteomics. 2008 Aug;8(16):3284-93. doi: 10.1002/pmic.200800163. PMID: 18646009.

[68] Jennewein, M.F.; Alter, G. The Immunoregulatory Roles of Antibody Glycosylation. Trends Immunol. 2017 May;38(5):358-372. doi: 10.1016/j.it.2017.02.004. Epub 2017 Apr 3. PMID: 28385520.

[69] Biermann, M.H.; Gri_ante, G.; Podolska, M.J.; Boeltz, S.; Stürmer, J.; Munoz, L.E.; Bilyy, R.; Herrmann, M. Sweet but dangerous-the role of immunoglobulin G glycosylation in autoimmunity and inflammation. Lupus. 2016 Jul;25(8):934-42. doi: 10.1177/0961203316640368. PMID: 27252272.

[70] T. Fujimaru, J. H. Park, and J. Lim Sensory characteristics and relative sweetness of tagatose and other sweeteners. J Food Sci. 2012 Sep;77(9):S323-8. doi: 10.1111/j.1750-3841.2012.02844.x. Epub 2012 Aug 21. PMID: 22908895.

[71] P. Kim, Current studies on biological tagatose production using L-arabinose isomerase: a review and future perspective. Appl Microbiol Biotechnol. 2004 Aug;65(3):243-9. doi: 10.1007/s00253-004-1665-8. Epub 2004 Jul 10. PMID: 15248040.

[72] H. F. Bunn and P. J. Higgins, Reaction of monosaccharides with proteins: possible evolutionary significance. Science. 1981 Jul 10;213(4504):222-4. doi: 10.1126/science.12192669. PMID: 12192669.

[73] M. Ensor, A. B. Banfield, R. R. Smith, J. Williams, and R. A. Lodder Safety and efficacy of D-tagatose in glycemic control in subjects with type 2 diabetes. J Endocrinol Diabetes Obes. 2015;3(1):1065. Epub 2014 Dec 31. PMID: 27054147; PMCID: PMC4820068.

[74] T. K. Abouzed, S. Munesue, A. Harashima et al. Preventive effect of salicylate and pyridoxamine on diabetic nephropathy. J Diabetes Res. 2016;2016:1786789. doi: 10.1155/2016/1786789. Epub 2016 Nov 30. PMID: 28042580; PMCID: PMC5155113.

[75] Calay ES, Hotamisligil GS. (2013) Turning off the inflammatory, but not the metabolic, flames. Nat Med. 2013 Mar;19(3):265-7. doi: 10.1038/nm.3114. PMID: 23467233.

[76] Kahn, S. E., et al. Mechanisms linking obesity to insulin resistance and type 2 diabetes. Nature. 2006 Dec 14;444(7121):840-6. doi: 10.1038/nature05482. PMID: 17167471.

[77] Benetti E, Chiazza F, Patel NS, Collino M. The NLRP3 Inflammasome as a novel player of the intercellular crosstalk in metabolic disorders. Mediators Inflamm. 2013;2013:678627. doi: 10.1155/2013/678627. Epub 2013 Jun 13. PMID: 23843683; PMCID: PMC3697790.

[78] S. D. Purvis, Massimo Collino, Haidee M. A. Tavio, Fausto Chiazza, Caroline E. O'Riodan, Lynda Zeboudj, Nick Guisot, Peter Bunyard, David R. Greaves, Christoph Thiemermann. Inhibition of Bruton's tyrosine kinase reduces NF-kB and NLRP3 inflammasome activity preventing insulin resistance and microvascular diseaseGareth. BioRxiv 745943; doi: https://doi.org/10.1101/745943

[79] Chiazza F, Couturier-Maillard A, Benetti E, et al. Targeting the NLRP3 Inflammasome to Reduce Diet-Induced Metabolic Abnormalities in Mice. Mol Med. 2016 Mar;21(1):1025-1037. doi: 10.2119/molmed.2015.00104. Epub 2016 May 9. PMID: 26623925; PMCID: PMC4982477.

[80] Brabant, G., et al., Hepatic leptin signaling in obesity. ASEB J. 2005 Jun;19(8):1048-50. doi: 10.1096/fj.04-2846fje. Epub 2005 Mar 23. Erratum in: FASEB J. 2013 May;27(5):2080-1. PMID: 15788447.

[81] Hondam, S.K., D.J. Cuthbertson, and J.P.H. Wilding, The influence of Glucose-dependent Insulinotropic Polypeptide (GIP) on human adipose tissue and fat metabolism: Implications for obesity, type 2 diabetes and Non-Alcoholic Fatty Liver Disease (NAFLD). Peptides. 2020 Mar;125:170208. doi: 10.1016/j.peptides.2019.170208. Epub 2019 Nov 20. PMID: 31759125.

[82] Ma, X., et al., Suppression of Ghrelin Exacerbates HFCS-Induced Adiposity and Insulin Resistance. Int J Mol Sci. 2017 Jun 19;18(6):1302. doi: 10.3390/ijms18061302. PMID: 28629187; PMCID: PMC5486123.

[83] Matthews, V.B., Allen, T.L., Risis, S., Chan, M.H.S., Henstridge, D.C., Watson, N., et al., 2010. Interleukin-6-deficient mice develop hepatic inflammation and systemic insulin resistance. Diabetologia. 2010 Nov;53(11):2431-41. doi: 10.1007/s00125-010-1865-y. Epub 2010 Aug 11. PMID: 20697689.

[84] Opal, S.M., DePalo, V.A., 2000. Anti-inflammatory cytokines. Chest. 2000 Apr;117(4):1162-72. doi: 10.1378/chest.117.4.1162. PMID: 10767254.

[85] Gilroy DW, Lawrence T, Perretti M, et al. Inflammatory resolution: new opportunities for drug discovery. Nat Rev Drug Discov. 2004 May;3(5):401-16. doi: 10.1038/nrd1383. PMID: 15136788.

[86] Pipicz M, Demján V, Sárközy M, Csont T. Effects of Cardiovascular Risk Factors on Cardiac STAT3. Nat Rev Drug Discov. 2004 May;3(5):401-16. doi: 10.1038/nrd1383. PMID: 15136788

Acknowledgments

Throughout the writing of this dissertation I have received a great deal of support and assistance from many important persons that I would like to mention.

I would first like to thank my supervisor, Professor Massimo Collino, whose expertise was invaluable in formulating the research and methodology. His insightful feedback pushed me to sharpen my thinking and brought my work to a higher level.

I would like to acknowledge my colleagues at the University of Turin for their wonderful collaboration. I would particularly like to mention Fausto Chiazza, Gustavo Ferreira Alves, Roberta Verta, Eleonora Aimaretti and Giacomo Einaudi. Also from the pathology department I want to tank Dr Raffaella Mastrocola for her patient support and for all of the opportunities I was given to further my research.

A special thanks to Professor Arianna Carolina Rosa who taught me how to manage the animal house activities and whom I always work with extreme empaty.

I would also like to thank my tutors in my abroad experiences, Dr. Lokesh Josh, Dr. Marie Le Berre from the National University of Ireland (Advanced Glycoscience Research Cluster, NCBES Biomedical Science), in Galway and Professor Maria Rosa Saiz Menedez from the University of Oviedo, Spain (Institute of Oncology “Principado de Asturias”) for their valuable guidance throughout my research. Each one of you provided me with the tools that I needed to choose the right direction and successfully complete my dissertation.

Thank you Professor Giuseppina Mattace Raso and Monica Montagnani for being on my dissertation committee. I truly appreciate the work you both did during the review of my thesis: your experience and expertise were fundamental in tailoring a professional work.

In addition, I would like to thank my parents for their wise counsel and sympathetic ear. They have been always there for me. Thanks also to my entire family including my Mexican family. Also, I could not have completed this dissertation without the support of my ex-students now friends, who provided stimulating discussions as well as happy distractions to rest my mind

outside of my research. Flogerta, Valentina, Barbara and Giulia you are a precious treasure I found in the middle of my path.

Last but not least, Omar with whom I am building a family, infact soon we will be three, we I give birth to our sweet daughter Marina! You with unlimited patience and love were able to support me during my intense days of study and research. Only with you I was really able to let off steam. Thanks for giving me the strength and the courage to face every challenge during the PhD program, from speaking in front of an audience, to live in other countries. Your kindnesses allowed me to improve my self every day, and now more and more also as a mother!